Molecular Modeling of Asymmetric Induction in Heterogeneously Catalyzed Hydrogenation of the C=O Bond

Antti Taskinen

Laboratory of Physical Chemistry
Department of Natural Sciences
Åbo Akademi University
2010

Supervisor

Professor Matti Hotokka
Laboratory of Physical Chemistry
Department of Natural Sciences
Åbo Akademi University
Turku, Finland

Reviewers

Professor Tapio Rantala
Department of Physics
Tampere University of Technology
Tampere, Finland

and

Professor Dage Sundholm
Department of Chemistry
University of Helsinki
Helsinki, Finland

Opponent

Dr. Philippe Sautet
Director of the Chemistry Laboratory
Institute of Chemistry
University of Lyon
Lyon, France

ISBN 978-952-12-2480-5
ISBN 978-952-12-2481-2 (digital)
Uniprint – Turku, Finland 2010

To render my works properly requires a combination of extreme precision and irresistible verve, a regulated vehemence, a dreamy tenderness, and an almost morbid melancholy.

—Hector Berlioz (1803–1869)

Acknowledgments

This work was carried out at Åbo Akademi University, Department of Physical Chemistry, during the years 2002–2006. Part of the work is based on studies conducted at the Laboratory of Industrial Chemistry and Reaction Engineering in 2007–2009. The work was supported by the Graduate School of Computational Chemistry and Molecular Spectroscopy (Laskemo), Academy of Finland, the Rector of Åbo Akademi University, and the Research Institute of the Åbo Akademi Foundation.

I would like to express my gratitude to my supervisor, professor Matti Hotokka, for this project. I am especially grateful to him for his support and patience. I would also like to thank Professor Dmitry Murzin for his constant interest and enthusiasm for my work. Professor Reko Leino is thanked for his valuable advice. Professor Björn Rosenholm and Professor Tapio Salmi are acknowledged for giving me the opportunity to work at their laboratories.

I owe my gratitude to Dr. Ville Nieminen, Docent Esa Toukoniitty, and Dr. Igor Busygin for scientific collaboration and many fruitful discussions. M.Sc. Max Johansson is thanked for the nice company at work and for sharing his knowledge of computers with me. Moreover, I would like to express my special gratitude to Ph.L. Thomas Sandberg for his friendship at work and leisure time. I also wish to thank all the co-authors of the articles I have contributed to. People at the Department of Physical Chemistry and the Laboratory of Industrial Chemistry and Reaction Engineering are acknowledged for the inspiring and friendly atmosphere. Computer resources provided by CSC, the Finnish IT center for science, are kindly acknowledged.

I would like to thank all my friends in Akademiska Orkestern vid Åbo Akademi for the wonderful and unforgettable moments we have experienced together—this orchestra has influenced my life in so many ways. My parents deserve special thanks for all their support. Finally, I am most indebted to my wife Kirsi. Thank you for all the moments we have shared during this journey!

Piikkiö, June 2010

Antti Taskinen

Abstract

Modification of metal surfaces by strongly adsorbed chiral organic molecules is perhaps the most relevant technique known today to create chiral surfaces. It can be utilized in catalytic production of enantiomerically pure chiral compounds increasingly needed, for example, as drugs and aroma chemicals. Despite many benefits of asymmetric heterogeneous catalysis over other strategies to obtain chiral compounds, it has not become a standard tool for large-scale applications yet. This, for one, is due to the lack of deeper knowledge of catalytic reaction mechanisms and origins of asymmetric induction.

In this study, molecular modeling techniques were employed to investigate asymmetric heterogeneous catalytic systems, specifically hydrogenation of prochiral carbonyl compounds to corresponding chiral alcohols over Pt catalysts modified by cinchona alkaloids (called modifiers). 1-Phenyl-1,2-propanedione (PPD) and some other compounds containing a prochiral C=O moiety were used as model reactants. Conformations of the reactants and modifiers as well as hydrogen-bonded one-to-one complexes between them were studied in the gas and solution phase with methods based on wave function theory and density functional theory (DFT). For the assessment of proton affinities, highly accurate compound methods such as G2(MP2) were also used. The relative population of the modifier conformations depended on the solvent, the modifier itself, and whether the modifier was protonated or not. Several reactant–modifier interaction geometries were considered. Conclusions about the sense of stereoselectivity were based on the relative thermodynamic stabilities of the diastereomeric reactant–modifier complexes and the energies of the π and π^* orbitals of the reacting carbonyl group.

Adsorption and reactions on the Pt(111) surface were modeled by DFT. Regioselectivity in the hydrogenation of PPD and 2,3-hexanedione could be explained by molecule–surface interactions. The size and shape of the cluster used to model the Pt surface affected not only the adsorption energies but also the relative stabilities of different adsorption modes of a molecule. The populations of the modifier conformations in the gas and solution phase did not correlate with those on the Pt surface nor with the enantioselectivity in the hydrogenation of PPD over Pt–cinchona catalysts. Some modifier conformations and reactant–modifier interaction geometries were stable only on the metal surface. Theoretically obtained potential energy profiles for hydrogenation of chiral α-hydroxyketones on Pt implied the preference for pairwise hydrogen addition mechanism and selectivities consistent with experiments.

The attained results increase understanding of chiral heterogeneous catalytic systems and could thus be utilized to develop new, more active and selective chiral catalysts.

Sammanfattning

Modifiering av metallytor med starkt adsorberade kirala organiska molekyler är eventuellt den mest relevanta teknik man vet i dag för att skapa kirala ytor. Den kan utnyttjas i katalytisk produktion av enantiomeriskt rena kirala föreningar som behövs t.ex. som läkemedel och aromkemikalier. Trots många fördelar av asymmetrisk heterogen katalys jämfört med andra sätt för att få kirala föreningar, har den ändå inte blivit ett allmänt verktyg för storskaliga tillämpningar. Detta beror t.ex. på brist på djupare kunskaper i katalytiska reaktionsmekanismer och ursprunget för asymmetrisk induktion.

I denna studie användes molekylmodelleringstekniker för att studera asymmetriska, heterogena katalytiska system, speciellt hydrering av prokirala karbonylföreningar till motsvarande kirala alkoholer på cinchona-alkaloidmodifierade Pt-katalysatorer. 1-Fenyl-1,2-propandion (PPD) och några andra föreningar, som innehåller en prokiral C=O-grupp, användes som reaktanter. Konformationer av reaktanter och cinchona-alkaloider (som kallas modifierare) samt vätebundna 1:1-komplex mellan dem studerades i gas- och lösningsfas med metoder som baserar sig på vågfunktionsteori och täthetsfunktionalteori (DFT). För beräkningen av protonaffiniteter användes också högst noggranna kombinationsmetoder såsom G2(MP2). Den relativa populationen av modifierarnas konformationer varierade som funktion av modifieraren, dess protonering och lösningsmedlet. Flera reaktant–modifierare-interaktionsgeometrier beaktades. Slutsatserna på riktning av stereoselektivitet baserade sig på den relativa termodynamiska stabiliteten av de diastereomeriska reaktant–modifierare-komplexen samt energierna hos π- och π^*-orbitalerna i den reaktiva karbonylgruppen.

Adsorption och reaktioner på Pt(111)-ytan betraktades med DFT. Regioselektivitet i hydreringen av PPD och 2,3-hexandion kunde förklaras med molekyl–yta-interaktioner. Storleken och formen av klustret använt för att beskriva Pt-ytan inverkade inte bara på adsorptionsenergierna utan också på de relativa stabiliteterna av olika adsorptionsstrukturer av en molekyl. Populationerna av modifierarnas konformationer i gas- och lösningsfas korrelerade inte med populationerna på Pt-ytan eller med enantioselektiviteten i hydreringen av PPD på Pt–cinchona-katalysatorer. Vissa modifierares konformationer och reaktant–modifierare-interaktionsgeometrier var stabila bara på metallytan. Teoretiskt beräknade potentialenergiprofiler för hydrering av kirala α-hydroxiketoner på Pt implicerade preferens för parvis additionsmekanism för väte och selektiviteter i harmoni med experimenten.

De uppnådda resultaten ökar uppfattningen om kirala heterogena katalytiska system och kunde därför utnyttjas i utvecklingen av nya, mera aktiva och selektiva kirala katalysatorer.

List of original publications

The thesis consists mainly in the following publications, which are referred to by their Roman numerals (**I**–**IX**) in the text. The thesis also contains some unpublished results, which are cited accordingly.

I Toukoniitty, E.; Nieminen, V.; Taskinen, A.; Päivärinta, J.; Hotokka, M.; Murzin, D. Yu. A combined experimental and theoretical study of 1-phenylpropane-1,2-dione hydrogenation over heterogeneous cinchonidine-modified Pt catalyst. *J. Catal.* **2004**, *224*, 326–339.

II Taskinen, A.; Toukoniitty, E.; Nieminen, V.; Murzin, D. Yu.; Hotokka, M. Ab initio study of solvent effects on reactant–modifier complexes in enantioselective hydrogenation. *Catal. Today* **2005**, *100*, 373–377.

III Taskinen, A.; Nieminen, V.; Toukoniitty, E.; Murzin, D. Yu.; Hotokka, M. Proton affinities of ketones, vicinal diketones and α-keto esters: a computational study. *Tetrahedron* **2005**, *61*, 8109–8119.

IV Nieminen, V.; Taskinen, A.; Toukoniitty, E.; Hotokka, M.; Murzin, D. Yu. One-to-one reactant–modifier interactions in enantio- and diastereoselective hydrogenation of chiral α-hydroxyketones on Pt(111). *J. Catal.* **2006**, *237*, 131–142.

V Nieminen, V.; Taskinen, A.; Hotokka, M.; Murzin, D. Yu. Revealing regioselectivity in hydrogenation of 1-phenyl-1,2-propanedione on Pt catalysts. *J. Catal.* **2007**, *245*, 228–236.

VI Taskinen, A.; Nieminen, V.; Hotokka, M.; Murzin, D. Yu. The role of modifier structure in heterogeneous enantioselective hydrogenation: one-to-one interactions of 1-phenyl-1,2-propanedione and methyl pyruvate with modifiers on the Pt(111) surface. *J. Phys. Chem. C* **2007**, *111*, 5128–5140.

VII Nieminen, V.; Honkala, K.; Taskinen, A.; Murzin, D. Yu. Intrinsic metal size effect on adsorption of organic molecules on platinum. *J. Phys. Chem. C* **2008**, *112*, 6822–6831.

VIII Busygin, I.; Nieminen, V.; Taskinen, A.; Sinkkonen, J.; Toukoniitty, E.; Sillanpää, R.; Murzin, D. Yu.; Leino, R. A combined NMR, DFT, and X-ray investigation of some cinchona alkaloid *O*-ethers. *J. Org. Chem.* **2008**, *73*, 6559–6569.

IX Busygin, I.; Taskinen, A.; Nieminen, V.; Toukoniitty, E.; Stillger, T.; Leino, R.; Murzin, D. Yu. Experimental and theoretical analysis of asymmetric induction in heterogeneous catalysis: diastereoselective hydrogenation of chiral α-hydroxyketones over Pt catalyst. *J. Am. Chem. Soc.* **2009**, *131*, 4449–4462.

Contribution of the author

The author is responsible for the computational work in the publications **II**, **III**, **VI**, and **IX**. About half of the computations for the publications **I**, **IV**, **V**, and **VIII** were performed by the author, whereas the contribution of the author to the publication **VII** was less.

Contents

Chapter 1

Introduction

1.1 Chirality and life

Chirality, handedness (from Greek *cheir* – hand) is an essential feature of the universe and, especially, life.[1–3] Chirality is the geometric property of a rigid object or spatial arrangement of points or atoms of being non-superimposable on its mirror image.[4] Chiral, "handed" objects are related to their mirror images in the same way that the left hand is related to the right hand—they are similar but not identical (Figure 1.1).

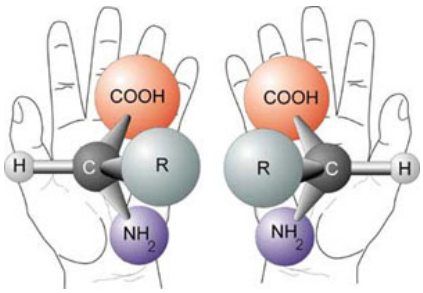

Figure 1.1. A chiral molecule and its non-superimposable mirror image are related like the left and the right hand. They are called enantiomers.[5]

Fundamental parts of all living organisms such as proteins, nucleic acids, and polysaccharides are made of chiral building blocks: amino acids, nucleotides, and sugars. Chirality is also common in the nonliving world. For example, the crystals of quartz (SiO_2), the most abundant mineral in the Earth's continental crust, are chiral.[6] However, equal amounts of left- and right-handed forms of quartz exist. Instead, chemistry of life is homochiral; monomeric building blocks of the biopolymers have the same handedness,

which also leads to homochirality in higher-order structures of the corresponding biopolymers (Figure 1.2). For example, L-amino acids and D-sugars[†] are found in the living systems almost exclusively.[3,7] The origin of homochirality in life is still one of the greatest unsolved problems.[1,2,7–9]

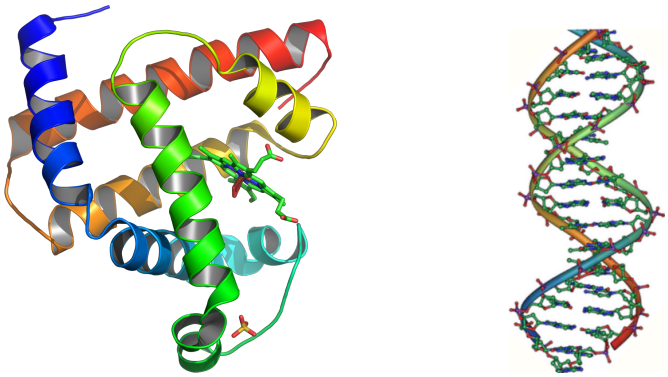

Figure 1.2. A right-handed α-helix (secondary structure) and the fold (tertiary structure) in a protein (left), and a part of a right-handed DNA double helix (right).[10]

Due to the homochirality of life, the enantiomers of a chiral compound may show different behavior when interacting with living beings. For example, enantiomeric compounds can have different odors: chiral (*R*)-carvone smells like spearmint whereas its enantiomer (*S*)-carvone like caraway[‡].[13,14] This ensues from the fact that one smells a molecule by binding it in a chiral receptor molecule, and one enantiomer may bind differently from the other or not at all. The stereoselective interactions are profoundly important for the function of pharmaceuticals. While one enantiomer of a compound can have beneficial effects, the other may be disastrous. This is the case, for example, with thalidomide, a chiral compound once used as an antinausea drug for pregnant women (Figure 1.3). Thalidomide was sold for years as a racemate[§]. As a result, thousands of children were born without limbs or with severe deformities due to the teratogenic effects of (*S*)-thalidomide.[15,16]

Since one enantiomer may be unsafe or merely inactive baggage, the drug industry has shifted to make single-enantiomer forms of chiral compounds.[15,17] In 2006, 80% of small-molecule drugs approved by the U.S.

[†] The D/L-nomenclature is based on the arbitrary stereochemical convention called Fischer–Rosanoff convention.[4] [‡] The (*R*)/(*S*) notation is for specifying the three-dimensional arrangement of substituents around a chirality center in a molecule (i.e., absolute configuration). It is based upon the Cahn–Ingold–Prelog priority system.[11,12] [§] An equimolar mixture of a pair of enantiomers is called a racemate.

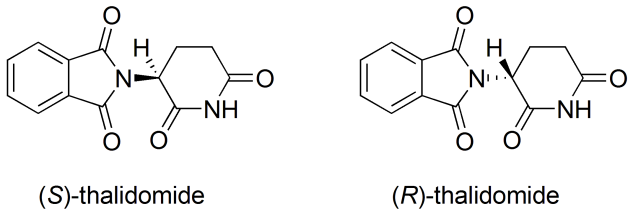

Figure 1.3. The (S) and (R) enantiomers of thalidomide.

Food & Drug Administration were chiral and 75% were single enantiomers.[15] Worldwide sales of single-enantiomer drugs is now more than $160 billion and grows strongly.[18–20] Demand for enantiomerically pure chiral compounds is also rising in three other sectors: flavor and aroma chemicals, agricultural chemicals, and specialty materials.[17]

1.2 Obtaining single enantiomers

Various strategies exist to obtain chiral compounds in enantiopure form (Figure 1.4).[20] The so-called chiral pool consists of a rich diversity of chiral molecules such as carbohydrates, amino acids, lipids, terpenes, and alkaloids, which can be used as a source of starting materials for synthetic routes. These molecules exist as pure enantiomers in nature and can be extracted from plant and animal sources.[21] For many decades, the chiral pool was the only source for enantiopure compounds.[22]

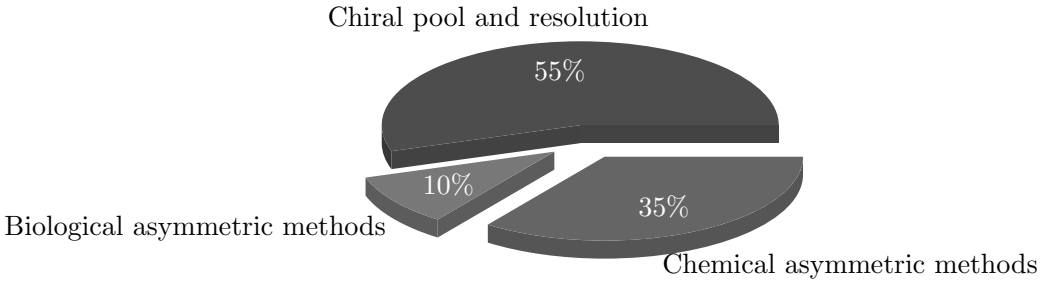

Figure 1.4. Techniques used to produce chiral compounds in 2002.[17]

Resolution (i.e., separation) of racemates constitutes the main method for the industrial synthesis of pure enantiomers.[21] Resolution techniques include crystallization as well as chromatographic and kinetic resolutions. Preparative chromatography is now blooming in the pharmaceutical industry.[15] This

technique is applicable to most chiral small molecules and is very scalable. In addition, it is often cheaper than traditional techniques such as crystallization or asymmetric synthesis to produce single-enantiomer drugs.[15] However, as any racemate contains only 50% of the desired enantiomer, the yield of the resolution technique can be 50% at best.

Usually, the chemical synthesis of molecules containing stereocenters leads to racemates. However, a chiral feature present in the substrate, reagent, catalyst or environment may lead to the preferential formation of one stereoisomer over the other—this is called asymmetric induction.[4] Stoichiometric amounts of chiral reactants can be used to convert prochiral molecules[†] to chiral. However, this approach, which is traditionally called asymmetric synthesis, has a disadvantage: the chiral starting materials may be poorly available and expensive. A more efficient approach is asymmetric, stereoselective catalysis where only a small, catalytic amount of chiral species is required to convey the chiral information to large amounts of products.

Catalytic stereoselective methods are the most desirable of all the methods to produce single-enantiomer compounds and have gained tremendous academic and industrial interest in recent years.[17,23,24] However, asymmetric catalysis is generally not yet competitive against alternative methods for producing chiral molecules. Therefore, it has not made a big breakthrough in industrial chemistry.[15] Noncatalytic, stoichiometric reactions are generally preferred because they are usually easier to control and more robust.[17,23] Several critical factors have to be considered when contemplating a catalytic step in a synthetic route: material availability, development time, ease of implementation, access to the technology, and cost.[24] A big problem with application of asymmetric catalysis is the still highly empirical nature of catalyst selection—which catalyst will work is often unpredictable and depends on reaction conditions and substrates.[24] Catalytic processes may be so fragile that minor variations in operating parameters lead to significant changes in yield or selectivity.

Depending on the type of catalyst used, asymmetric catalysis can be divided into biocatalysis and chemocatalysis. Microbial and other enzymes are extremely efficient catalysts. They can accelerate chemical reactions up to 10^{17}-fold and exhibit superb chemo-, regio-, and stereoselectivity (the "lock-and-key" selectivity) across a diverse range of reactions under mild conditions of pH, temperature, and pressure.[25,26] Many enzymes can be isolated and even immobilized, making them more stable and easier to handle, even separable and recoverable, and usable in standard reactors.[25] The role of biocatalysis is expected to grow impressively in the future.[17,27,28]

[†] Prochiral molecules are molecules that can be converted from achiral to chiral in a single step.

Asymmetric chemical catalysis has probably the greatest potential for general asymmetric synthesis.[29] The best synthetic catalysts are enantioselective over a wide range of different reactions, creating effective asymmetric environments for mechanistically unrelated reactions.[30] In the past decades homogeneous catalysis has seen phenomenal progress.[31–33] Excellent selectivities and activities can be obtained but the homogeneous catalysts are often expensive and their separation and recycling and, thus, industrial application may be difficult.[34,35] Some of the problems can be tackled by "heterogenizing" (i.e., immobilizing) homogeneous catalysts on suitable support materials.[23,36–38]

Molecular chiral imprinting,[39–41] metals supported by chiral materials (e.g., quartz, silk, and cellulose),[42] intrinsically chiral inorganic crystalline surfaces (e.g., quartz and certain high Miller index metal surfaces),[43–45] and supramolecular chirality[46,47] are examples of chiral heterogeneous catalysts. However, these techniques are limited by the generally low number density and structural instability of the chiral sites as well as relatively demanding procedures to prepare them.[48] From a practical catalysis point of view, the most promising solid chiral catalysts are metals modified by the addition of a chiral compound.[34,48–51] Thus far the application of these catalysts has been mainly limited to the asymmetric hydrogenation of unsaturated compounds.

Chemical manufacturers are especially keen to exploit heterogeneous catalytic systems because they can offer benefits such as significant improvement in handling, process efficiency and control, as well as cost savings.[17,23] In spite of the advantages of chiral heterogeneous catalysis, it has not experienced such a development as its homogeneous counterpart. In terms of performance and scope of applications, chiral heterogeneous catalysis lags far behind homogeneous catalysis at the moment. Part of the reason is that chiral heterogeneous systems are relatively few in number and can be quite complex, and they are useful for only a limited number of reactants.[23] It is difficult to create well-defined catalytically active and stable chiral sites on a solid surface.[48] Furthermore, there is lack of deeper knowledge of catalytic reaction and enantiodifferentiation mechanisms.[34] As mechanistic studies continue to reveal additional details of the catalytic systems, asymmetric heterogeneous catalysis has potential to move toward large-scale application.[23]

1.3 Aims of this work

Hydrogenation of a carbonyl compound (i.e., a molecule containing the C=O double bond) that is prochiral yields enantiomeric alcoholic (CH−OH) products. The reaction may be enantioselective if catalyzed by supported plat-

inum nanoparticles modified with large chiral organic molecules (modifiers) such as cinchona alkaloids under suitable reaction conditions (Figure 1.5). Moreover, if the reactant contains several carbonyl groups, the hydrogenation reaction may yield more complex product distribution showing both enantio- and diastereoselectivity as well as regioselectivity. For example, the hydrogenation of 1-phenyl-1,2-propanedione over modified Pt catalyst exhibits such a high complexity (Figure 1.6).

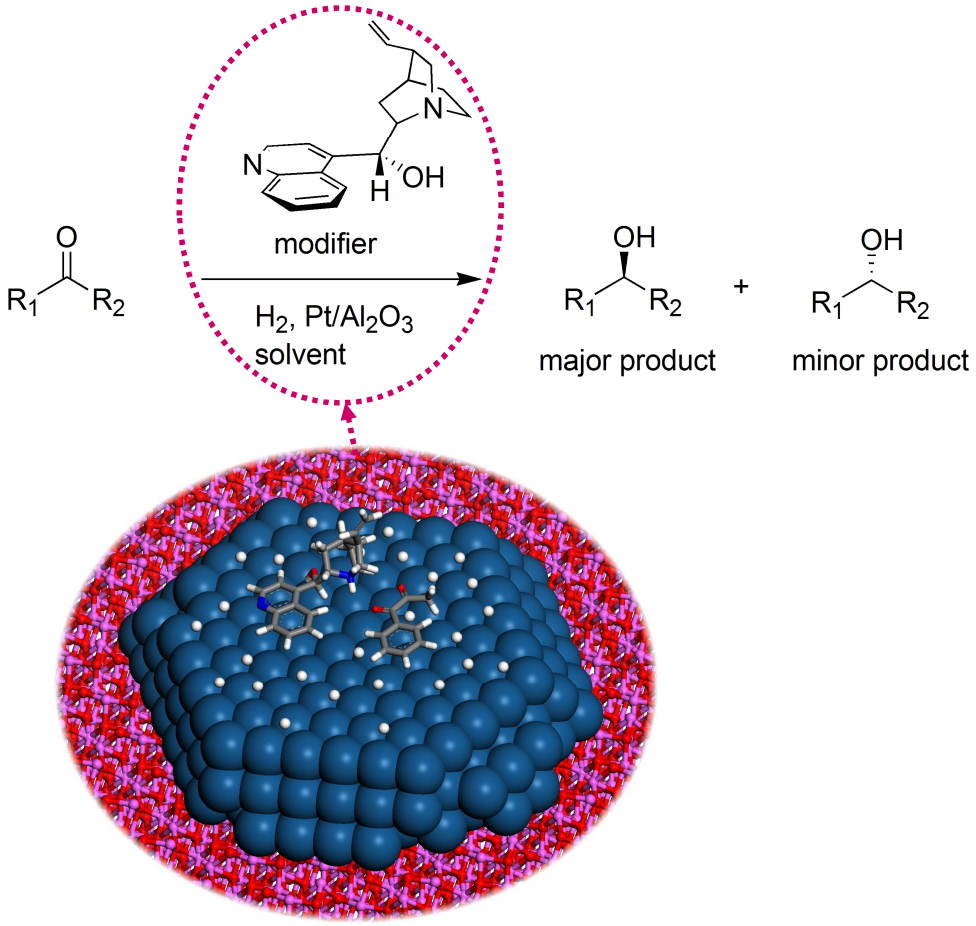

Figure 1.5. Hydrogenation of a prochiral C=O moiety ($R_1 \neq R_2$) may yield an excess amount of one stereoisomeric product over the other when carried out over chirally modified Pt catalysts. Here, cinchonidine exemplifies a typical modifier. The colored part illustrates an Al_2O_3 supported Pt cluster covered with hydrogen atoms (white balls) and cinchonidine and a reactant interacting with each other.

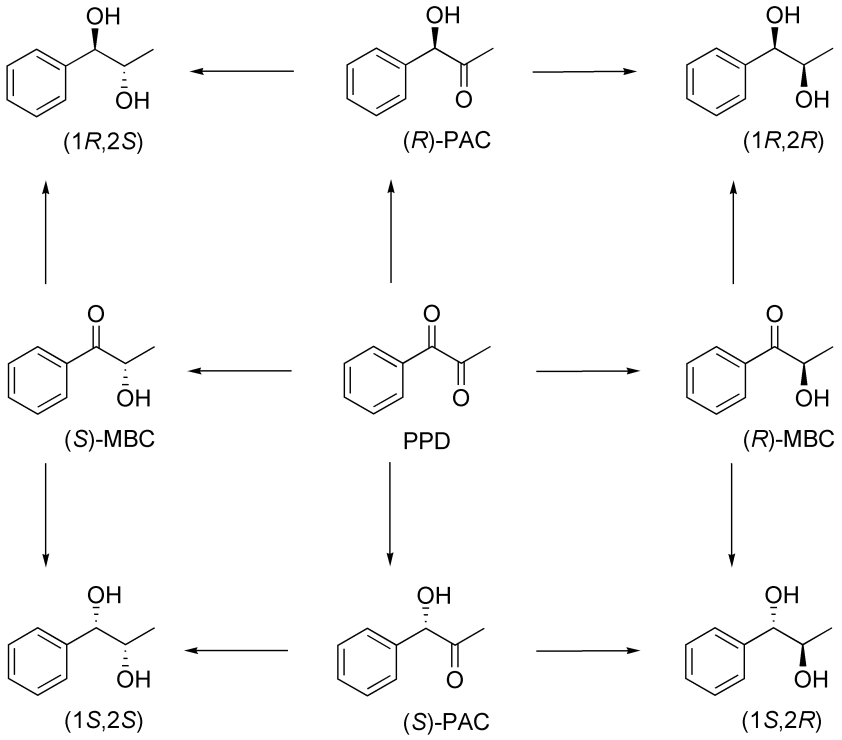

Figure 1.6. Reaction scheme for the hydrogenation of 1-phenyl-1,2-propanedione (PPD). PAC and MBC stand for phenylacetylcarbinol and methylbenzoylcarbinol, respectively.

In this work, issues related to the hydrogenation of carbonyl compounds over chirally modified Pt catalysts were investigated by molecular modeling techniques, mainly by quantum chemical calculations. The following questions were especially addressed:

- What is the origin of asymmetric induction at the molecular level?
- Why and how does the molecular structure of the reactant and the modifier affect stereoselectivity?
- What is the role of the solvent in stereodifferentiation?

In addition to these subjects, the detailed hydrogenation mechanism of the C=O bond and regioselectivity in the α-diketone hydrogenation were considered. The effect of metal particle size on adsorption of organic molecules was also investigated. Elucidating the above-mentioned topics would increase the understanding of the chirally modified catalytic system at the molecular

level. Consequently, it also would help in predicting the performance of other similar types of catalytic systems. Ultimately, the attained knowledge could be utilized to develop new, more active and selective chiral heterogeneous catalysts for the needs of, for example, pharmaceutical and fine chemical industries.

The structure of the rest of the thesis is as follows. Appendix A lists the abbreviations used in the thesis, whereas Appendix B contains some background information about the three key concepts in this work—chirality, catalysis, and molecular modeling. Chapter 2 summarizes characteristic features of the catalytic system studied. Various mechanistic models suggested to be the origin of stereodifferentiation in this system are also presented. Chapter 3 gives a short overview of the computational methods used in this work, whereas details of the methods can be found in Appendix C. The main results of this work are presented and discussed in Chapter 4. Chapter 5 lists the main conclusions and suggestions for future investigations.

Chapter 2

Heterogeneous Pt–cinchona catalysts

Among the techniques known today to create chirality on metal surfaces (see Section 1.2), modification of the surfaces by strongly adsorbed chiral organic molecules is the most relevant from a practical catalysis point of view. Generally, only a very small quantity (a sub-monolayer) of the chiral modifier is required to induce stereoselectivity into the catalytic process. So far the application range of chirally modified metals has been quite narrow. The best understood subject is asymmetric hydrogenation of unsaturated compounds containing C=O and C=C double bonds.[34,48–51] Platinum group metals and nickel have been used as catalytically active metals.

Chirally modified catalytic systems are highly specific with respect to reactants and modifiers, whose interaction may be described by a lock-and-key model familiar from biocatalysis. The origin of almost enzymatic specificity is probably due to the deviations in the adsorption of the reactant and the modifier, but the details are still poorly understood.[51] Under optimized reaction conditions high enantioselectivities ($> 90\%$ enantiomeric excess, ee[†]) are obtained. The three most important chirally modified metal catalysts are (i) Raney Ni modified by tartaric acid for hydrogenation of unfunctionalized and β-functionalized ketones, especially β-keto esters and β-diketones, (ii) Pd modified by cinchona alkaloids for hydrogenation of activated C=C bonds, for example, in α,β-unsaturated carboxylic acids and 2-pyrones, and (iii) Pt modified by cinchona alkaloids for hydrogenation of α-functionalized (activated) ketones such as α-keto esters and α-diketones. The Pt–cinchona catalytic system (iii) has been of interest in the present work and will be surveyed in this chapter. More details can be found in many excellent reviews.[34,48–58]

[†] Enantiomeric excess of the (R) enantiomer over the (S) enantiomer is defined as $ee(\%) = 100 \times ([R] - [S])/([R] + [S])$, where $[R]$ and $[S]$ are the concentrations of the enantiomers.

2.1 Characteristic features

The activity and (stereo)selectivity of chirally modified supported metal catalysts depend on many factors: structure and concentration of the reactants and the modifiers, metal, metal particle size and shape, support, solvent, temperature, and hydrogen pressure among others. All these variables have to be optimized in order to achieve products with high yields and selectivities. The most crucial parameters for the Pt–cinchona system are structure and concentration of the modifier, the structural properties of the supported Pt, and the solvent used.[56]

2.1.1 Reactants and modifiers

Reactant structure

The structure of the reactant molecule plays an important role for achieving high enantioselectivities over a chirally modified metal catalyst—a certain structure is required for optimal interaction with a particular modifier.[34] The Pt−cinchona catalyst was originally reported for enantioselective hydrogenation of α-keto esters by Orito et al. in 1979.[59,60] The application range of the catalyst extends now to several other ketones (Figure 2.1). The highest *ee*s have been observed for ketones possessing an electron-withdrawing functional group at the α-position. Despite the remarkable progress in the past years, the synthetically useful substrate scope of the cinchona-modified platinum catalysts as of the other chirally modified supported metal catalysts is still relatively narrow.[50]

Modifier structure

The key component of the catalytic system is the chiral modifier which generates chiral sites by adsorbing onto the metal surface. The number of efficient modifiers is small and the applicability of the modifier is highly specific to the metal. For the enantioselective hydrogenation of α-functionalized (activated) ketones, the most suitable chiral modifiers are cinchona alkaloids and their simple derivatives (examples shown in Figure 2.2). They possess all three elements that are believed to be crucial:[51] (i) an extended, flat aromatic ring (the "anchoring moiety", shown in blue in Figure 2.2) that allows strong adsorption of the modifier on the metal surface, (ii) the amine group (shown in green) with a basic nitrogen atom capable of interacting with the reactant, and (iii) one or more stereogenic centers (shown in red) in the neighborhood of the other two functions to define the chiral pocket that induces stereoselectivity.

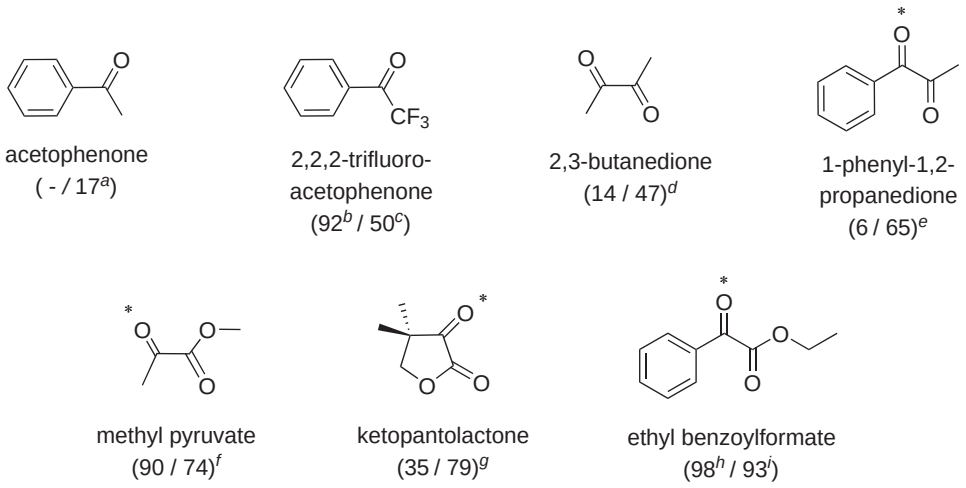

Figure 2.1. Examples of molecules whose keto carbonyl group is hydrogenated enantioselectively over cinchonidine-modified Pt under suitable reaction conditions. The experimentally observed maximum values for the *ee* (%) are given in parentheses (*ee* in acetic acid / *ee* in toluene); the (*R*) enantiomers were formed in excess except in the hydrogenation of acetophenone. If the molecule contains nonequivalent carbonyl groups, the *ee* refers to the hydrogenation of the group indicated with an asterisk. [a] Ref 61. [b] Toluene with some trifluoroacetic acid, ref 62. [c] Ref 63. [d] Ref 64. [e] Ref **I**. [f] Ref 65. [g] Ref 66. [h] AcOH–toluene mixture (1:1 v/v), ref 67. [i] Ref 68.

The stereochemistry of the main product isomer of the catalytic hydrogenation is determined by the configuration of the modifier. For example, in the hydrogenation of 1-phenyl-1,2-propanedione (PPD) and ethyl pyruvate (EP), (*R*)-1-hydroxy-1-phenyl-2-propanone [henceforward called (*R*)-PAC where PAC stands for phenylacetylcarbinol] and (*R*)-ethyl lactate [(*R*)-EL] are formed in excess as cinchonidine (CD) is used as the chiral catalyst modifier (Figure 2.2). By using cinchonine (CN), the opposite product enantiomers are formed in excess. Substitution of the hydroxyl group at the C(9) position of cinchona alkaloids may also affect selectivity and the effect depends sensitively on the reactant. For example, in the hydrogenation of activated α-substituted ketones such as EP, the *ee*s are of similar magnitude whether the modifier is CD or *O*-methylcinchonidine (MeOCD).[69–72] Instead, the replacement of CD by MeOCD leads to a remarkable loss of enantioselectivity or even to an inversion in the sense of enantioselectivity in the hydrogenation of substituted acetophenones,[73] PPD,[74–76] and α-hydroxyketones.[74,77]

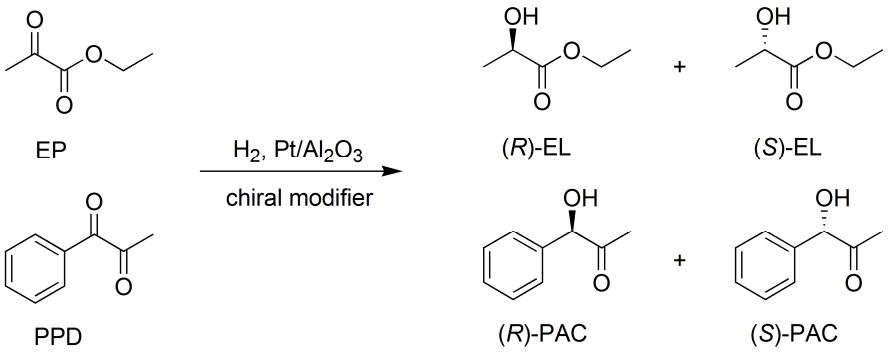

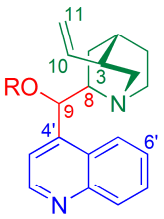

Modifier		*ee* (%) EL	*ee* (%) PAC[a]
CD:	(8*S*,9*R*)-, R = H	74 (*R*)[b]	63 (*R*)
MeOCD:	(8*S*,9*R*)-, R = CH_3	74 (*R*)[b]	10 (*S*)
PhOCD:	(8*S*,9*R*)-, R = C_6H_5	7 (*S*)[b]	28 (*S*)
CN:	(8*R*,9*S*)-, R = H	65 (*S*)[c]	19 (*S*)
MeOCN:	(8*R*,9*S*)-, R = CH_3	46 (*S*)[c]	32 (*R*)
PhOCN:	(8*R*,9*S*)-, R = C_6H_5	n.a.[d]	33 (*R*)

Figure 2.2. Enantiomeric excess (*ee*) observed in the hydrogenation of EP and PPD over Pt/Al_2O_3 catalyst modified with cinchona alkaloids CD and CN and their *O*-ethers in toluene. The structural depiction of the modifier highlights in different colors the three main functionalities that are believed to define the performance of the modifier as a chiral promoter (see the text). [a] At 50% conversion of PPD, ref 74. [b] Ref 71. [c] Ref 69. [d] Not available.

Concentration

The concentration of the reactant can affect the reaction rate and enantioselectivity.[34] The study of EP hydrogenation over a Pt–CD catalyst revealed a weak *ee* maximum at EP concentration of about 2 M (mol dm^{-3}) in the range of 0.4–9 M.[78] In the hydrogenation of PPD, the *ee* increased slightly with increasing PPD concentration, but the maximum *ee* was probably not achieved at such low initial dione concentrations (0.01–0.025 M).[79]

The concentration of the modifier is an important parameter controlling both the rate of hydrogenation and the *ee*. Even very small quantity of the modifier (the molar ratio modifier/$Pt_{surf} \ll 1$) is sufficient to induce enantiodifferentiation.[56] The modifier/reactant molar ratio necessary to obtain the

highest *ee* may be as low as 4 ppm.[80] In the hydrogenation of PPD over Pt catalysts, the *ee* increased with increasing CD concentration until it attained its maximum value at 2:1 molar ratio of CD/Pt_{surf}, whereafter it decreased as the concentration of CD was further increased.[79] In EP hydrogenation, the *ee* also increased first with increasing modifier concentration, whereafter a constant *ee* level[81] or a decline in *ee*[64,82] was observed, depending on the solvent and the modifier. In general, the choice of the reactant, modifier, solvent, and/or catalyst has an effect on the general form of the curves representing the *ee* as a function of the modifier concentration.[64,81,82]

2.1.2 Catalysts

Supported metal catalysts contain polycrystalline metal particles that expose terraces, steps, and kinks to the fluid phase.[83] These particles have a wide size distribution and surface morphologies that depend on their size and on their chemical and thermal history.[83] As enantioselective hydrogenations are structure sensitive reactions (i.e., reactions whose turnover frequencies[†] vary with different metal dispersions), the metal and metal particle size are some of the most important factors affecting the activity and enantioselectivity of chirally modified metal catalysts.[34] The spatial demands on the active surface are such that metal particle morphology is of much greater importance than in simpler (unmodified) reactions.[55]

Metal and metal particle size

Pt is the most suitable metal in the hydrogenation of ketones with cinchona alkaloids as modifiers. Other Pt group metals (Ru, Rh, Pd, Os, Ir) are usually inferior to it. Nickel is not suitable when using cinchona alkaloids.[34] The differences between metals originate from different surface processes during hydrogenation.[34]

The highest enantioselectivities have been obtained with supported catalysts having a low dispersion of metallic platinum.[55] This has been interpreted to mean that the average Pt particle has to be large enough to favor adjacent adsorption of one large modifier molecule and one reactant molecule. In EP hydrogenation, the mean Pt particle diameter had to be larger than about 3 nm to obtain good *ee*s.[85–87] The optimum size for supported Pt particles leading to the maximum *ee* was around 4 nm in the hydrogenation of PPD.[88,89] However, high, over 90% *ee*s have been achieved in the

[†] Turnover frequency (TOF) is the number of molecules A that a catalyst can convert into molecules B in a unit time per active site (or per gram catalyst).[84]

hydrogenation of α-keto esters by using CD-modified colloidal, highly dispersed polyvinylpyrrolidone-stabilized Pt clusters with a mean size less than 2.0 nm. For example, the maximum *ee* of 97.6% in methyl pyruvate (MP) hydrogenation was obtained with Pt particle size of 1.4 nm.[65,90]

The above examples show that more understanding is needed to fully explain all the particle size and morphology effects. One should be careful when drawing conclusions because contradictory observations on the effect of metal particle size on enantioselectivity in various reactions are probably partly due to different surface impurities originating from catalyst preparation and to side reactions that are also structure sensitive.[51] It should also be noted that the shape and size of colloidal and supported metal particles can undergo remarkable changes during catalytic reactions.[51]

Support, modification, and pretreatment

Support material and its pore size distribution as well as catalyst modification and pretreatment procedures are other important factors in enantioselective hydrogenations.[34,56] Most conventional support materials like Al_2O_3, SiO_2, and carbon are suitable when using Pt–cinchona catalysts.[54] Catalyst modification and pretreatment affect the metal surface structure and the presence of other adsorbents on the surface.[34] These procedures can differ from case to case because, for instance, the presence of oxygen and traces of organic impurities may have either positive or negative effect on the *ee*.[34] For example, hydrogenation of α-keto esters led to higher *ee*s when the catalyst was modified under aerobic rather than anaerobic conditions.[91–93] Small amounts of oxygen (and other impurities) enhanced the *ee* in PPD hydrogenation as well.[94]

Catalyst pretreatments are highly catalyst specific and have sometimes dramatic influence on catalyst performance.[51] Effective and widely used pretreatments are prereduction in hydrogen at elevated temperature (in the gas phase or in solution) and ultrasonication (in solution in the presence of the modifier).[51] These pretreatments lead to restructuring of the metal particles. Restructuring changes relative abundance of special surface sites and, thus, influences the adsorption of the reaction components.[51] Reductive and oxidative pretreatments of Pt/Al_2O_3 are also accompanied by the removal or formation of impurities on the metal surface, strongly influencing the adsorption of cinchona alkaloids.[51]

2.1.3 Solvents

Solvent may have a large impact on reaction selectivity (see, e.g., Figure 2.1). In principle, enantioselective hydrogenation is possible in the gas phase,[34,55] but it is usually more convenient to carry out the reaction in some solvent. The dependence of the catalytic activity and selectivity on solvent may be due to several factors: (i) solubility of liquid and gaseous reactants and modifiers and their adsorption on the catalyst surface, (ii) competitive adsorption of solvent molecules, (iii) interactions of solvent molecules with the reactant and the modifier either in the liquid phase or on the catalyst surface, as well as (iv) catalyst deactivation caused by the solvent.[34] Solvents may also promote undesired side reactions.[95] In addition, complex organic molecules can commonly adopt several conformers, and the population of these conformers can vary as a function of solvent properties [e.g., solvent polarity (dielectric constant)] and thus affect the selectivity.[34] The change of the active metal, reactant, and modifier can all affect the choice of the solvent. Due to the various different roles of the solvent, it is usually very difficult to understand solvent effects completely.

In the hydrogenation of carbonyl compounds over Pt–cinchona catalysts, the highest *ee*s have been obtained using solvents with the dielectric constant between 2 and 10, such as acetic acid and toluene.[34,56,96] In EP hydrogenation, the *ee* decreased linearly with increasing dielectric constant,[97] whereas in the hydrogenation of PPD[98] and ketopantolactone (KPL)[99] an exponential decline in *ee* was observed. Alcohols, such as ethanol and propanol, afford also reasonable high *ee*s, but they can undergo undesired side reactions with the reactant leading to hemiketal formation.[56]

2.1.4 Other issues

Temperature, pressure, additives, and side reactions are further issues that need to be considered in the context of enantioselective hydrogenation over chirally modified, supported metal catalysts. The best enantioselectivities are generally obtained under mild conditions, at or slightly below room temperature and at 1–100 bar.[34,51,56] Additives can act as catalyst poisons, change the chemical structure of the modifier (e.g., by protonating it), or interact with the modifier and/or the products.[34] The mechanism of how an additive acts in favor of enantioselectivity depends on the reactant and modifier structure, the relative rates of the modified and unmodified hydrogenations, as well as the desorption of the product.[34]

In an ideal catalytic cycle for the hydrogenation of ketones over a modified catalyst, the modifier—without transformation—is involved in the next

cycle after formation of the chiral alcohol product.[57] This model, however, does not reflect the real complexity of the system, because the reactant and the modifier are involved in several other reactions, either in solution or on the Pt surface.[57] For example, the saturation of the aromatic ring of the modifier (i.e., the "anchoring moiety") is a side reaction, which leads to partial or complete loss of enantioselectivity.[57] Some other side reactions are Pt-catalyzed decarbonylation and oligomerization, and the amine-catalyzed aldol reaction and cyclization.[51,57] Maybe the most unpleasant consequence of numerous side reactions is that they are the major source of difficulties in the spectroscopic analysis of the reactant–modifier–metal interactions.[51]

Another interesting feature of enantioselective hydrogenations over Pt–cinchona catalysts is the dependence of the *ee* on the conversion of the reactant. It is very characteristic to the structure of the reaction mechanism, and different trends in the development of the *ee* as a function of conversion have been observed depending on the metal and the reaction.[34] In the hydrogenation of PPD, the *ee* increased with increasing conversion of PPD, the initial *ee* values at 10% conversion being ca. 30% less than at 90% conversion.[79] Transient development of the *ee* was also observed in EP hydrogenation where, however, the *ee* rose to a plateau already at 10–20% conversion.[100] The strong increase of the *ee* at high conversion levels ($> 90\%$) of PPD was due to the kinetic resolution, where different hydroxyketones reacted with different rates to corresponding diols.[79]

The production of fine chemicals is usually carried out in batch reactors. Traditionally, continuous operation has been used in gas-phase reactions but it can also be applied in the liquid-phase reactions. Continuous operation has many advantages compared to batch operation, making it a tempting choice for heterogeneous enantioselective hydrogenations.[34] For instance, continuous operation allows higher production capacity and, from the mechanistic point of view, helps to increase the understanding of different phenomena during the reaction. Thus far continuous operation has been used relatively seldom in heterogeneous enantioselective hydrogenations.[34] Examples are the hydrogenation of α-keto esters[80,91,101] and PPD[102] over cinchona-modified Pt.

2.2 Origin of asymmetric induction

As with all catalysis, asymmetric catalysis is a kinetic phenomenon and all asymmetric inductions share the common principle that competing reactions via diastereomeric transition states proceed at different rates.[21] A chiral catalyst is a prerequisite for energetically different diastereomeric transition states and asymmetric induction in transformations of a prochiral reactant (Fig-

ure 2.3a). In the absence of a chiral catalyst, the enantiomeric excess will be zero even under thermodynamic control due to the equal energies of the enantiomeric products. Instead, the origin of diastereoselectivity is based on the chirality of the substrate itself. Energetically different diastereomeric transition states ($\Delta G_1^{\ddagger} \neq \Delta G_2^{\ddagger}$) and products ($\Delta G_1 \neq \Delta G_2$) ensue from a chiral reactant even with an achiral catalyst, and the diastereomeric excess (de) will be nonzero (Figure 2.3b). A chiral catalyst (or other chiral species) may enhance diastereoselectivity.

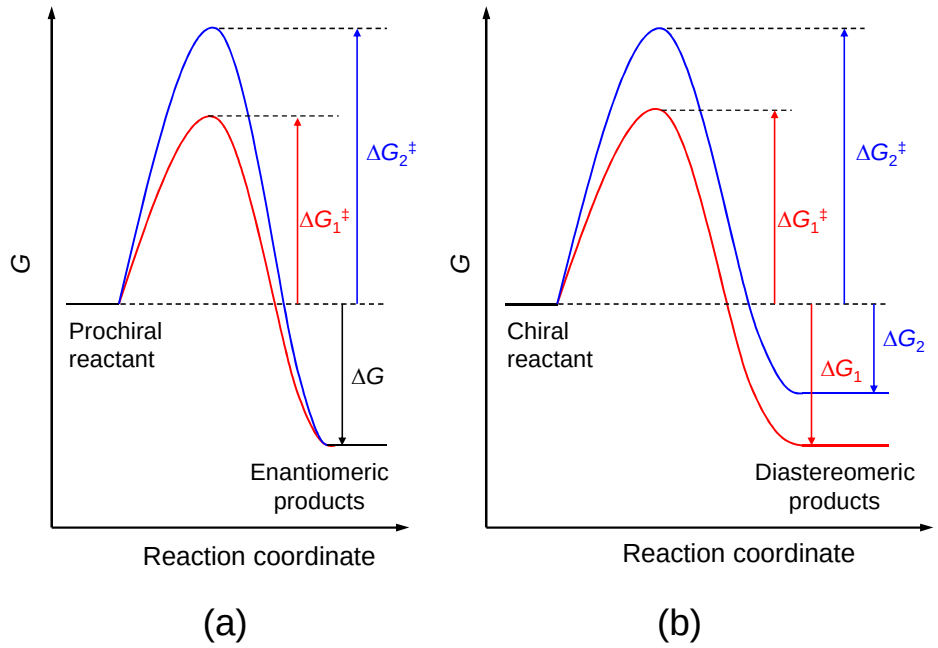

Figure 2.3. Energy profiles for (a) enantioselective and (b) diastereoselective reactions.

Today, most researchers agree that the enantioselective hydrogenation of the C=O double bond catalyzed by heterogeneous Pt–cinchona catalysts proceeds through a mechanism, where the active chiral sites are formed by adsorption of the chiral modifier on the Pt surface. The kinetic results have been compatible with the Langmuir–Hinshelwood formalism, which states that the reactions occur in the adsorbed state.[78,103] As any catalytic reaction, enantioselective hydrogenation is made up of several steps. These steps form a cyclic process called a catalytic cycle. There are three competing catalytic cycles for the hydrogenation of activated ketones on modified Pt.[49,50] Two of them are for the modified active site which yields (R) and (S)

products—preferentially only one product. As it is not possible to modify all catalytically active sites, one cycle is for the unmodified site leading to racemic product mixture. The basic catalytic cycle consists of a fast adsorption of ketone and hydrogen from the fluid or gas phase on an active site, the addition of two hydrogen atoms to the C=O bond and, finally, the fast desorption of the alcohol.[49,50] In the presence of a modified active site, the prochiral ketone adsorbs reversibly on these sites via its two enantiofacial configurations *re* and *si*, forming the diastereomeric intermediate complexes pro-*R* and pro-*S*, respectively, which upon hydrogenation afford the (*R*) and (*S*) products, respectively (Figure 2.4). In the final step, the products are desorbed to regenerate the chiral surface sites. The resulting enantiomeric excess will depend on the ratio of modified to unmodified sites and on the relative turnover frequencies of the cycles.[81]

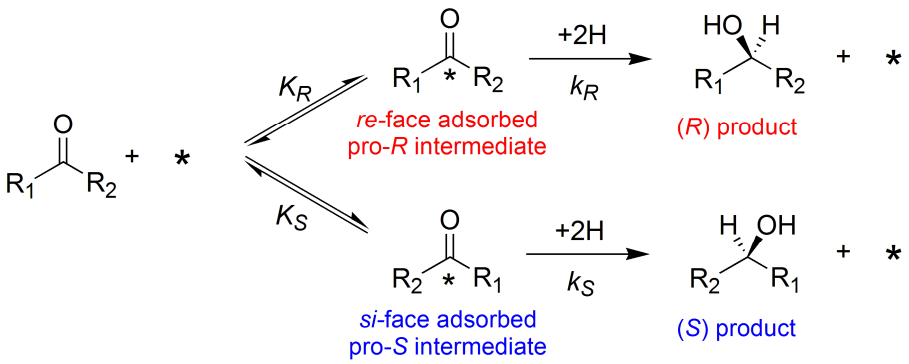

Figure 2.4. The general mechanism of enantioselective hydrogenation of a prochiral ketone on chirally modified metal surface (denoted by ⋆, following ref 55). For simplicity, it is assumed that the reactant contains only one carbonyl group that can be reduced.

Basically, asymmetric induction at chirally modified sites arises from the combination of thermodynamic and kinetic factors (see, e.g., refs 55, 58, 104, and Figure 2.5). In this context, the thermodynamic factor means the (relative) thermodynamic stabilities of the adsorbed diastereomeric reactant–modifier adducts, whereas the kinetic factor means the (relative) intrinsic hydrogenation rates of the reactant in diastereomeric reactant–modifier complexes, that is, the pre-exponential factors and activation energies.

If the adsorption step is the only discriminating factor, that is, there is no kinetic distinction in the hydrogen addition steps ($k_R = k_S$ corresponding to $E_R = E_S$ in Figure 2.5), and adsorption equilibrium is achieved, the relative

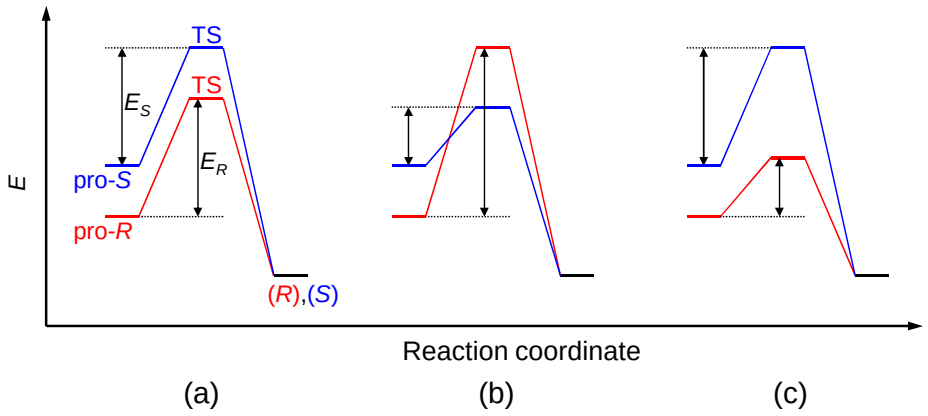

Figure 2.5. Three possible combinations of kinetic factors, described by E_R and E_S, in the process from two diastereomeric complexes to enantiomeric products (following refs 55 and 58): (a) $E_R = E_S$; (b) $E_R > E_S$; (c) $E_R < E_S$. The initial states (left) represent diastereomeric pro-R and pro-S complexes with different energies. The transition states (TS, center) represent the hydrogen addition steps. The final states (right) represent the (R) and (S) products after release from the chiral site.

populations of the intermediates and products will be

$$\frac{[R]}{[S]} = \frac{K_R}{K_S} = \exp\left(\frac{-\delta\Delta G^{\ominus}_{\text{ads}}}{RT}\right) \quad . \tag{2.2.1}$$

In (2.2.1), $\delta\Delta G^{\ominus}_{\text{ads}}$ is the difference between the Gibbs energies of adsorption for the pro-R and pro-S intermediates,[55] R is the gas constant, and T is temperature in kelvins. The energy of adsorption is defined here as

$$\Delta E_{\text{ads}} = E_{\text{intermediate}} - E_{\text{reactant}} - E_{\text{modified site}} \tag{2.2.2}$$

where $E_{\text{intermediate}}$ is the energy of the modified site with the reactant adsorbed, and E_{reactant} and $E_{\text{modified site}}$ are the energies of the isolated reactant and the modified site, respectively. For a reaction where the only difference between the two pathways is the (electronic) adsorption energy ΔE_{ads}, $\delta\Delta G^{\circ}_{\text{ads}}$ may be replaced with $\delta\Delta E_{\text{ads}}$ obtained, for example, from first-principles electronic structure calculations. The enantiomeric excess can then be estimated theoretically as[104]

$$ee = \frac{1 - \exp\left(\frac{-\delta\Delta E_{\text{ads}}}{RT}\right)}{1 + \exp\left(\frac{-\delta\Delta E_{\text{ads}}}{RT}\right)} \quad . \tag{2.2.3}$$

Thus, the *ee* is exponentially related to the difference between the adsorption energies of the pro-R and pro-S intermediates implying that very small adsorption energy differences lead to significant enantiomeric excesses. For example, $ee = 66.7\%$ at 300 K if $\delta\Delta E_{\mathrm{ads}} = 4$ kJ mol^{-1}.

In general, the pro-R and pro-S intermediates may be hydrogenated at different rates ($k_R \neq k_S$) corresponding to Figure 2.5 (b) and (c). If the energy barrier for conversion of the intermediates to corresponding products is the only difference between the two pathways (i.e., $K_R = K_S$ in Figure 2.4) and if the rate constants can be modeled using an activation energy approach, an equation analogous to (2.2.3) can be written with the difference in barrier height $\delta\Delta E^{\ddagger}_{\mathrm{ads}}$ playing the role of $\delta\Delta E_{\mathrm{ads}}$.[104]

In more complicated cases (i.e., $K_R \neq K_S$ together with $k_R \neq k_S$) the theoretical estimation of even the sense of enantioselectivity becomes difficult. In principle, assessing the *ee* is possible from potential energy diagrams, including transition-state energies, for whole reaction paths on chirally modified metal surface. However, determination of these diagrams using first-principles electronic structure calculations is a formidable task and would require huge computational resources, beyond the scope of most computational chemists.[104] Thus far, full potential energy profiles have been determined computationally for systems which are small enough (see, e.g., refs 105 and 106). Instead, molecular modeling of enantioselective hydrogenations over chirally modified metal surfaces has concentrated on the study of modifier conformations and their interactions with various reactants. The effect of the solvent or the catalyst metal surface (with adsorbed hydrogen) has been possible to take into account in calculations only quite recently.

A way to assess the effect of the kinetic factor on stereoselectivity without performing first-principles calculations on transition states was suggested by Vargas et al.[107,108] The hydrogenation rate of substituted acetophenones over Pt was found to correlate with the stability of the reactive keto carbonyl π orbitals of the isolated reactants calculated using the Hartree–Fock theory with the 6-31G* basis set; the sum of bonding π and antibonding π^* orbital stabilization was proposed to be the most general parameter as a measure for the reactivity.[107,108] The orbital stabilization was suggested to result in lowering of the transition state energy, hence decreasing the activation energy and increasing the rate of the hydrogenation reaction. Applied to enantioselective hydrogenation, a stability difference between the keto carbonyl orbitals of the reactant in the pro-R and pro-S complexes would affect enantioselectivity. For example, if the keto carbonyl orbitals of the reactant were more stable in the pro-R than in the pro-S complex, the reactant in the pro-R complex would be hydrogenated faster. In other words, the kinetic factor would favor an excess formation of the (R) enantiomer.

Another challenge to the direct calculation of the *ee* is that extremely small energy differences (close to the error expected in current simulations) along the pathways to two enantiomers can lead to large effects on selectivity.[104] Due to the incompleteness of the computational methods and models used to describe the catalytic system, it will often be possible to achieve "only" a qualitative understanding of the system.[104]

2.3 Mechanistic models for enantioselectivity

The mechanisms of the heterogeneous enantioselective hydrogenations are not completely understood in spite of many efforts.[34] The mechanistic models developed for homogeneous catalysts provide only strongly limited help to understand the functioning of chirally modified metals.[51] Despite the analogies between the chiral homogeneous and heterogeneous catalysts, several phenomena makes the latter ones far more complex and difficult to understand. These phenomena include the complex metal surface structure including edges and corners, the anchoring of the modifier, and the mobility of organic molecules on the metal surfaces.[34,51]

The mechanistic models for Pt–cinchona catalyzed hydrogenations are based on the catalytic experimental results, molecular modeling, and physicochemical measurements regarding interactions in the reactant–modifier–catalyst system.[34] Most mechanistic studies consider the chiral induction in α-keto ester hydrogenation, usually taking the example of ethyl or methyl pyruvate.[57] Due to the rareness of truly in situ spectroscopic measurements at the liquid–solid interfaces that would be in the key role for revealing the real enantiodetermining step, the proposed models are mainly based on the systematic variation of reactant and modifier structure.[57] The adsorption modes of the modifiers and reactants on the metal surface during their interaction is only speculated based on ex situ measurements and theoretical calculations.[51] Hence, remarkably different mechanistic models have been proposed for the most studied reactions, and even the basic elements of the origin of enantioselectivity are debated.[51]

Most scientists agree that direct one-to-one reactant–modifier interactions on the metal surface are responsible for enantioselectivity.[51] However, many variations in the details of molecular interactions exist. Supramolecular chirality has also been suggested to be responsible for enantiodifferentiation in Pt–cinchona systems; the so-called template model by Wells et al. assumed that ordered arrays of cinchonidine on the Pt surface are responsible for enantiodifferentiation in pyruvate hydrogenation.[87,109] Later, the model was revised to emphasize the role of one-to-one reactant–modifier interactions,

because disordered adsorption of cinchona alkaloids and other amine type of modifiers was confirmed.[110]

Baiker's model

Baiker's model for the origin of enantioselectivity is perhaps the most widely discussed today.[52,56,58] It dates back to the early 1990's.[111,112] According to the model, a single modifier molecule anchored to the Pt catalyst surface interacts with an adsorbed reactant molecule through an attractive N−H−O type hydrogen bond. Nowadays, it is assumed that the intermolecular interaction arises through an $N^+-H\cdots O$ bond between protonated quinuclidine nitrogen of the modifier and keto carbonyl oxygen of the reactant (Figure 2.6a). The protonated modifier is always the interacting species, both in protic and aprotic solvents; the Pt−hydrogen system can protonate the basic nitrogen atoms of, for example, CD[113] and pyridine.[114] The CD modifier is bound to the surface via the aromatic quinoline moiety and the basic quinuclidine nitrogen atom points away from the quinoline ring—the modifier adopts an "open" conformation. The keto group of the reactant is assumed to adsorb parallel to the Pt surface during hydrogenation.

It is less clear what is the nature of the second interaction between the reactant and the modifier that ensures the preferential adsorption of the reactant on one enantioface (*re* or *si*) and an excess formation of the product alcohol thereof. A repulsive interaction between the reactant and the anchoring group of the modifier was previously suggested to determine the adsorption mode of the ketone,[57,58] but now the enantiodifferentiating effect has rather been attributed to the directing effect of the electron-withdrawing (and activating) functional group of the ketone that is related to the electronic environment provided by the chiral modifier.[115,116] The position of the activating group determines the direction and extent of enantioselectivity, and the steric bulkiness on any side of the keto carbonyl group and additional electronic effects of substituents play only secondary roles.[115,116]

McBreen's model

Another model that is based on the formation of adsorbed 1:1 reactant–modifier hydrogen-bonded complexes was proposed by McBreen et al.[117–121] In this "generalized two-point H-bonding model", the prochiral complex is formed by two separate H-bonding interactions (Figure 2.6b): (i) the prochiral keto carbonyl forms a $C{=}O\cdots H-C$ bond, at the surface, to the chemisorption activated aromatic anchor of the modifier, and (ii) the ester carbonyl forms a conventional H-bond, above the surface, to the protonated tertiary

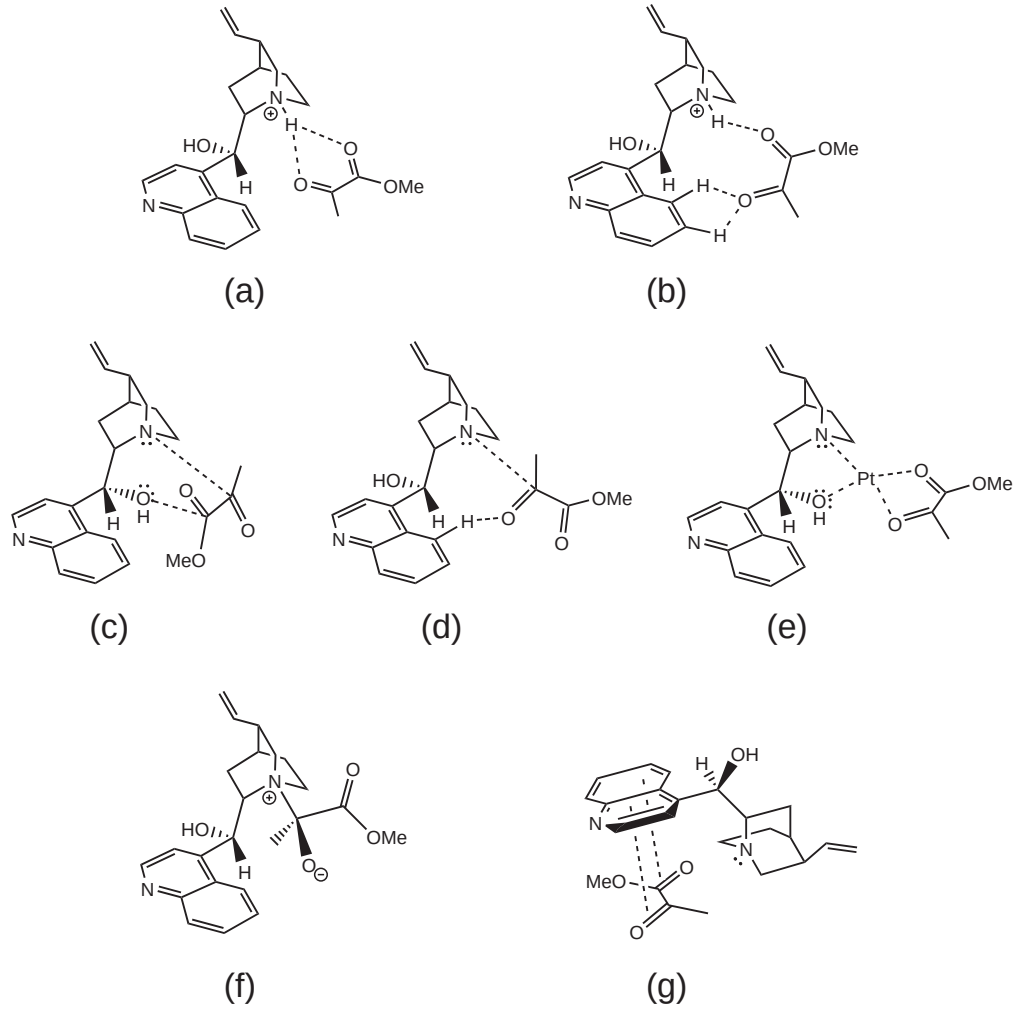

Figure 2.6. Proposed 1:1 reactant–modifier interaction geometries illustrated for methyl pyruvate and cinchonidine: (a) Baiker's model, (b) McBreen's model, (c) Augustine's model, (d)–(e) Bartók's models, (f) Vayner's model, and (g) Margitfalvi's model.

amine function of the modifier. McBreen's model is suggested to be valid for stereoselective hydrogenation of all activated ketones on chirally modified Pt.[117] However, the model has problems with explaining, for example, why the cinchona alkaloids quinidine and quinine are effective modifiers. These modifiers have a methoxy group at the C(6')-position of the anchoring moiety (see Figure 2.2), which would hinder the C−H$\cdots$O=C interaction. In addition, the model does not provide any explanation for the inversion of the

ee, which is observed when the OH group of cinchonidine is replaced by a methoxy group in the hydrogenation of, for example, PPD.[75]

Augustine's model

Besides the models involving an N−H···O=C type hydrogen bond interaction between the (protonated) modifier and the carbonyl oxygen, N···C type interaction based on the nucleophilic attack of the quinuclidine N atom on the electron deficient carbonyl C atom has been suggested. Augustine et al.[122,123] proposed an enantiodifferentiating "bidentate" complex where the lone electron pairs of the quinuclidine N and the oxygen of the C(9)−OH group of cinchonidine interact attractively with the keto carbonyl C and ester carbonyl C atoms, respectively (Figure 2.6c). In the first version of Augustine's model, cinchonidine was adsorbed edge-on onto the Pt surface through the quinoline N atom,[122] whereas later the quinoline portion was considered to be adsorbed parallel to the Pt surface.[123] In both versions, coordinatively unsaturated corner atoms or adatoms on the metal surface were considered as the active sites for hydrogenation.

Augustine's model has several shortcomings. For example, it does not explain enantioselectivity when the quinuclidine nitrogen is protonated—good *ee*s have been obtained in EP hydrogenation with both CD and CD·HCl as the chiral auxiliary.[124] Further, the bidentate interaction leading to the formation of a pseudo-six-membered ring species is sterically hindered on the Pt surface, particularly when MeOCD is used. Still, the experimentally observed *ee* is constant or slightly higher in pyruvate hydrogenation when using MeOCD instead of CD.[125]

Bartók's model

An N→C=O interaction between the quinuclidine skeleton of the modifier and the keto group of the reactant also plays a central role in the models suggested by Bartók et al.[126–129] for reactions in non-acidic solvents like toluene. Furthermore, a hydrogen bond between an aromatic H of the quinoline ring and the C=O group of the substrate was proposed (Figure 2.6d).[126] However, this model has problems similar to McBreen's model. Bartók et al.[128,130,131] also suggested organometallic type surface complexes, where the modifier and the reactant (the "ligands") bound to a surface Pt atom via the lone electron pairs of the N and O atoms as well as the two carbonyl O atoms, respectively (Figure 2.6e).

Vayner's model

On the basis of theoretical calculations, Vayner et al.[132] proposed that the initial step in the mechanism of hydrogenation of activated ketones on cinchona alkaloid modified Pt is nucleophilic addition (N→C=O) of the cinchona alkaloid to the ketone to form a zwitterionic adduct with a covalent N−C bond (Figure 2.6f); this adduct is likely to be stabilized by hydrogen bonding in acidic media. The adduct is adsorbed on Pt, and subsequently undergoes hydrogenolysis with inversion of configuration. The enantioselectivity of the reaction is determined by the relative stabilities of the diastereomeric adducts adsorbed on platinum.[132] The formation of zwitterionic species in acetone solution was supported by NMR studies[63,133] but strong experimental evidence against this mechanistic model was provided later.[134]

Margitfalvi's model

Margitfalvi et al.[135–139] proposed a model that is remarkably different from the others. According to this "shielding effect" model, a 1:1 complex is formed in solution between the reactant and the modifier (Figure 2.6g). Furthermore, the modifier adopts a closed conformation and not an open one as in all the other models. The reactant–modifier interaction takes place via π–π overlapping between the conjugated π-bonds of the α-keto ester and the aromatic ring of the modifier. In the closed conformation of the modifier, the lone pair of electrons of the quinuclidine nitrogen is directed towards the quinoline ring and the modifier can provide a concave, umbrella-like form required for steric shielding. Preferential shielding of one of the prochiral faces of the prochiral reactant and subsequent adsorption of the reactant by its unshielded side onto the Pt surface, followed by hydrogen uptake, results in enantiodifferentiation. Although reactant–modifier interaction in the liquid phase is probable, the shielding effect model contradicts many experimental observations (see, e.g., refs 51 and 57).

2.4 Reactant–modifier–catalyst interactions

As has been stated, the reactant–modifier interactions are the source of asymmetric induction in enantioselective hydrogenations over chirally modified Pt surfaces. Therefore, understanding these interactions is of fundamental importance. Most of the information about the reactant–modifier–catalyst interactions comes from the studies on enantioselective hydrogenation of α-keto esters over cinchona alkaloid modified platinum catalysts. Hydrogenation of

other kind of ketones such as the vicinal diketone PPD has also been under active investigation,[75,76,79,94,98,140–145] but (before this work) these studies have mainly concerned catalyst selection and characterization as well as kinetic aspects. The studies of adsorption of α-keto esters on a metal surface indicated that adsorption is affected by the presence of coadsorbed hydrogen and that lone-pair- and π-bonded α-keto esters possibly coexist on the surface.[119,120,146–151] The π-bonded species adopting the s-*cis* conformation was suggested to be relevant in the enantiodifferentiating 1:1 reactant–modifier complex.[146,148] Spectroscopic and theoretical data support the model assumption that the modifier (e.g., CD) is strongly adsorbed via its quinoline moiety oriented preferentially parallel to the Pt surface.[113,152–163] The quinoline part of the modifier is adsorbed even under hydrogenation conditions.[154,157,161]

1:1 Complexes between MP and (*S*)-(–)-1-(1-naphthyl)ethylamine, a chiral modifier, were observed by scanning tunneling microscopy (STM) on Pt(111) in the presence of coadsorbed hydrogen.[164] In situ attenuated total reflection (ATR) infrared spectroscopy studies during the enantioselective hydrogenation of EP over CD-modified Pt/Al_2O_3 catalyst showed the preferential adsorption of EP as an s-*cis* conformer and indicated a hydrogen bond between the keto-oxygen atom of EP and the quinuclidine nitrogen of coadsorbed CD.[165] A similar $N^+-H\cdots O{=}C$ hydrogen bonding interaction was also observed experimentally between KPL and CD over Pt/Al_2O_3 catalyst.[166]

Hydrogen bonding interactions between methyl/ethyl pyruvate and protonated modifier have also been investigated computationally.[112,167–170] The complexes where the pyruvate adopted the s-*cis* conformer were substantially more stable than the complexes with the s-*trans* conformer.[112,168–170] The steric constraints imposed by the adsorption of the complexes on a metal surface were modeled implicitly using geometry restrictions in the calculations.[168,169] The Pt(111) surface was taken explicitly into account only in some theoretical studies by molecular mechanics[65,132,139] and by DFT.[171,172] Recently, supramolecular docking structures of KPL within the chiral sites formed by CD adsorbed on the Pt(111) surface were explored by DFT.[173]

Chapter 3

Computational methods and models

This chapter summarizes the computational methods and models employed in this work. The methods are discussed in more detail in Appendix C. As the author of this thesis has contributed only to the computational work, the details of the experiments will not be considered here but they can be found in appropriate references [**I**–**IX**].

The catalytic three-phase system composed of hydrogenation of ketones in the presence of a solid catalyst and a dissolved catalyst modifier is intrinsically very complex (see Chapter 2). Modifiers, substrates, hydrogen, and solvent molecules adsorb onto the catalyst surface in competition with each other; if they are able to undergo dissociative adsorption and side reactions, variety of other species may be formed.[55] Oxygen in the air may be introduced in the dissolved state in the solvent to provide sufficient surface coverage of adsorbed oxygen.[55] Furthermore, the surface geometry of supported metal catalyst is intrinsically heterogeneous, containing various types of surface sites with different coordination (terrace, step, edge, kink, vacancy, adatom) and thus different adsorption properties.[51] Typically, the adsorption strength and geometry will change with coverage and coadsorption of other compounds.[51]

Equations derived at the most fundamental level of theory (e.g., relativistic quantum mechanics) to describe various aspects of catalysis in the above-mentioned system—spanning time scales from about 10^{-15} s to even days and length scales from picometers to meters—would be too demanding to be solved with current computational resources and methods (see also Section B.3.3). Therefore, approximations about the composition of the system and physics governing it have to be made in order to make the problems solvable. Reasonable approximations may reduce the complexity of the problem substantially but still provide information that is accurate enough to be

useful about the questions at hand. More discussion about the reliability of the methods and models used in this work can be found in **IV** and **VI**. Approximations which are incorporated into the computational methods and which affect the accuracy of the results are:

- Born–Oppenheimer approximation, that is, separation of nuclear and electronic motions (Section C.1.5)
- using the Schrödinger equation instead of the Dirac equation, that is, complete neglect of relativistic effects except when some of them are taken into account implicitly by using pseudopotentials (Section C.3)
- representing a one-electron wavefunction (orbital) by an expansion in a finite basis set (Section C.3)
- representing a many-electron wavefunction by one Slater determinant [Hartree–Fock (HF) method, Section C.2] or by a finite sum of Slater determinants [truncated configuration interaction (CI), coupled cluster (CC), and Møller–Plesset perturbation theory (MPPT) based methods, Section C.4]
- approximating the Hamiltonian describing the system, for example, approximating the exchange-correlation functional (whose exact form is not known) in density functional theory (DFT, Section C.5)
- neglecting the motion of the nuclei, that is, neglecting the zero-point vibrational energy and the thermal corrections to the energy (Section C.6)
- describing solvation by continuum solvation models (Section C.8)
- using classical mechanics instead of quantum mechanics in molecular mechanics methods (Section C.9)

3.1 Quantum mechanics methods

The quantum mechanics (QM) calculations with localized basis sets were performed with computational methods incorporated in the program packages Gaussian 98,[174,175] Gaussian 03,[176] and TURBOMOLE versions 5.6–5.9.[177–180] The DACAPO code[181,182] was used for DFT calculations with periodic boundary conditions and plane wave basis. The latter computations were performed only in **VII** and not by the author of the thesis.

Methods based on both wave function theory (WFT)[183] and DFT[184,185] were employed to calculate the electronic structure and some properties of molecules and molecular complexes in the gas phase. Of the WFT methods, the HF theory,[183] MPPT with second- and fourth order corrections (MP2 and MP4, respectively),[186–188] as well as the CC method including single and double excitations (CCSD)[189,190] were used. DFT was applied in the form introduced by Kohn and Sham[191] (including its spin-polarized extension[192]), mainly with the B3LYP hybrid exchange-correlation functional[193–196] and the BP86[194,197,198] gradient-corrected exchange-correlation functional. The basis sets used to construct the spin orbitals can be found in **I**–**IX** in connection with appropriate methods.

In addition to the aforementioned methods, the CBS-4M,[199] G2(MP2),[200] and G3(MP2)//B3LYP[201] model chemistries were employed. These compound methods consist of a number of predefined component calculations whose results are combined together in a specified matter with some empirical corrections. The compound methods allow very accurate calculations on molecules that would be too large to be handled with conventional WFT methods suchs as the CC method. More details of the compound methods can be found in Section C.7 and in **III**.

Processes on the metal surface (adsorption, reactions, etc.) were modeled by DFT. Calculations with localized basis sets were performed mainly using the BP86 functional in combination with the RI-J and MARI-J approximations (MARI-J stands for Multipole-Accelerated-Resolution-of-Identity-J).[202–205] Relativistic effects were taken into account implicitly using the relativistic effective core potential (ECP) from the TURBOMOLE library (called "def-ecp") to represent the 60 core electrons of Pt.[206] The 18 valence electrons of platinum and all electrons of the other elements were treated explicitly using mainly the SV(P) and SVP basis sets ("def-SV(P)" and "def-SVP").[207] SVP and SV(P) are double zeta valence basis sets including polarization functions for all elements and for all non-hydrogen elements, respectively.

DFT calculations with periodic boundary conditions utilized the PW91,[208] PBE,[209] and RPBE[210] gradient-corrected functionals. The core electrons of all atoms were treated with Vanderbilt ultrasoft pseudopotentials,[211] whereas the valence electrons were modeled by plane wave basis [**VII**].

Transition states for hydrogenation reactions and hydrogen diffusion on the Pt surface [**IX**] as well as energy barriers for conversion between various conformers of reactants [**IV**] and modifiers [**VIII**] were searched using constrained optimization. In this procedure, the reaction coordinate (e.g., interatomic distance, torsion angle) is fixed while all other degrees of freedom are optimized. The transition state is characterized by the configuration with the highest energy along the reaction coordinate.

3.2 Molecular mechanics methods

The molecular mechanics (MM) calculations (also called force field calculations) were performed with the Forcite molecular mechanics module in Materials Studio versions 3.2, 4.1, and 4.2 (Accelrys Software Inc.). The COMPASS (Condensed-phase Optimized Molecular Potentials for Atomistic Simulation Studies) force field[212] was employed with the atomic charges determined using the QEq charge equilibration method[213] as implemented in Materials Studio.

3.3 Models for catalyst surface

3.3.1 DFT calculations

Typically, the catalyst surface is represented by cluster or slab models.[214,215] Cluster models use a small number of atoms to represent the catalyst and often capture only the local environment around the catalytically active site.[215] By contrast, in the slab models the catalyst is represented by an infinite slab with a periodic structure along the surface. Both approaches have benefits and drawbacks discussed, for example, in ref 215. When considering adsorption of molecules on metal surfaces, the predicted structures of the adsorbates and relative energies of various adsorption modes do not usually depend on the approach.[216–218] However, it should be noted that active metal catalysts are often composed of highly dispersed metal particles on support materials, with the metal particle diameter as low as 1–2 nm. These nanoparticles have often properties which differ substantially from those of the bulk metal. Thus, cluster models should be the correct choice since clusters best mimic the experimental system.[215]

In this work, the Pt(111) catalyst surface was represented by clusters [**V**–**VII**,**IX**] and periodic slabs [**VII**]. Clusters consisted of two or three layers and 19−64 Pt atoms. These clusters were large enough to accommodate various molecules (reactants and modifiers) but small enough to make computations feasible. To account for surface relaxations effects, the coordinates of the central atoms (i.e., atoms not on cluster edges) on the top layer of the clusters were allowed to fully optimize. All other atoms were fixed at the crystal bulk structure with the Pt−Pt distance of 277.5 pm. Totally fixed clusters were also employed to study, for example, the effect of surface relaxation on adsorption. In periodic slab calculations, the catalyst surface was modeled by two or three atomic layer thick slabs and a (3×3) unit cell. All the atoms except atoms at the bottom Pt layer were relaxed.

3.3.2 MM calculations

As the COMPASS force field cannot be used to model chemisorption and, consequently, exact structures of the adsorbed molecules, the role of the metal surface in the MM calculations was mainly to act as a steric constraint to the formation of reactant–modifier complexes. The flat Pt(111) surface was represented by three atomic layer thick slabs of finite dimensions. During the calculations, all Pt−Pt distances were kept fixed to the experimental value of 277.5 pm of bulk Pt. The atomic charges of all Pt atoms were set to zero.

3.4 Models for solvent

The quantum mechanical treatment of solvation effects was carried out either implicitly with Conductor-like Screening Model (COSMO) [219] as implemented in TURBOMOLE or explicitly by representing the solvent by individual solvent molecules (in **II**). COSMO is a continuum solvation model, where the solute molecule forms a cavity within the dielectric continuum of permittivity ε that represents the solvent. The charge distribution of the solute polarizes the dielectric medium and the response of the medium is described by the generation of screening charges on the cavity surface.

Chapter 4

Results and discussion

The main results of the thesis are summarized and discussed in this chapter. Sections 4.1 and 4.2 deal with the effects of the structure of reactants and modifiers on stereoselectivity, whereas the role of the solvent in stereodifferentiation is considered in Section 4.3. The origin of regioselectivity, which may arise in hydrogenation of reactants that contain several reacting carbonyl groups (e.g., PPD), is discussed in Section 4.4. In Section 4.5, effects of the size of catalyst metal particles on the adsorption (and reaction selectivity) of organic molecules are considered. Finally, reaction mechanisms and the origins of asymmetric induction in diastereoselective hydrogenation of chiral ketones over unmodified Pt catalyst are discussed in Section 4.6.

4.1 Effect of reactant on stereoselectivity

To study the effect of reactant structure on the stereodifferentiating one-to-one reactant–modifier interactions, CD was used as the modifier. MeOCD was also applied and the results with this modifier will be discussed in the next section. CD is a complex molecule and has many conformers of which the so-called Open(3) conformer has been shown to be the most stable in the gas phase and in solution.[66,73,99,132,143,220] Open(3) has also been proposed to be the actor species in enantiodifferentiation. Therefore, interactions between the Open(3) conformer of CD and various reactants were studied first. Later, other conformers were considered as well (Section 4.2).

Whatever the conformer of the modifier, it was supposed to be protonated at the quinuclidine nitrogen following the Baiker's model (see Section 2.3). The proton affinity (PA) of CD was indeed calculated to be quite high, around 1000 kJ mol^{-1} [**I**], which is in line with the model. The reactant–modifier

interaction involved at least one hydrogen bond between the carbonyl oxygen of the reactant and the NH^+ moiety of the modifier (C=O$\cdots$H−N^+). Two different interaction modes were found to be stable between PPD and CDH^+ in the gas phase: (i) bifurcated, where a bifurcated hydrogen bond existed between the carbonyl oxygens of the reactant and the NH^+ proton of the modifier (Figure 4.1) and (ii) cyclic, where one of the carbonyl oxygens of the reactant interacted with NH^+ of the modifier and the other one interacted with the hydroxyl group of the modifier (Figure 4.2).

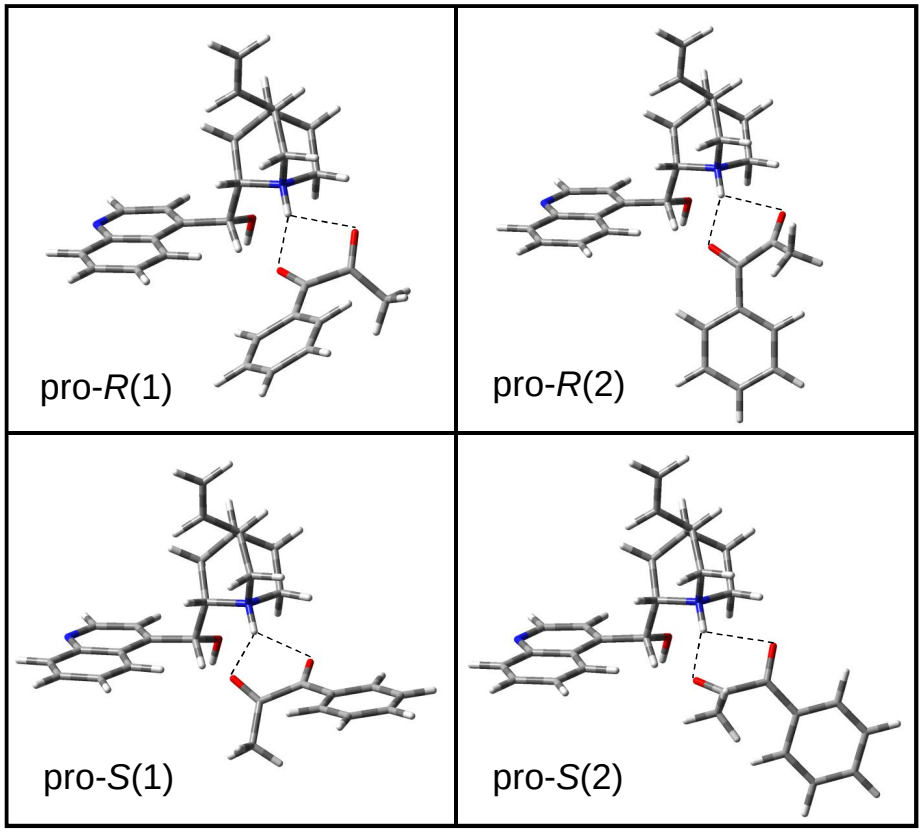

Figure 4.1. Bifurcated PPD−CDH^+ complexes optimized at the HF/6-31G* level of theory [**I**].

In the most stable PPD−CDH^+ complexes, PPD adopted an s-*cis* type of conformation with the torsion angle D(O=C−C=O) varying between −90° and +90° [**I**]. The complexes with an s-*trans*-like conformation of PPD were less stable by over 15 kJ mol^{-1} or not stable at all [**I**]. Instead, isolated PPD adopted an s-*trans*-like conformation (Figure 4.3).

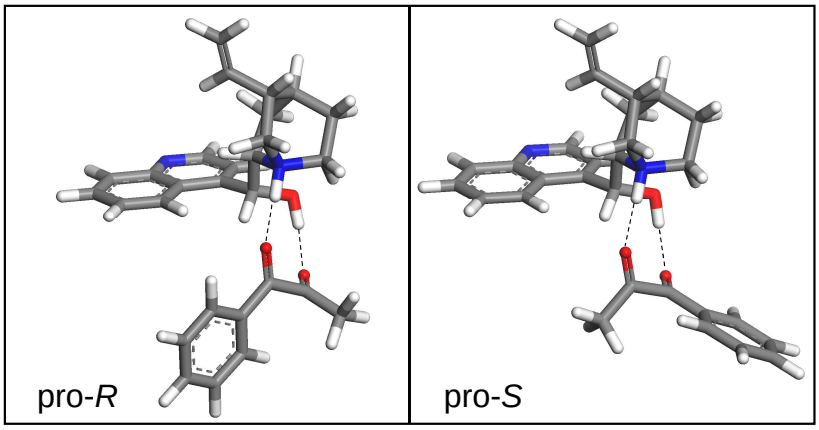

Figure 4.2. Cyclic PPD−CDH^+ complexes optimized at the B3LYP/-T(ON)DZP level of theory [**VI**].

In addition to the thermodynamic stabilities of the reactant–modifier complexes, energies of the keto carbonyl bonding π and antibonding π^* orbitals of the reactant were also of interest. As discussed in Section 2.2, stabilities of these orbitals reflect the kinetic factor, that is, the reactivity of the reactant towards hydrogenation. Appearances of these orbitals for isolated PPD are shown in Figure 4.4.

Investigation of the interactions between PPD and CDH^+ in the gas phase at the HF/6-31G* level revealed that the diastereomeric complexes were almost of equal thermodynamic stability [**I**]; the complexation energies differed at most by 2 kJ mol^{-1}. Some of the complexes could be excluded from being actor species in enantiodifferentiation on geometrical grounds—the C=O group next to the phenyl group did not have access to the Pt surface (and reactive hydrogen) in some complexes. In fact, only the pro-$R(1)$ and pro-$S(1)$ complexes (Figure 4.1) fulfilled the geometrical criteria. The pro-$R(1)$ complex was only slightly ($\sim$1 kJ mol^{-1}) more stable than the pro-$S(1)$ complex but the sum of the keto carbonyl π orbital energies was lower in the pro-$R(1)$ than in the pro-$S(1)$ complex by 13 kJ mol^{-1} [**I**]. Therefore, the experimentally observed *ee* of 65% of (R)-PAC was proposed to be mainly due to the kinetic factor [**I**]. The results thus suggested that the sense of enantioselectivity could be assessed by studying reactant–modifier interactions in the gas phase provided that both the thermodynamic and kinetic factors together with geometrical constraints were taken into account and the modifier adopted the Open(3) conformation.

The computational model that gave a reasonable explanation for the ex-

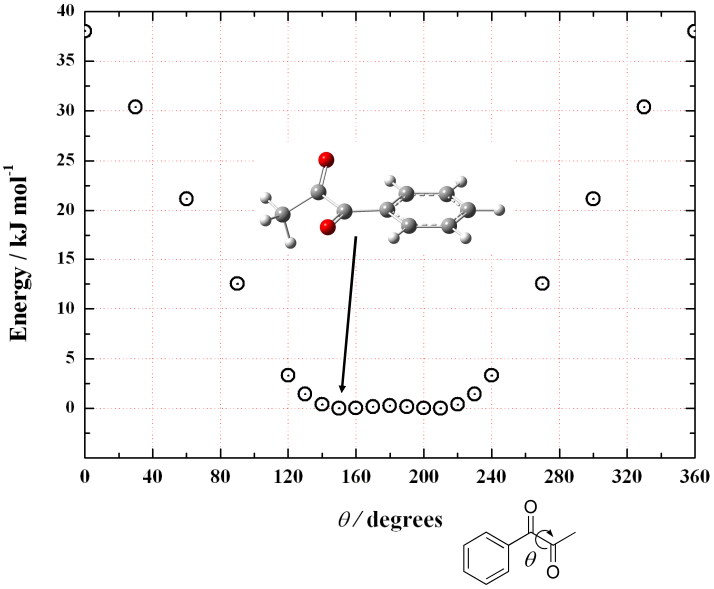

Figure 4.3. The total electronic energy of PPD as a function of the O=C−C=O torsional angle (θ), calculated at the B3LYP/6-31G* level.[221]

perimentally observed enantioselectivity in PPD hydrogenation did not work as well for α-keto esters [**II**]. The pro-R and pro-S complexes between MP and CDH^+ adopting the Open(3) conformation were of equal energy, and the keto carbonyl π orbitals of MP were only 2 kJ mol^{-1} more stable in the pro-R complex. These results suggested a slight excess formation of the (R)-methyl lactate but, on the contrary, quite high *ee* of 74% was observed experimentally in toluene.[65] Taking electron correlation into account at the MP2/6-31G*//HF/6-31G* level did not have any significant effect on the energetics and neither did the enlargement of the basis set from 6-31G* to 6-31G** [**II**]. In the case of KPL–CDH^+ complexes, both thermodynamic and kinetic factors suggested an excess formation of (S)-pantolactone upon hydrogenation [**II**], thus contradicting the experimental observation of an excess formation of (R)-pantolactone (Figure 2.1). The theoretical results thus suggested that the diastereomeric, bifurcated complexes between the above-mentioned α-keto esters and CD adopting the Open(3) conformation were not controlling enantiodifferentiation. Alternatively, the computational model that omitted the platinum surface among others was too simple for evaluating the experimental *ee*.

Subsequently, effects of a flat Pt(111) surface on the reactant–modifier interactions were addressed using MP, PPD, and the α-hydroxyketone deriva-

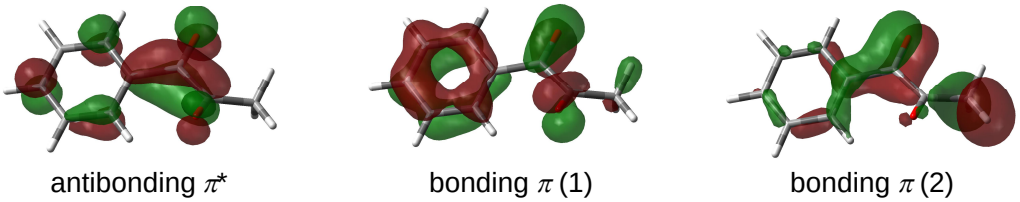

Figure 4.4. One antibonding and two bonding keto carbonyl π orbitals of 1-phenyl-1,2-propanedione [**I**].

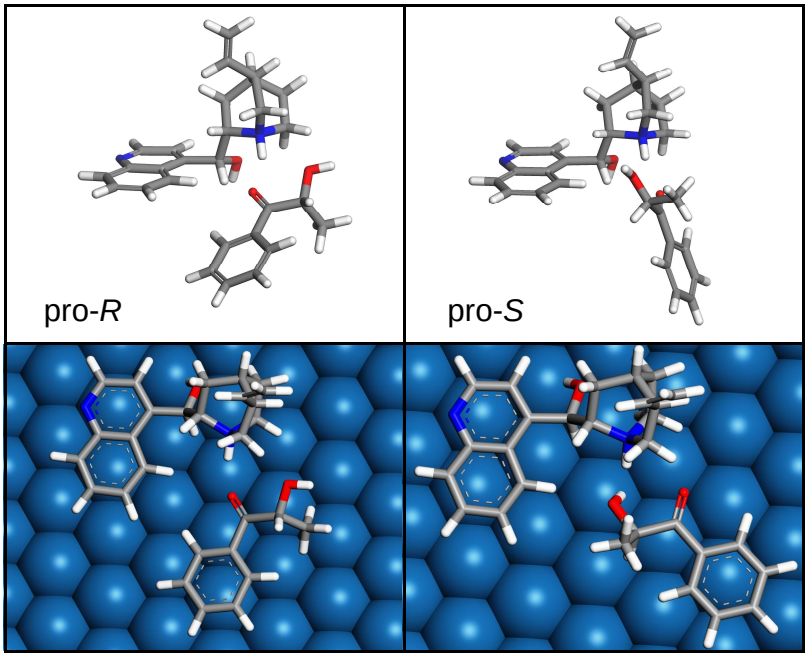

Figure 4.5. Optimized geometries of the bifurcated complexes between 2-hydroxy-1-phenyl-1-propanone and CDH^+ in the gas phase (above, by DFT) and on the Pt(111) surface (below, by MM) [**IV**].

tives of PPD as reactants and CDH^+(Open3) as the modifier [**IV**,**VI**]. The cyclic hydrogen-bonded complexes were stable in the absence of the Pt surface and of almost equal energy as the corresponding bifurcated complexes, evaluated using DFT with the B3LYP hybrid functional and the TZVP and T(ON)DZP basis sets [**IV**,**VI**]. However, according to the molecular mechanics (MM) calculations with the COMPASS force field, neither PPD nor MP

was able to form cyclic complexes with CDH^+ on the Pt surface as opposed to the situation in the gas phase [**VI**]. Further, most of the cyclic complexes between α-hydroxyketones and CDH^+ were not stable on the Pt(111) surface as opposed to the bifurcated ones (Figure 4.5). As the feasible cyclic complexes were less stable than the bifurcated complexes, the relevance of the cyclic complexes to stereodifferentiation was considered negligible [**IV**]. The geometries of the bifurcated complexes were actually often closer to single hydrogen-bonded than bifurcated [**IV**,**VI**]. In any case, the reactants adopted an s-*cis* conformation in the complexes even on the Pt(111) surface. Only 1-hydroxy-1-phenyl-2-propanones adopted conformations closer to s-*trans* than s-*cis* due to the sp^3-hybridized carbon atom next to the phenyl ring [**IV**]. Instead, the s-*cis* conformers were the most stable of all isolated α-hydroxyketones due to the intramolecular O−H$\cdots$O=C hydrogen bonds [**IV**].

In the case of PPD and MP, the bifurcated pro-R complexes were thermodynamically more stable than the corresponding pro-S complexes by 1 kJ mol^{-1} and the keto carbonyl π orbital stabilization was more pronounced in the pro-R complexes by 32–52 kJ mol^{-1} [**VI**]. These DFT results are in line with the experimental enantioselectivities (at least qualitatively), whether the selectivity is controlled by the thermodynamic or kinetic factor. Combination of the results of the DFT and MM calculations led also to a reasonable explanation for the experimentally observed enantio- and diastereoselectivities in α-hydroxyketone hydrogenation [**IV**].

4.2 Effect of modifier on stereoselectivity

As exemplified in Figure 2.2, modifier structure has a crucial effect on stereoselectivity. For example, substitution of CD by its near-enantiomer CN in PPD hydrogenation was followed by a change of the major product from (*R*)-PAC to (*S*)-PAC. This experimental observation is in line with the theoretical result of kinetic preference for the formation of the (*S*) product [**I**]. The relation between the stereoselectivity of the reaction and the configuration of the modifier is quite reasonable. Instead, it is more difficult to explain the dependence of stereoselectivity on the substituent at the C(9)-*O*- position of the modifier. For example, under optimal conditions the main product in PPD hydrogenation, (*R*)-PAC, could be obtained in 65% *ee* using CD as the chiral catalyst modifier [**I**]. When *O*-methyl, *O*-phenyl, and *O*-silyl ether derivatives of CD were used, a loss ($ee = 0\%$) or inversion of enantioselectivity resulted with 10–28% *ee* of (*S*)-PAC produced (Table 1 in **VIII**). The same trend was observed with CN and its derivatives as chiral modifiers. With

CN the main product (*S*)-PAC was obtained in 19% *ee* but when *O*-methyl, *O*-phenyl, and *O*-silyl ether derivatives of CN were used, an inversion of enantioselectivity resulted with (*R*)-PAC being produced in 28–33% *ee* (Table 1 in **VIII**).

4.2.1 Modifier conformations

Cinchona alkaloids and their derivatives can adopt many stable conformations (Figure 4.6), which complicates finding the species relevant to stereodifferentiation. The conformers of CD, CN and their derivatives can be distinguished by the relative orientation of the quinoline and quinuclidine moieties and, especially, by the direction where the quinuclidine nitrogen points at. In the closed conformers the quinuclidine nitrogen points towards the quinoline moiety, whereas in the open conformers the nitrogen points away from the quinoline moiety.

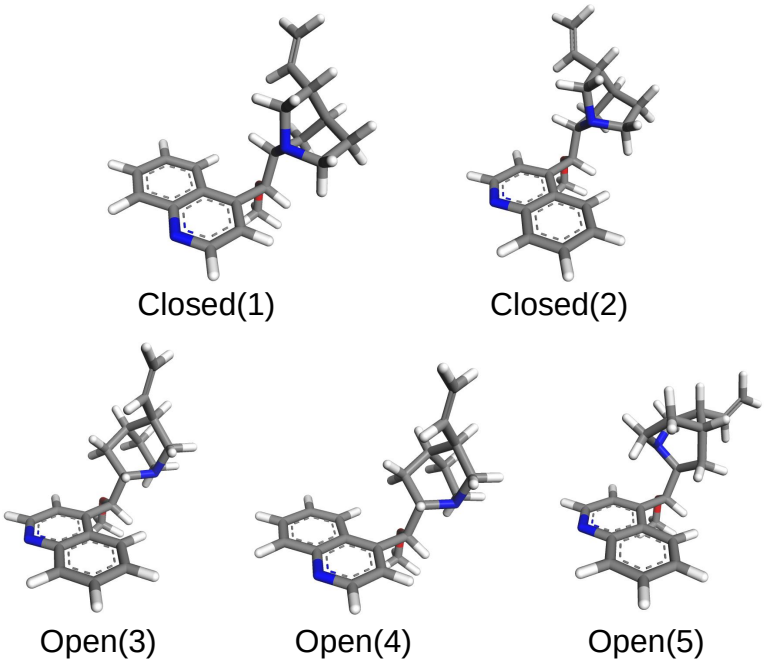

Figure 4.6. Some stable conformations of MeOCD optimized at the B3LYP/T(ON)DZP level of theory [**VIII**].

Theoretical and experimental studies of various *O*-ether derivatives of CD and CN showed that the equilibrium populations of the modifiers in the gas (and liquid) phase did not directly correlate with the enantioselectivity

observed in the hydrogenation of PPD over modified Pt catalyst [**VIII**]. For example, on the basis of computational electronic energies, Open(3) was the most stable and thus the most populated conformer of MeOCD, *O*-methylcinchonine (MeOCN), *O*-(*tert*-butyldimethylsilyl)cinchonidine (TBDMSOCD), and *O*-(propyldimethylsilyl)-10,11-dihydrocinchonidine (PDMSODHCD, Tables 3 and 4 in **VIII**). The Closed(1) and Closed(2) conformers were the next most populated, whereas the populations of the Open(4) and Open(5) conformers were negligible. Computational Gibbs energies at 25°C and 1 bar gave rather similar results for the relative stabilities of the conformers of MeOCD and MeOCN as the electronic energies. However, the most stable conformer of TBDMSOCD in the gas phase was Closed(2) followed by Open(3) and Closed(1) according to the Gibbs energies. The notable differences between the relative Gibbs and electronic energies in the case of TBDMSOCD were attributed to errors in the computational entropy term, caused by poor description of low-frequency vibrations within the harmonic oscillator approximation [**VIII**].

The conformational analysis of the modifiers implied that specific interactions between the modifier and the catalyst surface play a crucial role in creating sites that are able to chiral recognition in stereoselective hydrogenation reactions [**VIII**]. The possible protonation of the basic nitrogen atoms on the catalyst surface[113,114] and its effect on conformational equilibria should also be borne in mind. Specifically, it should be noted that on the metal surface cinchona alkaloids may adopt conformations that are not stable in the gas or liquid phase. If these conformers are able to stereospecific interactions with reactant molecules, their role in stereodifferentiation should be considered.

Computational studies showed indeed that some conformations of CD and MeOCD were stable only on the Pt surface [**VI**]. These conformations were adsorbed on the surface via the quinuclidine moiety in addition to the quinoline ring and were called, accordingly, Quinuclidine Adsorbed-Open(3) and -Open(4) [QA-Open(3) and QA-Open(4)]. In principle, they could be generated from the adsorbed Open(3) and Open(4) conformations, respectively, by rotating around the C(4')−C(9) bond (Figure 2.2). The vinyl moiety [the C(10)=C(11) double bond] of the qa-open conformations lay close and almost parallel to the surface, which provided a reasonable explanation for its fast hydrogenation to the ethyl moiety observed experimentally under catalytic conditions.[70,152,154]

According to the MM calculations, the qa-open conformers were more stable on the flat Pt(111) surface than any of the gas-phase conformers [**VI**]. Similar conformations were found to be stable on Pt(111) by molecular dynamics[159] and by DFT calculations.[162,163,173] However, Vargas and

Baiker[162,163] considered these conformations as transient species converting to some other conformation after the detachment of the quinuclidine moiety due to the hydrogenation of the vinyl group to ethyl. Instead, our DFT calculations showed that the quinuclidine moiety may stay adsorbed even if the vinyl group is hydrogenated (Figure 2 in **VI**). Moreover, as the quinuclidine N was protonated (which takes place under hydrogenation conditions[165,166]), the QA-Open(4) conformations of CD and MeOCD were more stable than the Open(3) conformations on the Pt(111) surface (Figure 2 in **VI**). In addition to the high stability of the qa-open conformations on Pt(111), their geometries were such that they were able to form hydrogen-bonded complexes with adsorbed reactants [**VI**]. These facts suggested that the qa-open conformations might have some role in stereoselective hydrogenation over modified Pt catalyst.

Table 4.1. Adsorption energies (kJ mol^{-1}) for various conformations of CD, CDH$^+$, and their *O*-methyl ether derivatives MeOCD and MeOCDH$^+$ adsorbed on a Pt_{38} cluster with two layers and the (111) surface, calculated at the BP86/SV(P)–MARI-*J* level.[222,a]

Conformation	CD	CDH$^+$	MeOCD	MeOCDH$^+$
Closed(1)	−198[b]	−153	−167	−115
Closed(2)	−200[b,c]	−151	−167	−119
Open(3)	−193[b,c]	−169	−159	−112
Open(4)	−183[b]	−161	−152	−111
Open(5)	−160[b,c]	−167	−137	−117
QA-Open(4)	−166	−189	−163	−180

[a] Adsorption energies were calculated with respect to the Open(3) conformer as in **VI**. The nine central atoms of the top Pt layer were allowed to fully optimize whereas all other Pt atoms were fixed at the crystal bulk structure with the Pt−Pt distance of 277.5 pm. All calculations were done spin unrestricted with the total spin state of $S = 3$. The following convergence criteria were used unless otherwise stated: 10^{-5} hartree for the SCF energy and the total energy; maximum norm of Cartesian gradient up to 10^{-3} atomic units (bohr) for structure optimization.
[b] 10^{-6} hartree for the SCF energy. [c] Total energy up to 10^{-6} hartree.

Subsequent, more extensive DFT studies on the adsorption of some cinchona alkaloids (Table 4.1, see also Figure 4.7) demonstrated that Closed(1) and Closed(2) were actually the most stable conformers of CD on the Pt(111) surface, Open(3) being less stable by about 5 kJ mol^{-1}.[222] This is in contrast to the situation in the gas and liquid phase, where Open(3) is the most populated conformer at room temperature.[99] Open(4), QA-Open(4) and Open(5)

were the least stable conformations of CD on Pt(111). The stability order for the open and closed conformations on the Pt(111) surface is in line with previous findings.[162,163] The absolute values of the adsorption energies may vary between different studies due to the computational details, the details of the Pt clusters (partly relaxed or totally frozen), and the adsorption site (edge or center of the cluster).

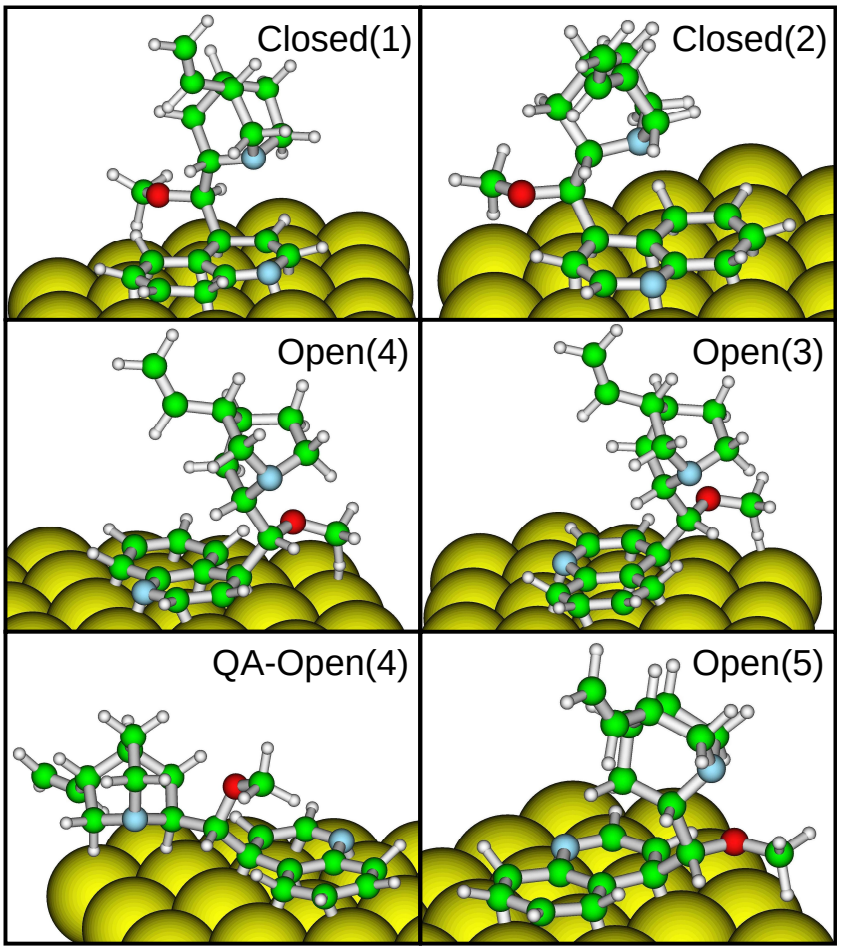

Figure 4.7. Optimized structures of some conformers of MeOCD on the Pt(111) surface. For computational details and relative stabilities of the conformers, see Table 4.1.

Adsorption energies of the closed and open conformers of MeOCD varied between −137 and −167 kJ mol^{-1}, being 23–35 kJ mol^{-1} less negative than for CD (less negative adsorption energy means weaker adsorption). However, the stability order was qualitatively and almost even quantitatively the

same as for CD: Closed(1) ≈ Closed(2) > Open(3) > Open(4) > Open(5). These results are in reasonable agreement with the results of Vargas and Baiker.[223] However, contrary to the results for CD, the QA-Open(4) conformer of MeOCD was 4 kJ mol^{-1} more stable than Open(3), being just 4 kJ mol^{-1} less stable than the closed conformers. A so-called tilted adsorption mode of the Open(3) conformation of MeOCD was also optimized on Pt(111). In the tilted adsorption modes of cinchona alkaloids the quinoline ring lies tilted rather than parallel to the metal surface, with only one edge of the ring chemisorbed to the surface.[154,224] The tilted mode of Open(3) was less stable than the parallel adsorption mode by 52 kJ mol^{-1}. In spite of this, tilted adsorption modes may become relevant in reactions where high modifier concentrations are applied.[225]

Protonation of CD and MeOCD had a large effect on both adsorption energies and relative stabilities of the conformers. The protonated CDH$^+$ and MeOCDH$^+$ conformations adsorbed by about 20–50 kJ mol^{-1} less strongly on the Pt(111) surface than the corresponding unprotonated species with two exceptions. First, the adsorption of CDH$^+$(Open5) was stronger than the adsorption of the unprotonated species by 7 kJ mol^{-1}. Therefore, the Open(3) and Open(5) conformers of CDH$^+$ were approximately equally stable on the Pt(111) surface, as was also observed in the gas phase [**VI**]. The Open(5) conformer of MeOCDH$^+$ was more stable than Open(3) on Pt(111), which was the case even in the gas phase (according to the electronic energies, **VI**). Second, the adsorption of the protonated QA-Open(4) conformation was stronger than the adsorption of the unprotonated species by 17–23 kJ mol^{-1}. Consequently, the QA-Open(4) conformation of CDH$^+$ was more stable than the second most stable conformer Open(3) by 20 kJ mol^{-1}. Interestingly, the closed conformations of CDH$^+$ were less stable than Open(3) by 16–18 kJ mol^{-1}. In other words, the closed conformations were greatly destabilized with respect to the open conformations owing to the protonation. Among the protonated MeOCDH$^+$ conformations, QA-Open(4) was by far the most stable on the surface, the other conformers being less stable by 60–70 kJ mol^{-1}. Open(3) and Open(4) were the least stable conformers of MeOCDH$^+$ on Pt(111).

The above DFT results show that the conformational equilibria of adsorbed CD and MeOCD differ significantly from each other whether the modifiers are protonated or not. On general level, this provides a reasonable explanation for the drastic change and even inversion of enantioselectivity observed, for example, in the hydrogenation of PPD as the modifier is changed from CD to MeOCD.[75,76] However, similar change in the *ee* as a function of modifier structure has not been observed in the hydrogenation of, for example, α-keto esters such as EP, where the *ee* is very similar whether

CD or MeOCD is used.[69–72] Therefore, analyzing modifier conformations on the metal surface is probably not enough to explain observed selectivities. The reactant–modifier interactions have to be studied in detail to understand the origins of stereodifferentiation on modified surfaces as well as the alteration of stereoselectivity as a function of reactant and modifier structure. It should also be noted that the liquid phase populations of the modifier conformations, which depend on whether the modifier is protonated or not, may have an effect on which modifier conformations exist on the surface and to which extent (and which conformation is the active one in stereodifferentiation).[226,227] Specifically, some conformers such as Open(3) and Open(4) adsorbed on the surface cannot interconvert simply via conformational rearrangement around the C(4')−C(9) and C(8)−C(9) bonds as on the contrary can happen in vacuum or in solution (see Figure 2.2). In fact, the interconversion between those conformers requires a desorption–adsorption step of the quinoline moiety:

$$\text{Closed(1)} \overset{\text{rotation}}{\rightleftharpoons} \text{Open(4)} \overset{\text{desorption–adsorption}}{\rightleftharpoons} \text{Open(3)} \overset{\text{rotation}}{\rightleftharpoons} \text{Closed(2)} \ .$$

4.2.2 Reactant–modifier interactions

To better understand the crucial role of the C(9)−OH group of CD for achieving high enantioselectivity in the hydrogenation of PPD,[75,76] one-to-one reactant–modifier interactions were addressed in detail [**VI**]. Interactions of PPD and MP with the protonated modifiers CDH^+ and $MeOCDH^+$ were studied by DFT and MM calculations. The Open(3), Open(5), QA-Open(3), and QA-Open(4) conformations of the modifiers were considered. Instead, the closed conformers were neglected because they cannot serve as an efficient source of stereodifferentiation when adsorbed on the metal. This is due to the orientation of the quinuclidine N towards the anchoring moiety.

Neither the isolated qa-open conformations nor the complexes between them and the reactants were stable according to the DFT calculations; they relaxed to some other structures during the geometry optimization calculations [**VI**]. For example, QA-Open(4) relaxed either to Open(4) or Open(3). Therefore, the stability and other properties of the reactant–modifier(qa-open) complexes could only be investigated in the presence of the surface. However, studying systems consisting of the modifier, the reactant, and the surface with DFT was challenging due to the huge demand of computer resources. In **VI**, results based on MM calculations were reported for such systems. However, computations on the Pt surface at the MM level should be regarded only as indicative. The MM calculations did not take electronic effects into account and did not allow, for instance, charge transfer between

the charged adsorbate and the electrically neutral adsorbent. Chemisorption and, consequently, rehybridization of the atoms of the adsorbates could not be observed, either. Instead, the force fields are able to describe physisorption and steric constraints imposed by the surface. The MM calculations thus gave valuable suggestions about possible molecular and supramolecular structures that could exist on the surface. Later, it was also possible to investigate reactant–modifier interactions on large Pt clusters by DFT computations.[228,229]

The C(9)−OH moiety of CD could obviously play an important role in stereodifferentiation if it was involved directly in the hydrogen bonding interaction between the reactant and the modifier. This interaction would lack if the modifier was MeOCD, which could be the reason for the change of stereoselectivity in the hydrogenation reaction. Of the one-to-one reactant–modifier complexes studied in **VI**, the C(9)−OH moiety of CD took part in the reactant–modifier interaction in the cyclic complexes where CDH^+ adopted either the Open(3) or Open(5) conformation (Figure 3 in **VI**) and in the complexes on Pt(111) where CDH^+ adopted the QA-Open(3) or QA-Open(4) conformation (Figure 5 in **VI**).

The Open(5) conformer of CDH^+ was stated to be unimportant in stereodifferentiation due to the thermodynamic instability and low reactivity of the reactant–CDH^+(Open5) complexes compared to the other complexes (Tables 1 and 3 in **VI**). When CDH^+ adopted the Open(3) conformation, the isolated, cyclic PPD–CDH^+ complexes were approximately as stable as the bifurcated ones (Table 1 in **VI**). Further, the keto carbonyl orbitals of PPD were of similar stability in both cyclic and bifurcated PPD–CDH^+(Open3) complexes. Although the thermodynamic factor did not favor an excess formation of either one of the enantiomeric (*R*)-PAC and (*S*)-PAC hydrogenation products, the keto carbonyl orbitals of PPD were clearly more stable in both cyclic and bifurcated pro-*R* than pro-*S* complexes indicating a faster production of (*R*)-PAC due to the kinetic factor.

The DFT calculations on isolated MP–CDH^+(Open3) complexes showed in turn that the cyclic complexes were less stable than the bifurcated ones by 5–6 kJ mol^{-1} (Table 3 in **VI**). On the other hand, the keto carbonyl orbital stabilization was more pronounced in the cyclic complexes. This would in principle lead to a higher hydrogenation rate of MP in the cyclic than in the bifurcated complexes. However, as the thermodynamic and kinetic factors favored an excess formation of (*R*)-methyl lactate from both bifurcated and cyclic complexes by approximately the same amount, the *ee* did not depend on the detailed geometry of the intermediate complex. As already noted in Section 4.1, the MM calculations implied that the cyclic PPD–CDH^+(Open3) and MP–CDH^+(Open3) complexes could not exist on the Pt(111) surface due

to steric constraints. Thus, the results from the DFT and MM calculations indicated together that the cyclic complexes were not important in the enantioselective Pt-catalyzed hydrogenation of PPD and MP.

Even though the most favored interaction geometry for both the reactant–CDH^+ and reactant–$MeOCDH^+$ complexes was the same (i.e., bifurcated with the Open(3) conformation of the modifier), the thermodynamic and/or kinetic factors that control the enantioselectivity were not of the same magnitude in both cases, probably due to steric or electronic effects. The relative energies of the bifurcated PPD–CDH^+(Open3) and PPD–$MeOCDH^+$-(Open3) complexes calculated by DFT revealed that the thermodynamic factor favored an excess formation of (*R*)-PAC by about the same amount (1–2 kJ mol^{-1}) in the case of both modifiers (Tables 1 and 2 in **VI**). However, the kinetic factor, that is, stabilization of the keto carbonyl orbitals of PPD favored an excess formation of (*R*)-PAC by 52 kJ mol^{-1} in the case of CDH^+ but only by 6 kJ mol^{-1} in the case of $MeOCDH^+$. These results indicated that the substitution of the OH moiety of CD with OMe decreased the enantiomeric excess of (*R*)-PAC considerably. Thus, the calculations were well in line with the experiments.[75,76]

The DFT computed complexation energies and stabilization of the keto carbonyl orbitals of MP in the bifurcated MP–CDH^+(Open3) and MP–$MeOCDH^+$(Open3) complexes indicated that the thermodynamic and kinetic factors favored an excess formation of (*R*)-methyl lactate by the same amount (within 1 kJ mol^{-1}) in the case of both modifiers (Tables 3 and 4 in **VI**). The MM calculations on isolated complexes and complexes on the Pt surface supported these results. As the experimental *ee*s are very similar with CD and MeOCD,[69–72] the computational results were again well in accord with the experimental ones. Summarizing, combination of the results from the DFT and MM calculations led to a reasonable explanation for the observed enantioselectivities in the hydrogenation of PPD and MP over Pt catalyst modified by CD and MeOCD [**VI**].

The above discussion ignored the reactant–modifier complexes where the modifiers adopted qa-open conformations. This is because these complexes were not stable in the gas phase. Therefore, any information regarding their thermodynamic stability or reactivity towards hydrogenation could not be gained from the gas-phase DFT calculations. However, the MM calculations suggested that the reactant–modifier complexes were the most stable on Pt(111) when the modifier adopted either one of the qa-open conformations (Tables 1–4 in **VI**). The adsorbed reactants were also able to interact simultaneously with the protonated quinuclidine nitrogen and the functional group at the C(9) position of the modifier.

These findings prompted us to investigate the role of qa-open conforma-

tions in asymmetric induction in more detail. For this endeavor, reactant–modifier interactions on the flat Pt(111) surface were studied by DFT computations.[228,229] PPD and protonated 10,11-dihydrocinchonidine ($DHCDH^+$) were chosen as the reactant and the modifier, respectively. The optimized structures of the complexes are shown in Figure 4.8 and Figure 4.9. The modifier adopts the QA-Open(4) conformation in Figure 4.8, whereas it adopts the Open(3) conformation in Figure 4.9. The titles of the structures describe the adsorption geometry of PPD: the enantiotopic face of the chemisorbed PPD exposed to the Pt surface (*re* or *si* yielding (*R*)-PAC and (*S*)-PAC upon hydrogenation, respectively) and the conformation of the O=C−C=O moiety of PPD (s-*cis* or s-*trans*). Structures with physisorbed PPD are denoted accordingly.

The adsorption energies of the Open(3) and QA-Open(4) conformers on Pt(111) were −153 and −181 kJ mol^{-1}, respectively. These adsorption energies were about 35 kJ mol^{-1} more negative than found previously (Figure 2 in **VI**), probably due to the different clusters used to model the Pt surface; a frozen Pt_{64} cluster was used here, whereas a relaxed Pt_{38} cluster was employed in **VI**. However, the relative stabilities of the conformations of $DHCDH^+$ were about the same on both clusters—Open(3) was less stable than QA-Open(4) by 26 kJ mol^{-1} on Pt_{38} and by 28 kJ mol^{-1} on Pt_{64}.

Several different positions of PPD relative to $DHCDH^+$ could be realized on Pt(111). On one hand, the relative positions of the reactant and the modifier were intrinsically constrained by the Pt(111) surface geometry but on the other hand, the Pt surface enabled interaction geometries that were not stable in the gas phase. In addition, PPD could be either chemisorbed or physisorbed. The structures where PPD was physisorbed but interacted with the modifier by a bifurcated hydrogen bond (see physisorbed pro-*R* and pro-*S* at the bottom of Figure 4.9) were among the most unstable ones with 70 and 67 kJ mol^{-1} higher energies with respect to the most stable structure, *re*-(s-*cis*) in Figure 4.8. The structures where PPD adopted its most stable adsorption modes (see Section 4.4) but where it was located far from $DHCDH^+$ were of similar (un)stability as the physisorbed structures (see the second lowest row in Figure 4.9). The s-*trans* conformation of PPD resulted in more stable structure than the s-*cis* conformation which is consistent with the results of PPD adsorption presented in Section 4.4.

It is notable that the quinuclidine NH^+ moiety of $DHCDH^+$(Open3) was located too far from the Pt(111) surface in order to form such bifurcated complexes with PPD where at least one of the carbonyl moieties of PPD would have been chemisorbed (and activated towards hydrogenation). A bifurcated hydrogen bond was feasible only when PPD was physisorbed. Cyclic complexes as exemplified in Figure 4.2 were not stable on Pt(111). Instead, a

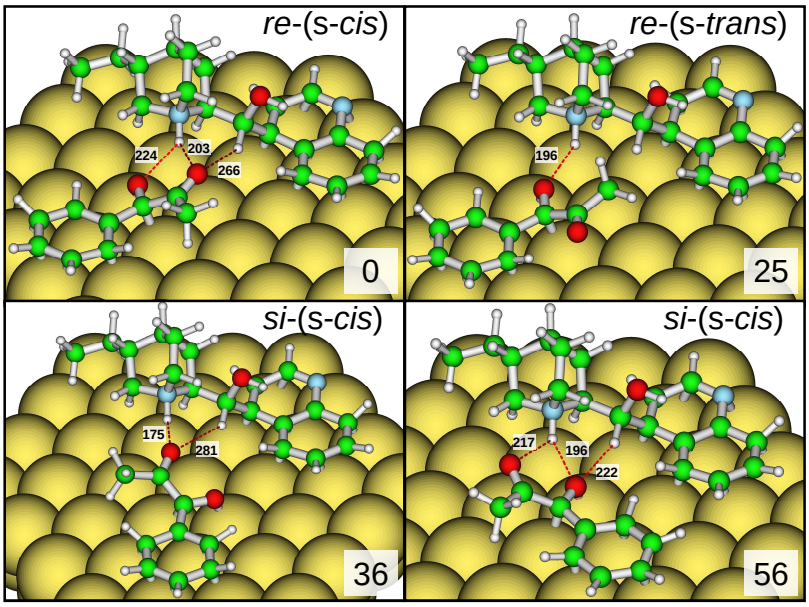

Figure 4.8. BP86/SV(P)–MARI-J optimized structures of PPD and $DHCDH^+$(QA-Open4) on the Pt(111) surface. The titles of the structures describe the adsorption mode of PPD. The surface was modeled with a frozen Pt_{64} cluster with two atomic layers and total spin state of $S = 5$. The following convergence criteria were used: 10^{-6} hartree for the SCF energy and 10^{-5} hartree for the total energy; maximum norm of Cartesian gradient up to 10^{-3} atomic units (bohr) for structure optimization. Energies (kJ mol^{-1}) of the systems, shown at the down right corner of each structure, are with respect to the energy of the most stable system where PPD adopts the *re*-(s-*cis*) adsorption mode. Some intermolecular distances (pm) are also given.

structure congruent with McBreen's model was identified (upper left corner in Figure 4.9). In this structure, denoted as *re*-(s-*cis*), the C1=O1 group of PPD (i.e., the C=O group next to the phenyl ring) was chemisorbed and close to an aromatic C−H hydrogen of the quinoline moiety, whereas the C2=O2 group formed a hydrogen bond to the quinuclidine NH^+ above the surface. The C2=O2 moiety was also close to another aromatic C−H. This structure was actually the most stable one found between PPD and $DHCDH^+$ adopting the Open(3) conformation. The corresponding *si*-face adsorption mode *si*-(s-*cis*) (upper right corner in Figure 4.9) was less stable by 17 kJ mol^{-1}, presumably due to the lack of stabilizing interaction between the C1=O1 moiety of PPD and the modifier present in *re*-(s-*cis*).

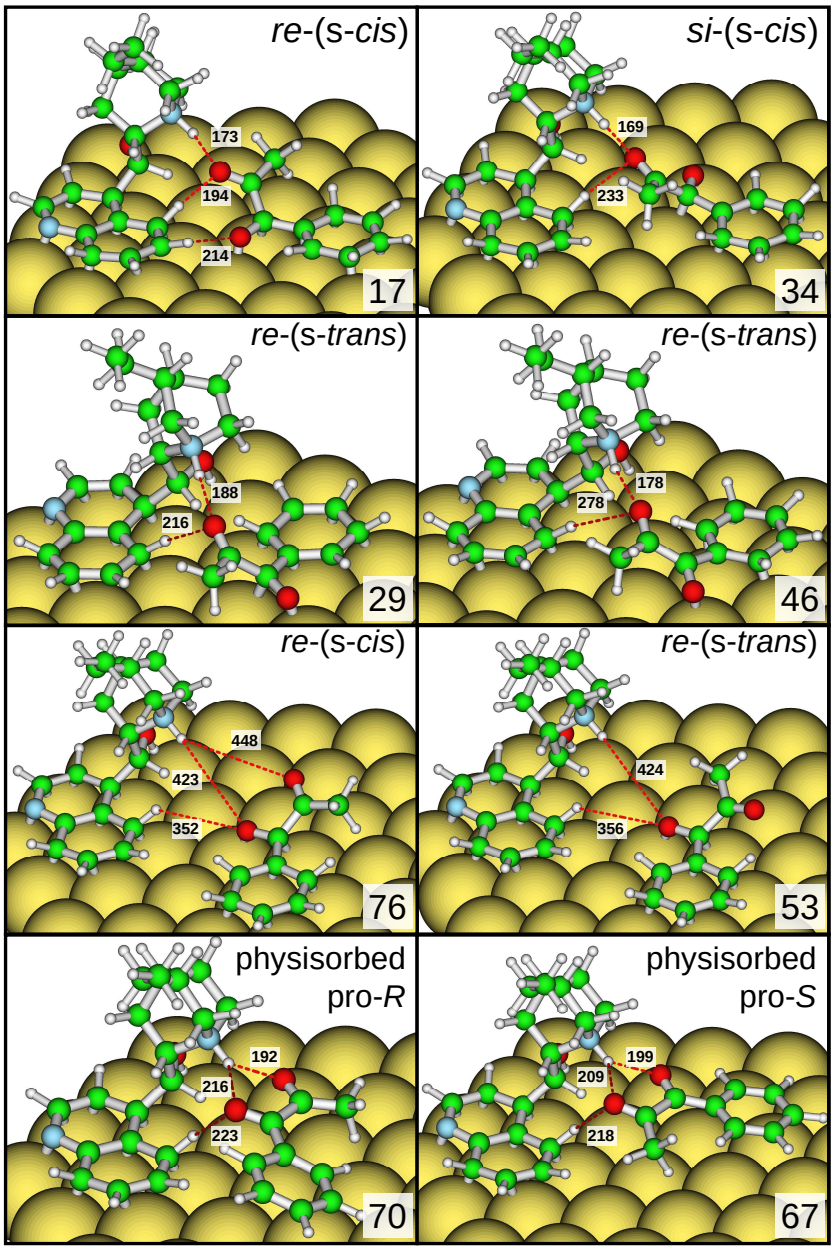

Figure 4.9. DFT optimized structures of PPD and $DHCDH^+$(Open3) on the Pt(111) surface. For computational details, see Figure 4.8. Energies (kJ mol^{-1}) of the systems, shown at the down right corner, are with respect to the energy of the most stable system (see Figure 4.8). Some intermolecular distances (pm) are also given.

The above-mentioned "McBreen-like" *re*-(s-*cis*) structure was also more stable than any of the s-*trans* structures where only one carbonyl oxygen interacted with the modifier by hydrogen bonds (see the second uppermost row in Figure 4.9). Interestingly, the chemisorbed s-*trans* conformation of PPD was more stable than the s-*cis* conformation on unmodified Pt(111) (see Section 4.4), but the stabilization gained from an extra hydrogen bond between *re*-(s-*cis*) adsorbed PPD and the modifier was enough to overcome the higher stability of the s-*trans* conformation. While the relative energies of the structures in Figure 4.8 and Figure 4.9 have been discussed so far on the basis of the number of attractive, stabilizing hydrogen bonds, those energies are also affected by the detailed adsorption mode of PPD as well as possible destabilizing (e.g., steric) interactions between the reactant and the modifier.

In the two most stable DFT optimized structures between PPD and $DHCDH^+$(Open3), the C1=O1 group of PPD was chemisorbed by its *re*-face. This result is compatible with the experimentally observed excess formation of (*R*)-PAC over (*S*)-PAC from the hydrogenation of PPD over CD-modified Pt catalysts, at least if the intrinsic hydrogenation rates of various adsorption modes are assumed to be of similar magnitude. The same conclusion is made on the basis of thermodynamic stabilities shown in Figure 4.8; the *re*-face structures (top line) were more stable than the *si*-face structures (bottom line). Figure 4.8 also shows that the QA-Open(4) conformation of $DHCDH^+$ formed the most stable complex with PPD on Pt(111) [*re*-(s-*cis*)] and that a bifurcated hydrogen bond existed between PPD and quinuclidine NH^+ in this complex. The corresponding *re*-(s-*trans*) structure was less stable by 25 kJ mol^{-1} because it was single hydrogen-bonded. The *si*-(s-*cis*) structures were even less stable because either there existed only one hydrogen bond between C=O and NH^+ (the structure with relative energy of 36 kJ mol^{-1}) or the aromatic moieties of the molecules were too close to each other thus causing repulsive steric interactions (the structure with relative energy of 56 kJ mol^{-1}). The latter structure was destabilized further because the phenyl moiety of PPD had not adopted its most stable adsorption mode bridge(30) due to the constraints induced by the Pt(111) surface geometry.

Summarizing, the above DFT results on reactant–modifier interactions on Pt(111) surface underpin the observations **[VI]** that the QA-Open(4) conformations of cinchona alkaloids may have an important role in creating chiral sites on catalytic Pt surfaces. In the two most stable reactant–modifier structures, PPD adopted the s-*cis* conformation and exposed its *re*-face to the surface which is in line with the experimentally observed excess formation of the (*R*) product enantiomer.

4.3 Effect of solvent on stereoselectivity

As exemplified in Figure 2.1 and discussed in Section 2.1.3, solvent has a crucial impact on the asymmetric hydrogenation of prochiral ketones, α-diketones and α-keto esters over cinchona alkaloid modified platinum catalysts (i.e., the Orito reaction). Choosing the appropriate solvent is highly important when optimizing the performance of these catalytic systems. A solvent has many different roles. For example, the adsorption properties of cinchona alkaloids[224,230,231] together with their ability to bestow chirality on surfaces[98,232] depend greatly on the nature of the solvent.[233] Therefore, it is usually very difficult to understand solvent effects completely. It has been hypothesised that the trends observed in connection with solvent effects are mostly related to the rotational conformation space available to the chiral molecules due to the presence of several C−C single bonds.[231,233] For example, variations in solubility, adsorption, and catalytic performance seen between the near-enantiomers CD and CN (which display opposite chirality in C(8) and C(9) but the same chirality in the quinuclidine moiety) have been suggested to be mostly a result of a somewhat more restricted rotational conformational space for CN than for CD.[233] Protonation of CD has been shown to significantly restrict its rotational conformation space.[226,234] At the same time, protonation severely affects the catalytic performance of CD, however, depending on the reactant [**I**].[66,96,235]

The present-day mechanistic models cannot comprehensively explain the dependence of the *ee* and the reaction rate on the solvent, particularly carboxylic acids. For example, the dependence of the *ee* on the solvent (toluene vs acetic acid, see Figure 2.1) cannot solely be explained in terms of solvent polarity. The dielectric constant is 2.4 for toluene and 6.2 for acetic acid at 20°C, that is, these solvents do not differ that much in polarity. We tried to extend the understanding of solvent effects by studying (i) reactant–modifier interactions in the presence and absence of a solvent molecule [**II**], (ii) proton affinities of various reactant molecules [**III**], and (iii) the effect of the solvent on the conformational equilibrium of some modifiers [**VIII**].

4.3.1 Reactant–modifier interactions

Although the computational model used in **II** (bifurcated hydrogen-bonded complexes and CDH^+ adopting the Open(3) conformation) could not properly predict the enantioselectivity in the hydrogenation of MP and KPL in toluene, it was still interesting to examine if the model could reproduce the trend in the *ee* when changing the solvent from toluene to acetic acid (AcOH). It was assumed that toluene as a non-polar and aprotic solvent does not

bind to the positively charged reactant–modifier complexes in a way, for example by hydrogen bonds, which could change the relative stabilities of the diastereomeric complexes optimized in the gas phase [**II**]. To account for the effect of AcOH on the properties of the complexes, one AcOH molecule was placed near the reaction centre and the structures were fully optimized without restrictions (Figure 3 in **II**). This procedure, however, did not considerably change the relative stabilities of the pro-R and pro-S complexes or the structure of the reactant (Table 1 in **II**). Only in the case of MP (Figure 4.10) the presence of AcOH changed the stability order of the diastereomeric complexes in the direction consistent with experiments—the pro-R complex was slightly more stable with respect to the pro-S complex in AcOH than in toluene. In addition, the presence of the AcOH molecule increased considerably the stability of the keto carbonyl π orbitals of MP in the pro-R complex with respect to that in the pro-S complex. This is a plausible explanation for the increased *ee* of (R)-methyl lactate in AcOH.

Similar analysis did not hold so well for other reactants. Either the AcOH molecule had practically no effect on the thermodynamic and kinetic factors as in the case of KPL or the effect was to increase the enantioselectivity as in the case of PPD. Experimentally, the *ee*s of (R)-pantolactone and (R)-PAC are smaller in AcOH than in toluene. These results implied that the complexes used for PPD and KPL were not controlling enantiodifferentiation or the relatively simple model was not sufficient for describing the effect of the solvent on the experimental *ee*. Other reactant–modifier interaction geometries should also be investigated using more solvent molecules around the complexes and, preferably, in the presence of the Pt surface. This is a challenging task for the future.

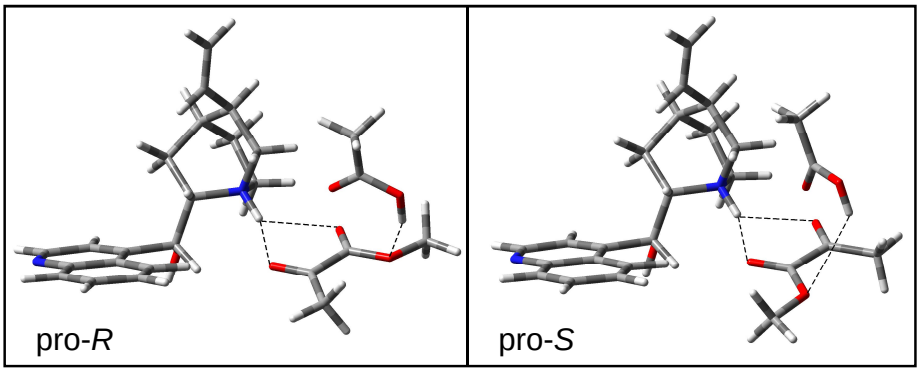

Figure 4.10. Bifurcated MP–CDH^+–AcOH complexes optimized at the HF/6-31G* level of theory [**II**].

4.3.2 Proton affinities

The thermodynamic proton affinity (PA) of a compound A is defined as the negative of the enthalpy change, $-\Delta_r H^\circ$, for the following gas phase reaction at standard conditions (usually at 298 K under pressure of 1 atm)

$$\mathrm{A} + \mathrm{H}^+ \longrightarrow \mathrm{AH}^+ \ .$$

The absolute gas-phase basicity, expressed in terms of PA, is an intrinsic property of individual molecules. In contrast, solution-phase basicities as well as solvation reflect solvent effects because these properties belong to the phase as a whole due to interactions between solute and solvent molecules.[236] In order to understand solvent effects, it is essential to know the PAs of the solute molecules under solvent-free conditions. PAs play an important role in reactions involving protons, protonated and unprotonated molecules. To the best of our knowledge, for most reactants frequently used in the Orito reaction[59,60] neither experimental nor theoretical PAs were available. The main aim of our study [**III**] was to fill this gap in fundamental knowledge.

The PAs of the ketones, vicinal diketones, and α-keto esters shown in Figure 2.1 were evaluated theoretically using the conventional ab initio HF and several post-HF methods (MP2, MP4, CCSD), DFT with the B3LYP hybrid functional, as well as some ab initio model chemistries [CBS-4M, G2(MP2), and G3(MP2)//B3LYP]. The PAs of these molecules varied between 750–890 kJ mol^{-1}, depending on the molecule and the computational method (Table 3 in **III**). Some of the results are visualized in Figure 4.11. Previously reported (experimental) PAs existed only for 2,3-butanedione, acetophenone, and 2,2,2-trifluoroacetophenone.[237] In the most stable protonated species, the proton was bound to one of the carbonyl oxygens. The preferred site depended on the molecule (Figure 1 and 2 in **III**): in MP and KPL the ester carbonyl oxygen was protonated, whereas in ethyl benzoylformate and PPD the keto carbonyl oxygen next to the phenyl group was protonated. These phenomena could be understood in terms of resonance stabilization of the resulting cations [**III**].

As expected, electron correlation had to be modeled very accurately in order to get reliable PAs. It was also essential that the basis set used in the calculations included polarization functions on all elements. Instead, inclusion of diffuse functions in the hydrogen basis set had only a minor effect on the PA. This is consistent with the fact that the evaluation of the PAs did not include any calculations of species such as anions, highly excited electronic states or loose supramolecular complexes where the diffuse functions are necessary in basis sets.[238] In most cases, the PAs evaluated with the CCSD/6-311+G(d,p)//B3LYP/TZVP and G2(MP2) methods were

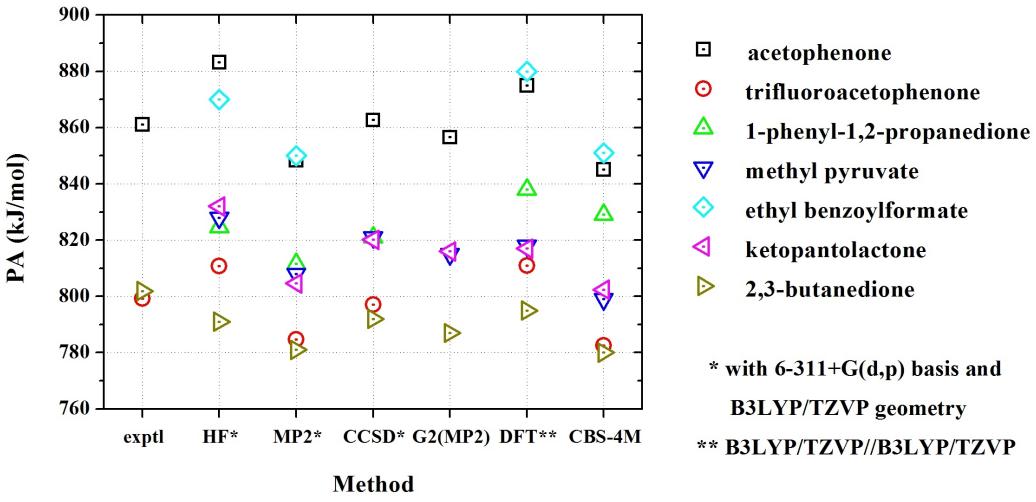

Figure 4.11. Experimental and theoretical PAs of the ketones, vicinal diketones, and α-keto esters studied in this work [**III**]. The PAs predicted by the CCSD and G2(MP2) methods lie between those given by MP2 and DFT. Generally, the PAs of the studied molecules differed from each other by about the same amount irrespective of the computational method.

in good agreement with the existing experimental ones [**III**]. However, the calculations underestimated the previously reported PA of 2,3-butanedione by 10–15 kJ mol^{-1} [**III**].

While the CCSD and G2(MP2) theories gave highly accurate results, they were computationally very expensive and, therefore, not practical for studying larger molecules [**III**]. On the other hand, the CBS-4M, MP2, and DFT methods were computationally much less demanding and could be applied to larger molecules, but they might suffer from inaccuracy. Nevertheless, the results showed that the CBS-4M, MP2, and DFT methods were competitive with the expensive G2(MP2), MP4, and CCSD methods to assess the PAs of the studied molecules. Specifically, very accurate PAs resulted when they were evaluated as the average of the PAs calculated with the B3LYP/TZVP//B3LYP/TZVP and the MP2/6-311+G(d,p)//B3LYP/-TZVP models, called just 'DFT' and 'MP2' at the rest of this section (Table 6 in **III**). For this combination method, referred to as $\frac{1}{2}$(DFT + MP2) in **III**, the mean absolute deviation (MAD) from the experimental PAs of 13 test molecules containing first- and second-row atoms was 4.0 kJ mol^{-1} (Table 6 in **III**). For 9 molecules composed only of first-row atoms the MAD was 2.5 kJ mol^{-1}. The reason for the good performance of the combination method was that its components 'DFT' and 'MP2' systematically over- and

underestimated, respectively, the experimental / accurate theoretical PAs by approximately the same amount. Therefore, it was suggested that if no experimental or highly accurate theoretical data is available (due to the computational cost), the PAs of similar compounds as investigated in this work could be evaluated with the combination method. For the studied molecules, this method gave the following PAs (in increasing order, in kJ mol^{-1}): 2,3-butanedione (788, exptl 802); 2,2,2-trifluoroacetophenone (798, exptl 799); KPL (811); MP (813); PPD (825); acetophenone (862, exptl 861); ethyl benzoylformate (865).

Under typical experimental conditions applied in heterogeneous enantioselective hydrogenation of activated ketones over Pt–cinchona catalysts, there may be many sources of proton donors, for example, traces of water as an impurity in the aprotic solvent (e.g., toluene), the protic solvent (e.g., AcOH), adsorbed hydrogen on Pt, or acidic sites of Al_2O_3 or SiO_2 which are commonly used as support materials. As long as proton donors are available the protonation of the quinuclidine N of CD is very likely due to its high PA (ca. 1000 kJ mol^{-1}, **I**). The PA of CD is also higher than the PA of any of the reactants by 130–200 kJ mol^{-1} (Table 4 in **III**), whereupon the protonation of CD would be the thermodynamically most favored under reaction conditions. Further protonation of the reactant molecules would probably lead to a non-favorable reactant–modifier interaction due to the repulsion of positive charges and, ultimately, to a reduced enantioselectivity (Scheme 3 in **III**). The protonation of the reactant could be a contributing factor, for example, for the decrease of the *ee* in EP hydrogenation observed in stronger acids than trifluoroacetic acid.[239]

If the enantioselectivity of the hydrogenation reaction was influenced by the PA of the reactant molecule, the *ee* could be expected to decrease in a protic solvent as a function of increasing PA. For example, the change of the solvent from toluene to AcOH should have the most detrimental effect on the *ee* in ethyl benzoylformate hydrogenation, because ethyl benzoylformate had the highest PA of the compounds studied. However, the *ee* was higher in AcOH than in toluene (Figure 2.1). Thus, comparison of the PAs with the experimental *ee*s showed that the PAs alone cannot be utilized to rationalize solvent effects. In the inherently complex asymmetric hydrogenation, many other solvent dependent factors such as modifier conformation, adsorption mode etc. may contribute simultaneously to the observed *ee*. Nevertheless, the PAs play an important role in fundamental understanding of the solute–solvent interactions and are required to explain solvation and solvent effects in enantioselective hydrogenation as well.

4.3.3 Modifier conformations

In order to better understand the solvent effects in heterogeneous enantioselective hydrogenation, the molecular structures and energies of MeOCD, MeOCN, and the silyl *O*-ether derivatives TBDMSOCD and PDMSODHCD were investigated in the gas phase, in chloroform ($CHCl_3$), and in toluene using DFT calculations at the B3LYP/T(ON)DZP level. The treatment of solvation effects were carried out implicitly using the COSMO continuum solvation model.[219] Energy barriers for the interconversion of the conformers were determined at the BP86/SV(P)–MARI-*J* level.

On the basis of the computational Gibbs energies at 25°C and 1 bar, Open(3) was the most stable conformation of both MeOCD and MeOCN in the gas phase and in toluene (Table 3 in **VIII**). Closed(1) and Closed(2) were the next most stable conformers. Open(4) and Open(5) were less stable than the other conformers by 10–20 kJ mol^{-1} for all cinchona alkaloid *O*-ethers investigated and, consequently, their population was considered negligible. The Closed(1), Closed(2), Open(4), and Open(5) conformations were stabilized relative to Open(3) when going from the gas phase to toluene. According to Boltzmann statistics, the populations of the Closed(1) and Open(3) conformers of MeOCN were about the same (Table 4.2). Instead, the population of the Closed(1) conformer of MeOCD was about one-third of the population of the Open(3) conformer. The results were in line with experiments.

Open(3) was the most populated conformer of TBDMSOCD in the gas phase and in toluene and $CHCl_3$ as far as the computational electronic energies and enthalpies were considered [**VIII**]. Deviation of the populations based on Gibbs energies was already discussed in Section 4.2.1. The closed conformers were stabilized relative to Open(3) when going from the gas phase to solution, as was also observed for MeOCD and MeOCN. The small deviations between the experimental and theoretical values may be attributed to the inaccuracy of COSMO when treating the screening effects of nonpolar solvents as discussed in **VIII**. Nevertheless, the computational results were well supported by the experimental results.

The computational populations of the conformers for PDMSODHCD in the gas phase were similar to those for TBDMSOCD (Table 4 in **VIII**). However, the *ee*s obtained in the hydrogenation of PPD over the catalyst modified by these modifiers were different. This example indicates that the conformational behavior of cinchona alkaloid *O*-ethers in the gas phase and in solution cannot explain their different behavior as chiral modifiers.

Table 4.2. The *ee*s (%) observed in the hydrogenation of PPD in toluene over Pt catalysts using cinchona alkaloid *O*-ethers as chiral modifiers, and populations (%) of some conformers of these modifiers in toluene estimated from DFT computed Gibbs energies and NMR data (in parenthesis if available, cf. Tables 1–4 in **VIII**).[a]

Modifier	*ee*[b]	Closed(1)	Closed(2)	Open(3)
MeOCD	10 (*S*)	22 (15)[c]	16 (29)	60 (56)
PhOCD	28 (*S*)	n.a.[d] (9)	n.a.[d] (33)	n.a.[d] (58)
TBDMSOCD	27 (*S*)	22[e] (29)	21[e] (29)	57[e] (42)
PDMSODHCD	1 (*S*)[f]	17[g] (10)[h]	11[g] (48)[h]	73[g] (42)[h]
MeOCN	32 (*R*)	46	3	51

[a] Populations of the Open(4) and Open(5) conformers were close to zero by the DFT calculations. [b] Taken from ref 74. Configuration of the major product enantiomer is given in parenthesis. [c] Populations of the conformers as studied by ^{1}H NMR are given in parenthesis. [d] Computational results not available.
[e] Estimated from computational enthalpies.
[f] Data for hydrogenation over Pt catalyst modified by *O*-(allyldimethylsilyl)cinchonidine which is converted rapidly to PDMSODHCD under hydrogenation conditions.
[g] Estimated from gas-phase electronic energies. [h] Population in $CDCl_3$.

DFT studies on the interconversion between the Closed(1) and Closed(2) conformations as well as between Open(3) and Open(4) (i.e., rotation around the C(4')−C(9) bond) showed that the bulkiness of the substituent had a large influence on rotational barriers (Figures 6 and 7 in **VIII**). The energy barrier for the interconversion between Closed(1) and Closed(2) decreased in the following order, where the height of the lowest barrier is given in parenthesis: TBDMSOCD (55 kJ mol^{-1}) > MeOCD (39 kJ mol^{-1}) > PhOCD (30 kJ mol^{-1}). Therefore, rotation around the C(4')−C(9) bond was less hindered for PhOCD than for MeOCD, most likely due to the flat geometry of the phenyl ring. The coalescence points in the NMR spectra decreased in the same order as the computational interconversion barriers. The DFT results were thus in good agreement with the NMR data. The energy barriers were somewhat higher for the Open(3)↔Open(4) interconversion compared to the Closed(1)↔Closed(2) interconversion, but the order remained the same (cf. above). The energy barriers for Closed(2)↔Open(3) interconversions of MeOCD (i.e., rotation around the C(8)−C(9) bond) were 3 and 11 kJ mol^{-1} for the forward and reverse process, respectively. These results were in line with the fact that it was not possible to separate the NMR signals of the Closed(2) and Open(3) conformers even at low temperature.

As the modification of the cinchona alkaloid structure induced changes in the conformational equilibria, it was investigated whether the enantioselectivity over the cinchona alkaloid *O*-ether modified metal catalysts correlates with the population of Open(3) or any other conformation in the solution phase. As a result of adsorption–desorption processes of the modifier, the conformational equilibria in solution could provide information on the distribution of the adsorbed species. The results presented in **VIII** (and Table 4.2) demonstrated, however, that direct correlation between the solution phase populations of the conformers and the enantioselectivities in PPD hydrogenation could not be established. Similarly, Vargas et al.[240] showed that the inversion in the sense of enantioselectivity, connected with the change of the modifier from CD to PhOCD in the Pt-catalyzed hydrogenation of KPL, could not be traced to the conformational behavior of the modifiers in the solution phase. Therefore, it seems that the adsorption behavior of the modifier has an important role in enantiodifferentiation. Particularly, the modifier may change its conformation upon adsorption onto the metal surface, and the population of a certain conformer on the metal surface is not necessarily correlated with the population in the solution phase. Adsorption and conformational behavior of the modifiers on the catalyst surface have to be emphasized more in future investigations.

4.4 Origin of regioselectivity

Complex organic molecules have normally more than one reactive site or functional group. The degree of difficulty of discriminating between reactive sites depends on the similarity of the functional groups. Discrimination is simpler if the functional groups belong to two different classes, such as C=O and C=C, than if they are members of the same class, such as two different C=O groups in the same molecule.[241] In most reactions, the functional groups in a molecule have different reactivity, at least to some extent.[241] The complete simulation of chemical reactivity processes requires a description of reaction pathways and associated transition states.[242] In this picture, selectivity arises from the competition between different pathways.

The hydrogenation of PPD over cinchona-modified Pt catalysts exhibits regioselectivity in addition to stereoselectivity (Figure 4.12): 1-hydroxy-1-phenyl-2-propanones (1-OH products) from the hydrogenation of the C1=O1 group adjacent to the phenyl ring were formed in excess with respect to 2-hydroxy-1-phenyl-1-propanones (2-OH products) from the hydrogenation of the C2=O2 group next to the methyl group.[243] Regioselectivity (*rs*) in this context is understood as the preferable reduction of one of the two carbonyl

groups and is defined as rs = [1-OH]/[2-OH]. In the absence of the modifier, rs was around 4 in the hydrogenation of PPD over Pt/Al_2O_3 catalyst. Regioselectivity increased with increasing modifier (CD) concentration to a maximum of 10 around a 1:1 CD/Pt_{surf} ratio, after which it gradually started to decrease.[243] Regioselectivity in the hydrogenation of PPD has been speculated to originate from the fact that the C1=O1 bond of the isolated molecule is longer and, thus, weaker than the C2=O2 bond.[243] However, this alone cannot explain why regioselectivity increased in the presence of the modifier. Interestingly, in the hydrogenation of 2,3-hexanedione over CD-modified Pt catalyst, equal amounts of both regioisomeric products were obtained and no regioselectivity was observed (Figure 4.12).[244]

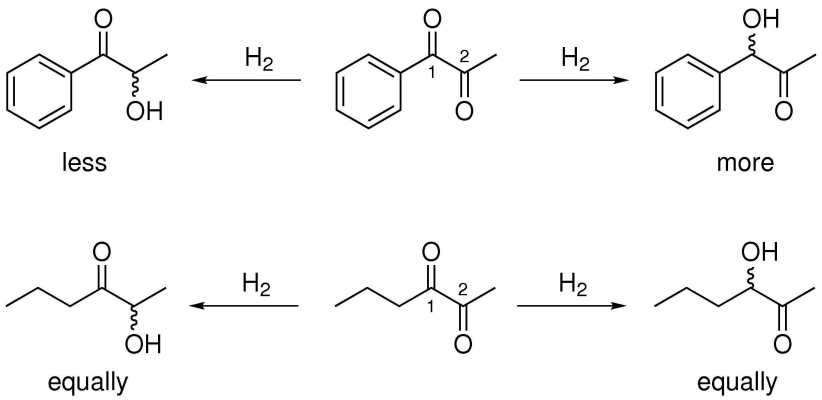

Figure 4.12. Regioselectivity is observed in the Pt-catalyzed hydrogenation of PPD (above) where 1-OH products are formed in excess.[243] Instead, hydrogenation of 2,3-hexanedione over Pt catalysts is not regioselective (below).[244] Numbering of the carbonyl groups follows ref **V**.

The main hydrogenation product of PPD, (*R*)-PAC, is an important intermediate in pharmaceutical synthesis, particularly in the production of ephedrine derivatives.[245] Keeping in mind the industrial applications, it is important to maximize both the enantioselectivity and the regioselectivity of the desired product. Therefore, although the main focus may often be on enantioselectivity, regioselectivity should not be neglected. In this work, adsorption of PPD and 2,3-hexanedione on the Pt(111) surface was studied by DFT to get further clues on the origins of regioselectivity [**V**].

Several adsorption geometries of the molecules were considered. They varied with respect to (i) the conformation of the O=C−C=O system (s-*cis* or s-*trans*), (ii) the adsorption mode of the phenyl moiety of PPD [bridge(30) or hollow-hcp(0)], and (iii) the adsorption mode of the C=O moiety (η^1 or

η^2), as discussed in **V**. As in the case of acetone and acetophenone, the η^2 adsorption mode of the carbonyl moiety was considered the activated species towards hydrogenation due to rehybridization of the carbonyl carbon and increased C=O bond distance.[146] The role of the η^2 mode as the key reaction intermediate was corroborated by recent studies.[172,246] The geometry of the η^1 adsorption mode was very similar to the geometry in the gas phase and, thus, the η^1 adsorption mode was considered a spectator species in hydrogenation.[146] However, it was also proposed that there exists a so-called μ_2(C$_1$,O) enolate species of acetone on Pt(111) besides the η^1 adsorbed acetone[247] suggesting that enol and enolate species are present on the Pt surface during hydrogenation of ketones for which keto–enol isomerization is possible. Nevertheless, deuterium labelling experiments showed that there was a direct addition of two deuterium atoms across the C=O double bond over Pt,[109] whereas over Pd the main product forming route was via the enol and C=C double bond hydrogenation.[248] The main hydrogenation route of PPD over Pd and Pt did not proceed via an enol form.[249] C1=O1 could not even form an enol tautomer via α-hydrogen abstraction because there is no such hydrogen. In **V** we thus concentrated on the comparison between the $\eta^2_{\mathrm{C1=O1}}$ and $\eta^2_{\mathrm{C2=O2}}$ adsorption modes where the carbonyl groups were activated.

The s-*trans* $\eta^2_{\mathrm{C1=O1}}$ mode was the most stable adsorption mode of PPD on the Pt(111) surface with an adsorption energy ΔE_{ads} of -169 kJ mol^{-1} (Table 1 in **V**). In s-*trans* $\eta^2_{\mathrm{C1=O1}}$, the C1=O1 moiety was chemisorbed to the Pt surface via oxygen and carbon. The C1=O1 bond distance was increased to 133 pm from 123 pm in the isolated molecule, and the C1 carbon was rehybridized from sp^2 to nearly sp^3. In addition, the phenyl moiety adopted the bridge(30) adsorption mode. Bridge(30) was the most stable adsorption mode of benzene on Pt(111) at low coverage followed by hollow-hcp(0).[217] In the s-*trans* $\eta^2_{\mathrm{C2=O2}}$ adsorption mode with $\Delta E_{\mathrm{ads}} = -111$ kJ mol^{-1}, the phenyl moiety adopted the bridge(0) site with some distortion (Figure 4.13). For comparison, ΔE_{ads} of the s-*trans* η^1_{O1} mode (Figure 6 in **V**) was only -19 kJ mol^{-1}, indicating a negligible presence of this mode on Pt(111), at least at low coverage.

Unlike in the gas phase, PPD could adopt the s-*cis* conformer on the Pt(111) surface (Figure 4.13). However, the repulsive interaction between the two oxygens in this conformation led to destabilization with respect to the s-*trans* conformation. This was marked by smaller adsorption energies in the case of the s-*cis* structures (Table 1 in **V**). For example, the s-*cis* $\eta^2_{\mathrm{C1=O1}}$ adsorption mode had an adsorption energy of -135 kJ mol^{-1}. It is less negative than ΔE_{ads} for the s-*trans* $\eta^2_{\mathrm{C1=O1}}$ mode by 34 kJ mol^{-1}, which is actually very close to the energy difference between the isolated s-*cis* and s-*trans* conformations of PPD (Figure 4.3). The adsorption energy of the

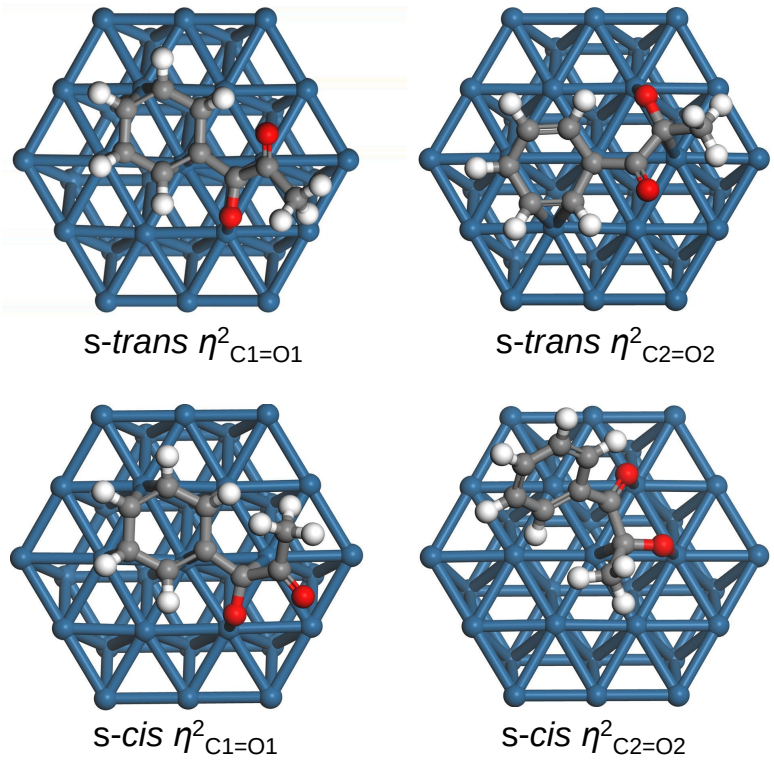

Figure 4.13. The $\eta^2_{C=O}$ adsorption modes of PPD considered as active species in the hydrogenation of the carbonyl group [**V**].

s-*cis* $\eta^2_{C2=O2}$ mode was only −38 kJ mol^{-1} because the phenyl ring was not chemisorbed. Similarly, ΔE_{ads} of the s-*cis* $\eta^1_{O1,O2}$ mode (Figure 6 in **V**) was only −3 kJ mol^{-1}, indicating again a negligible presence of the η^1 modes on Pt(111). ΔE_{ads} of the most stable spectator species of PPD, namely s-*trans* bridge(30), was −129 kJ mol^{-1}. Thus, it was less stable than the s-*trans* $\eta^2_{C1=O1}$ and s-*cis* $\eta^2_{C1=O1}$ modes.

The adsorption energies of the $\eta^2_{C=O}$ adsorption modes of 2,3-hexanedione varied between −33 and −36 kJ mol^{-1} for the s-*trans* conformations and between −38 and −39 kJ mol^{-1} for the s-*cis* conformations. Hence, the latter adsorption energies were equal to ΔE_{ads} of the s-*cis* $\eta^2_{C2=O2}$ mode of PPD having the phenyl ring not chemisorbed to the surface. The slightly stronger adsorption of the s-*cis* conformations of 2,3-hexanedione was probably due to a stabilizing interaction between the non-activated C=O group and the Pt surface, not present in the adsorption modes of the s-*trans* conformation (Figure 7 in **V**). This interaction energy apparently overcame the destabilizing effect of two adjacent oxygens repelling each other in the s-*cis* conforma-

tions. Spectator species (i.e., η^1-adsorption modes of 2,3-hexanedione) were not considered.

Vargas et al.[146] suggested that the probable reason for the higher hydrogenation rate of trifluoroacetone compared with acetone on Pt(111) was the increased proportion between activated species (η^2) and spectator species (η^1). Applying a similar analysis to the hydrogenation of PPD would mean that the relative rates for the formation of 1-OH and 2-OH products depend on the relative populations of the $\eta^2_{\mathrm{C1{=}O1}}$ and $\eta^2_{\mathrm{C2{=}O2}}$ adsorption modes. As the adsorption of the $\eta^2_{\mathrm{C1{=}O1}}$ modes of PPD was stronger than the adsorption of the $\eta^2_{\mathrm{C2{=}O2}}$ modes, the population of the $\eta^2_{\mathrm{C1{=}O1}}$ modes was higher on Pt(111), leading ultimately to regioselectivity. This analysis presumed of course that the hydrogenation rates of C1=O1 and C2=O2 were of the same order of magnitude. However, this should be a reasonable assumption.[243]

The DFT study of the adsorption of 2,3-hexanedione provided also a reasonable explanation for its hydrogenation not being regioselective. The adsorption energies of the s-*cis* and s-*trans* conformations of the $\eta^2_{\mathrm{C1{=}O1}}$ and $\eta^2_{\mathrm{C2{=}O2}}$ adsorption modes were practically equal suggesting that equal amounts of species activated at C1=O1 and C2=O2 existed on the Pt surface. Therefore, neither of the hydrogenation products 2-hydroxy-3-hexanone or 3-hydroxy-2-hexanone was formed in excess. This reasoning is also in accordance with the experimental findings thus supporting the conclusions made for PPD.

The reason for the increased regioselectivity observed in the hydrogenation of PPD in the presence of a modifier is not clear but the phenomenon might be explained as follows. As was shown in this work (see, e.g., Figure 4.8 and Figure 4.9), the reactant–modifier complexes were more stable when PPD adopted the s-*cis* rather than the s-*trans* conformation. Thus, the thermodynamic stabilities of the s-*cis* $\eta^2_{\mathrm{C1{=}O1}}$ and s-*cis* $\eta^2_{\mathrm{C2{=}O2}}$ adsorption modes should be considered in the case of modified hydrogenation. According to the results, proportional coverage of the $\eta^2_{\mathrm{C1{=}O1}}$ mode with respect to the $\eta^2_{\mathrm{C2{=}O2}}$ was higher when PPD adopted the s-*cis* conformation rather than the s-*trans* conformation [**V**]. This would indicate a higher regioselectivity in the modified hydrogenation. Although a proper explanation for the increase of regioselectivity in the PPD hydrogenation on a modified surface would require an explicit consideration of reactant–modifier interactions on the Pt surface and a complete simulation of the elementary hydrogenation steps, the regioselectivity in the unmodified hydrogenation of PPD and 2,3-hexanedione could well be explained by the interactions between the reactant and the metal surface.

4.5 Metal particle size effects

Catalysis by metal particles dispersed on support materials is an important method to produce vast variety of organic chemicals. The properties (rate etc.) of many catalytic reactions depend substantially on the size and shape of the supported metal particles;[250–252] these reactions are classified as structure sensitive, whereas the others are structure insensitive. The catalytic activity of the metal can be enhanced through the formation of very small particles with the diameter ranging from 1 to 10 nm. The nanosized particles have large surface-to-volume area (i.e., high dispersion) and an increased number of edges, corners, and faces leading to changes in electronic structure and variations in catalytic activity and selectivity.[252,253] The properties of particles with nanodimensions are between those of atoms and the bulk material.

A well-known example of the importance of size effect is gold, which was thought to be catalytically inert until the 1980s, when nanosized gold particles were found to be active in CO oxidation even at low temperatures.[254,255] The activity was lost with increasing particle size. The effect of particle size on catalytic properties has also been reported for other metals.[256] For example, the hydrogenation rate of ethene attained a maximum value on Pt particles with a diameter of ca. 0.6 nm,[257] and the adsorption energy of oxygen depended significantly on the Pt cluster size.[258,259] Further, experimental data for enantioselective hydrogenation of PPD demonstrated that kinetic regularities (e.g., activity, regio- and enantioselectivity) over nanometer-size metal particles were sensitive to the size of the particles.[260]

Different explanations have been proposed to rationalize the metal particle size effects. For example, the altered reaction rate for nm-size particles was related to changes in the ratio between different surface faces exhibiting different intrinsic kinetics.[261] For reactions involving complex organic molecules that require multicentered adsorption, not only this ratio but also the size of a particle face per se could be a parameter influencing the rates. In order to better understand why size matters in heterogeneous catalysis, the adsorption of ethene, acetone, and benzene on the Pt(111) surface was studied by DFT [**VII**]. The most stable adsorption modes and modes thought to be active in hydrogenation were considered (Figure 2 in **VII**). Eight different clusters with 19–38 Pt atoms, two or three atomic layers, and dimensions of 0.7×0.8 nm^2 to 1.1×1.4 nm^2 were employed to model the Pt(111) surface (Figure 1 in **VII**). For comparison, the Pt(111) surface was also modeled with two and three layer thick periodic slabs.

In most cases, adsorption geometries of the molecules depended only slightly on the surface model (cluster vs slab) and on the computational

details like basis sets [**VII**]. Instead, the adsorption energies depended prominently on the cluster size and the number of atomic layers both in clusters and slabs [**VII**]. For instance, the adsorption energy of η^1 adsorbed acetone varied from -39 kJ mol^{-1} on the Pt_{38} cluster to -60 kJ mol^{-1} on Pt_{22} and the adsorption strength decreased quite steadily with increasing cluster size (Figure 4.14). The role of cluster thickness in the η^1 adsorption was relatively small—the adsorption energies on Pt_{22} with two Pt layers and on Pt_{35} with three layers were quite close to each other. The adsorption energies from the slab calculations, -65 and -43 kJ mol^{-1} for the adsorption on the two and three layer thick slabs, respectively, were close to those from the cluster calculations. Interestingly, the adsorption energy of the η^2 mode depended more strongly on the cluster size than the adsorption energy of the η^1 mode. Adsorption through the η^2 mode was particularly weak on Pt_{38} and the three layer thick Pt_{35} cluster. The adsorption energies of the η^2 mode from the slab calculations were similar to those from cluster calculations using small clusters. The calculated adsorption energies were close to the experimental and previous theoretical values (for further details, see **VII**).

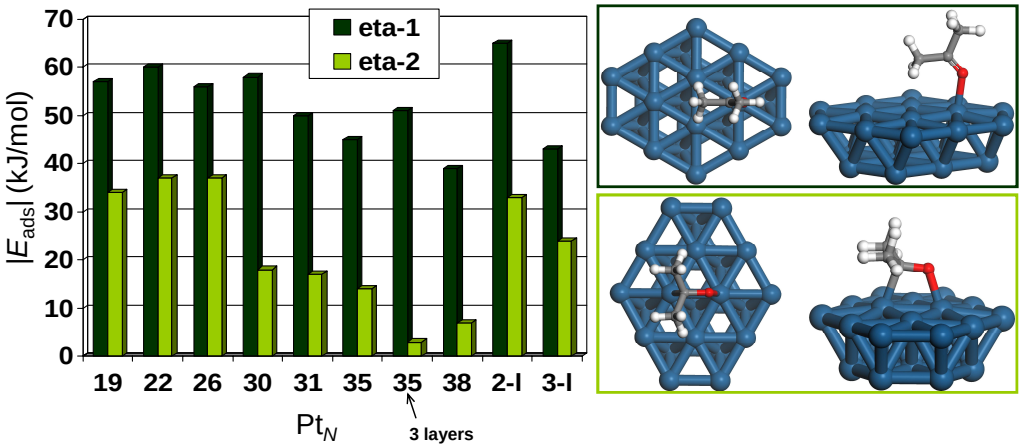

Figure 4.14. Absolute values for the adsorption energies of η^1 and η^2 adsorbed acetone as a function of Pt cluster size. The abscissa represents the total number of atoms (N) in the two layer thick Pt clusters (Tables 4 and 6 in **VII**); 2-l and 3-l represent two and three layer thick slabs, respectively (Tables 5 and 7 in **VII**). Top and side views of the adsorption modes η^1 (above) and η^2 (below) are also shown.

Relaxation of the central Pt atoms of the clusters (i.e., letting their coordinates optimize without any constraints) did not explain the size dependence of the adsorption energy. For example, although the adsorption of ethene

was weaker on frozen than on relaxed clusters by 20–40 kJ mol^{-1}, adsorption energies varied in a similar manner as the function of cluster size whether the clusters were relaxed or frozen (Table 1 in **VII**). The adsorption energy was independent of the number of relaxed cluster atoms as evidenced by a detailed decomposition analysis of the adsorption energy (Table 1 in **VII**). Interestingly, the adsorption energy of ethene on the three layer thick Pt_{35} cluster with 4 relaxed atoms was closer to the adsorption energy on Pt_{38} (9 relaxed atoms) than on Pt_{22} (4 relaxed atoms). In addition, possible correlation between the basis set superposition error (BSSE) and cluster size was searched. BSSE is an error in the interaction energy due to the finite basis set (see Appendix C). In the case of ethene adsorption, the BSSE was around 30 kJ mol^{-1} for all clusters with the functionals employed (Table 3 in **VII**). Therefore, the size effects were not due to the BSSE. The above-mentioned facts implied that the observed dependence of the adsorption energy on cluster size was indeed due to the cluster size (and shape) rather than some computational artifacts.

To account for the observed cluster size effects, the *d*-band center of the surface metal atoms was investigated. The *d*-band center has been shown to be a good descriptor of the catalytic reactivity of transition metal surfaces.[262,263] For example, it was proposed to be an important parameter in determining the strength of adsorption of ethene on the metal surface;[264] ethene was found to bind more strongly on surfaces, where the *d*-band center was closer to the Fermi level, and the activation barrier for the C−H bond cleavage was found to correlate with the position of the *d*-band center of the Pd atoms. According to our calculations (Table 11 in **VII**), the *d*-band center was almost independent of the cluster size. Accordingly, no correlation between the *d*-band center and the adsorption energy was found. Perhaps the variation in the cluster size was too small to be seen in the energy of the *d*-band center. It is also noted that only the Pt(111) surface was investigated here, whereas the aforementioned correlation is usually found for different transition metals and their different surfaces.

Although relation between catalyst particle size and catalytic activity was not explicitly studied in **VII**, the above theoretical results implied a connection between them. First, this could be due to the Brønsted–Evans–Polanyi (BEP) relationship[265] which relates the reaction energy and the activation energy (along with the reaction rate) as[253]

$$\delta E_{\text{activation}} = \alpha \cdot \delta E_{\text{reaction}} \quad (0 < \alpha < 1) \ .$$

If the reaction energy is a function of cluster size so is the rate. Second, the ratio of the adsorption energies of the η^2 and η^1 adsorption modes of acetone

was observed to vary as a function of cluster size (Figure 4.14). This suggests different proportions of active (η^2) and spectator (η^1) species on the catalyst surface and, thus, different reaction (e.g., hydrogenation) rates on catalyst particles of different size. For instance, an experimentally observed 400-fold enhancement in the turnover frequency of acetone hydrogenation on Pt was attributed to the presence of sites favoring the η^2 mode of acetone.[266]

4.6 Origin of asymmetric induction over unmodified Pt catalysts

The studies thus far have tried to elucidate the origins of stereodifferentiation in the hydrogenation of C=O bonds over chirally modified Pt catalysts. The reactants have mostly been prochiral vicinal diketones and α-keto esters. This section will discuss asymmetric induction in the hydrogenation of chiral α-hydroxyketones over unmodified, achiral Pt catalysts. Such kinds of diastereoselective heterogeneously catalyzed hydrogenations of prochiral double bonds have received relatively little attention,[267–269] presumably because high diastereoselectivities are commonly obtained by hydrogenation with homogeneous chiral metal catalysts.

As stated in Section 2.2, the origin of stereoselectivity in the hydrogenation of a chiral molecule over achiral Pt catalyst is based on the chirality of the molecule itself. Qualitatively, a stereogenic center in the molecule influences the mode of adsorption of the molecule on the catalyst surface;[268] adsorption takes place via the less hindered diastereotopic face of the molecule, whereupon the addition of hydrogen atoms from the catalyst surface to the adsorbed molecule leads to diastereoselectivity. Hence, the resulting diastereoselectivity depends crucially on the steric arrangement and conformational properties of the reactive molecule. The presence of a bulky substituent or polar group in the molecule is indispensable for directing the adsorption on the metal surface and obtaining a high diastereomeric excess (*de*). Most of the substrates reported to date also have a certain backbone rigidity,[270] which limits their conformational degrees of freedom. For example, rigid ring structures, which can adsorb on the metal surface of a heterogeneous catalyst through only one of their diastereotopic faces, usually give higher *de*s.[268] The *de* is also influenced by the catalytically active metal, the support, the solvent, and reaction conditions.

To further elucidate the mechanism of PPD hydrogenation over chirally modified Pt catalysts and the origins of asymmetric induction in heterogeneous catalysis in general, the hydrogenation of (*R*)-PAC over cinchonidine-

modified and unmodified Pt/Al_2O_3 was studied [**IX**]. Furthermore, hydrogenation of two other chiral α-hydroxyketones, (R)-2-hydroxycyclohexanone [(R)-adipoin] and (R)-3-hydroxybutanone [(R)-acetoin], were studied. These three compounds yield different *de*s upon hydrogenation over Pt/Al_2O_3 which gives a good opportunity to assess the validity of a theoretical model in the determination of the *de* (Figure 4.15). Theoretical aspects of stereoselectivity in the hydrogenation of chiral α-hydroxyketones over Pt–cinchona catalysts were studied already in **IV**. However, in that study the reactant–modifier interactions were investigated, whereas computational modeling of the actual hydrogenation over modified catalyst was not feasible due to the large size of the system. The unmodified system is computationally less demanding, whereupon it was possible to examine whole reaction paths for (R)-PAC hydrogenation and get more information about the mechanism of stereodifferentiation.

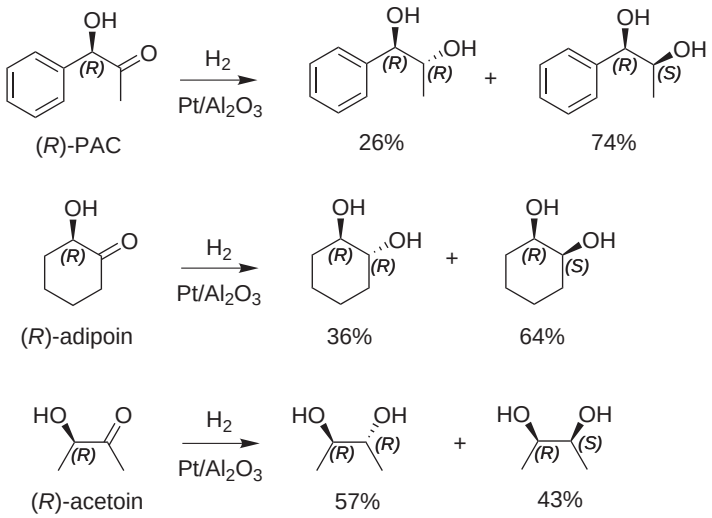

Figure 4.15. Hydrogenation of (R)-PAC, (R)-adipoin, and (R)-acetoin over Pt/Al_2O_3 yields different proportions of the diastereomeric products [**IX**].[271,272]

Hydrogenation of (R)-PAC produces two diastereomers, (1R,2S)-1-phenyl-1,2-propanediol and (1R,2R)-1-phenyl-1,2-propanediol, called (1R,2S)-diol and (1R,2R)-diol henceforward. When (R)-PAC was hydrogenated over the unmodified Pt/Al_2O_3 catalyst in toluene, significant diastereoselectivity was reached; the (1R,2S)-diol was formed in excess over the (1R,2R)-diol with

the *de*[†] of 49% (Figure 2 and Table 1 in **IX**). When CD was introduced into the reaction milieu, the *de* increased to 60%.

(*R*)-PAC is a conformationally flexible molecule as indicated by the low energy barriers for the rotations around its single bonds [**IV**]. Therefore, in qualitative terms, it is difficult to guess which diastereotopic face, *re* or *si* yielding (1*R*,2*R*)- and (1*R*,2*S*)-diols upon hydrogenation, respectively, is more easily exposed to the metal surface. Especially, any quantitative value for the *de* would be inaccessible. Basically, stereoselectivity originates from thermodynamic and kinetic factors, that is, relative thermodynamic stabilities of the diastereomeric adsorption modes and the difference in the reaction rate of those species. The inherently unequal thermodynamic stabilities of the product diastereomers may also contribute to the stereoselectivity. As the first step to rationalize the observed *de* the thermodynamic stabilities of the diastereomeric gas-phase products were determined by DFT. According to the calculations, (1*R*,2*R*)-diol was more stable than (1*R*,2*S*)-diol by 3 kJ mol^{-1} [**IX**]. This result implied an excess formation of (1*R*,2*R*)-diol assuming that the reaction was under thermodynamic control (i.e., product composition governed by the equilibrium thermodynamics) and that the difference between the total electronic energies of the diastereomers corresponded to the difference between their Gibbs energies. However, predominant formation of (1*R*,2*S*)-diol was observed in the experiments.

As the second step, adsorption of (*R*)-PAC on the Pt(111) surface was investigated. Complete characterization of the adsorption of such a complex molecule as (*R*)-PAC required considering many subtleties, which will be passed here but can be found in **IX**. The most stable adsorption modes of (*R*)-PAC were expected to have a bridge(30) adsorbed phenyl ring just as in the case of PPD adsorption [**V**]. Therefore, such modes were focused on. About 30 different adsorption modes of (*R*)-PAC were identified. In the two thermodynamically most stable modes (Figure 4.16), the C−OH bond was nearly parallel to the Pt surface, synperiplanar relative to the carbonyl group adsorbed by its *re*-face and antiperiplanar relative to the carbonyl group adsorbed by its *si*-face. The adsorption energies of the *re-(s-cis)-*π_S and *si-(s-trans,180)-*π_S adsorption modes were of similar magnitude but their absolute as well as relative values depended on the cluster used to model the Pt(111) surface [**IX**]. However, the choice of the cluster did not affect the conclusions about diastereoselectivity of the hydrogenation reaction [**IX**].

As the third step to reveal the origins of diastereodifferentiation, full potential energy profiles including transition states and stable intermediates were determined for various hydrogenation pathways by DFT. The hydro-

[†] Diastereomeric excess is defined here as
$de(\%) = 100 \times ([1R,2S] - [1R,2R])/([1R,2S] + [1R,2R])$.

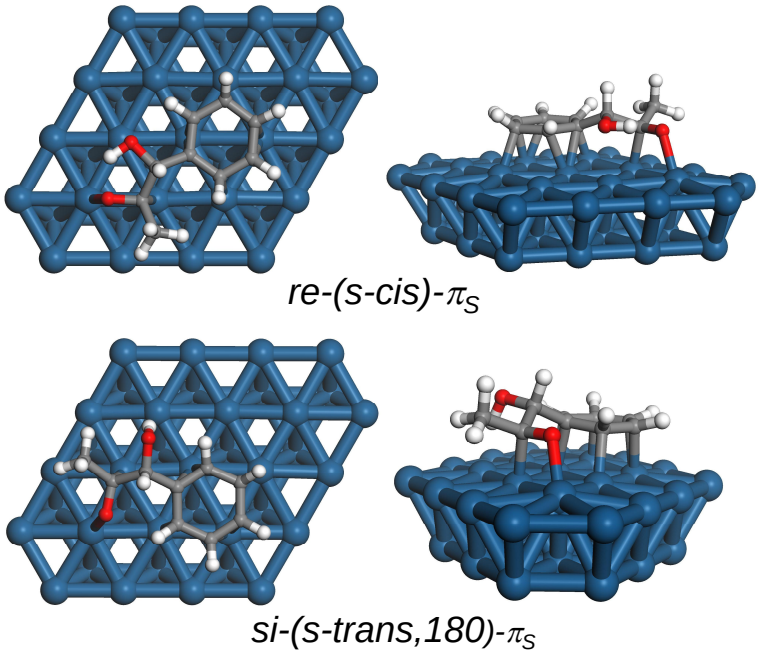

Figure 4.16. Top and side views of the DFT optimized, most stable *re*- and *si*-face adsorption modes of (*R*)-PAC on the (111) surface of a Pt_{38} cluster [**IX**].

genation mechanism of the C=O double bond on the Pt surface has commonly been thought to involve a series of surface catalyzed hydrogen addition steps (i.e., stepwise addition mechanism) and is known as the Horiuti–Polanyi mechanism.[273] In one pathway a hydroxyalkyl species is formed by adding the first hydrogen atom to the carbonyl oxygen, whereas in the other pathway the carbonyl carbon atom is attacked by the first hydrogen atom, forming an alkoxy species (Scheme 3 in **IX**). The second hydrogenation step leads to the product alcohol in both cases. Kinetic studies of the hydrogenation of simple ketones have suggested that either the first or the second H addition is the rate-determining step, depending on the catalyst and the reaction conditions.[266,274,275] In addition to these pathways, a pairwise addition mechanism, where both hydrogen atoms attack the C=O moiety simultaneously (Scheme 3 in **IX**), was studied in this work. To the best of our knowledge, this mechanism had not been investigated computationally before. However, the pairwise addition mechanism had been proposed for the hydrogenation of ketones[276,277] as well as of benzene and ethylbenzene.[278,279] In addition, it was recently demonstrated by NMR spectroscopy that hydrogen addition to

an alkene on supported metal catalysts occurs pairwise to some extent.[280]

According to the DFT calculations, all mechanisms considered for (*R*)-PAC hydrogenation on Pt(111) led to the diastereomeric excess of (1*R*,2*S*)-diol [**IX**]. The diastereodifferentiation was a result of both thermodynamic and kinetic factors. The adsorption of (*R*)-PAC with coadsorbed hydrogen was more stable through the *si*-face than through the *re*-face. In addition, the activation barriers for hydrogen addition to the *si*-face were nearly equal to or lower than the activation barriers for hydrogen addition to the *re*-face. The hydroxyalkyl hydrogenation route, where a hydrogen atom attacks the carbonyl oxygen first, had a high, over 100 kJ mol^{-1} activation energy barrier for the second hydrogen attack (Figure 4 in **IX**). Therefore, the thermodynamically quite stable hydroxyalkyl intermediate was more likely to be decomposed into (*R*)-PAC and hydrogen than to be hydrogenated further to the product diol. The alkoxy hydrogenation route was associated with a high, ∼100 kJ mol^{-1} activation barrier for the first reaction step, the formation of the C−H bond. The alkoxy intermediate was thermodynamically very unstable and had a low, 1–6 kJ mol^{-1} barrier for the backward dehydrogenation step. In addition, the reaction energy for the formation of the alkoxy intermediate was close to the desorption energy of (*R*)-PAC. Therefore, formation of the alkoxy intermediate was unlikely. The pairwise hydrogenation route, where two hydrogen atoms attacked the decoordinated carbonyl carbon and oxygen atoms simultaneously, was found to have a moderate, ∼50 kJ mol^{-1} activation barrier for the hydrogen addition step (Figure 4.17). Therefore, it corresponded to the minimum energy pathway from the adsorbed reactants to the adsorbed products and was proposed to be the main mechanism for (*R*)-PAC hydrogenation on Pt(111). Interestingly, the activation energy barriers were lower for hydrogen attacks that took place at the C=O moieties partially decoordinated from the surface rather than chemisorbed to the surface via the η^2 mode. Formation of the C−H bonds was endothermic, whereas formation of the O−H bonds was exothermic.

Hydrogenation of (*R*)-acetoin and (*R*)-adipoin was studied using a similar strategy as was applied for (*R*)-PAC hydrogenation. However, because searching for transition states was computationally very demanding, only stable species of the hydrogenation reaction were considered. The stability difference between the corresponding *si*- and *re*-face adsorbed species (e.g., hydroxyalkyl intermediates) in favor of the *si*-face species was less pronounced for (*R*)-adipoin than for (*R*)-PAC (Figure 7 in **IX**). This suggested that the *de* of (*R*,*S*)-diol (*meso*-diol) from (*R*)-adipoin hydrogenation was lower than the *de* of (1*R*,2*S*)-diol from (*R*)-PAC hydrogenation, which was in line with the experiments.[272] The *re*- and *si*-face adsorbed reactants and hydroxyalkyl intermediates of (*R*)-acetoin were almost equally stable, whereas the alkoxy

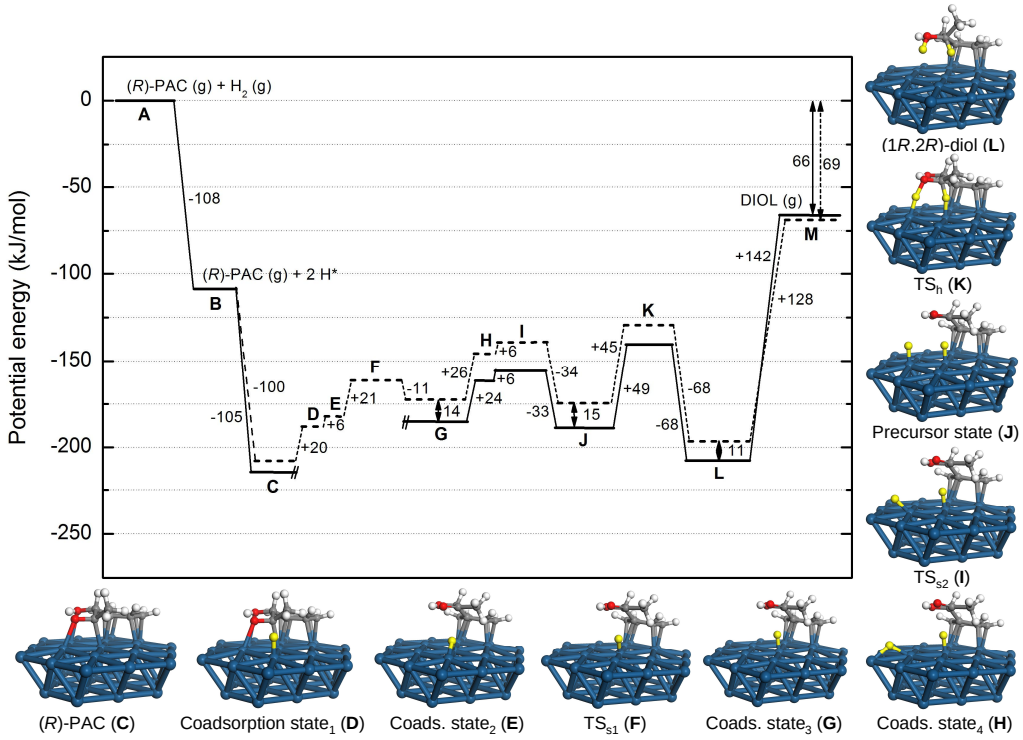

Figure 4.17. DFT computed potential energy profile for the hydrogenation of (*R*)-PAC on Pt(111) through pairwise mechanism [**IX**]. Represented are both *re*-face addition (dashed line) and *si*-face addition (solid line) leading to (1*R*,2*R*)- and (1*R*,2*S*)-diols, respectively. Side views of the reaction intermediates and transition states (TS) are shown for the *re*-face addition. Attacking hydrogen atoms are colored yellow.

intermediates and the precursor states of the pairwise addition mechanism were more stable when adsorbed through their *re*-face. These results implied a nonexistent to small *de* of (*R*,*R*)-diol, which was again consistent with the experiments (Figure 4.15).[271]

The results showed that cluster model DFT calculations as applied here can be used to assess (dia)stereoselectivity in metal-catalyzed hydrogenation of even quite complex organic molecules, provided that the whole reaction paths or at least the stable reaction intermediates are taken into consideration.

Chapter 5

Conclusions

In this doctoral thesis, molecular modeling tools were employed to study asymmetric heterogeneous catalysis, specifically hydrogenation of prochiral carbonyl compounds to corresponding chiral alcohols (i.e., C=O + H_2 → CH−OH) over Pt catalysts modified by cinchona alkaloids. Introduced by Orito et al. at the end of 1970s, this is one of the known heterogeneous catalytic systems which can yield high stereoselectivities. However, the activity and selectivity of this complex catalytic system is very sensitive to the structure of the reactant and the modifier (the chiral organic compound), the solvent, metal particle size, and reaction conditions among others. Molecular-level information about the system is required to fully understand these effects. Quantum mechanical calculations can help in this endeavor.

1-Phenyl-1,2-propanedione (PPD), its α-hydroxyketone derivatives, and some α-keto esters among others were used as reactants, whereas cinchonidine (CD), cinhonine, and their *O*-ether derivatives were used as modifiers. Adsorption and reactions were modeled on the Pt(111) surface which was represented by nanosized Pt clusters. The Conductor-like Screening Model (COSMO) was applied for the implicit treatment of solvation effects.

The relative thermodynamic stabilities of various modifier conformers depended on the solvent, the modifier itself, and whether the modifier was protonated or not. The populations of the modifier conformers in the gas and solution phase did not correlate with those on the Pt surface. Besides, some conformations were found to be stable only on Pt. For example, so-called QA-Open(4) was the most stable conformer of protonated CD and MeOCD on Pt(111). It was also observed that no correlation existed between the populations of the modifier conformers in the solution phase and the experimentally observed enantioselectivities of the PPD hydrogenation in the corresponding solvents. Therefore, the specific adsorption of the modifier on the catalyst

surface was suggested to be a crucial step in the generation of chiral sites, which can ultimately lead to the excess formation of one stereoisomer over the other.

Studies on the adsorption of some unsaturated organic molecules on Pt showed that the size of the cluster used to model the Pt surface may affect not only the adsorption energies but also the relative thermodynamic stabilities of different adsorption modes of a molecule. As different adsorption modes may possess different intrinsic reactivity, this observation actually implied size-dependent catalytic activity of nanosized metal particles, a well-known phenomenon. The relative populations of the modifier conformers on the Pt surface might also be influenced by the size of the catalyst particles, which could be a reason for the experimentally observed size-dependent stereoselectivity. The relative stabilities of the *re*- and *si*-face adsorption modes of the (*R*)-phenylacetylcarbinol reactant, yielding diastereomeric product diols upon hydrogenation, were shown to depend on the size and shape of the Pt cluster. These observations highlight the role of catalyst particles in the emergence of (stereo)selectivity and entail additional challenge to the molecular modeling of asymmetric heterogeneous catalysis.

To account for the experimentally observed enantio- and diastereoselectivities on modified Pt catalysts, the thermodynamic stabilities of the hydrogen-bonded one-to-one reactant–modifier complexes and the energies of the keto carbonyl π and π^* orbitals of the reactant in those complexes (approximating the kinetic factor) were studied. Due to many feasible conformers of the cinchona alkaloid modifiers, several reactant–modifier interaction geometries were considered. The stereoselectivities arising from the hydrogenation of PPD and methyl pyruvate over Pt catalysts modified by CD and MeOCD (in toluene) could be reasonably well explained by the formation of bifurcated hydrogen-bonded complexes (in the gas phase), where the modifier adopted the so-called Open(3) conformer. However, the bifurcated interaction mode could not explain the experimentally observed change in enantioselectivity associated with the change of the solvent from toluene to acetic acid. Either these interaction geometries were not controlling enantiodifferentiation or the relatively simple explicit model to account for solvent effects was not sufficient. The computed proton affinities of various reactant molecules did not correlate with the experimentally observed enantioselectivities in acetic acid either. Modeling and understanding the solvent effects in asymmetric heterogeneous catalysis remains undoubtedly one of the greatest challenges in this research field.

Similarly to modifier conformations, some reactant–modifier interaction geometries were stable only on the metal surface. In fact, the QA-Open(4) conformer of protonated 10,11-dihydro-CD formed the most stable complex

with PPD on the Pt(111) surface. A complex involving C−H$\cdots$O=C interactions was also detected. This complex, which is congruent with McBreen's model, was the most stable one formed by the Open(3) conformer. These findings provided additional evidence on the important role of the Pt surface in stereodifferentiation. However, although the thermodynamic stabilities of the diastereomeric complexes were qualitatively in line with the excess formation of the (R) enantiomer, the relevance of the new types of interaction modes in enantiodifferentiation could not be confirmed as the hydrogenation reaction was not studied explicitly. It is possible that the reactant in the thermodynamically most stable complex undergoes hydrogenation too slowly to be relevant to the outcome of the catalytic reaction. Nevertheless, the study of molecule–surface interactions, which also ignored the hydrogenation itself, was able to explain the experimentally observed regioselectivities in the hydrogenation of PPD and 2,3-hexanedione on Pt.

Full potential energy profiles were determined for the hydrogenation of chiral α-hydroxyketones over unmodified Pt particles. The results implied the preference for the pairwise hydrogen addition mechanism over the stepwise mechanisms. The asymmetric induction was a result of the whole reaction path but qualitatively correct conclusions about diastereoselectivity could be made by considering the stable reaction intermediates only.

It is noted that the catalytic system was approximated in many ways in the present work. For example, the catalytic Pt surface was modeled by a flat (111) surface, whereas the true catalyst particles may be hemisphere-like with several different surfaces exposed. The coadsorbed hydrogen, solvent molecules, and other impurities, which are likely to be present on the Pt surface under catalytic conditions, were also ignored. Moreover, effects of reactant and modifier concentrations as well as the catalyst support were not considered. These issues provide interesting topics for future studies.

In conclusion, computational investigations gave valuable information about molecular-level interactions that may occur in stereoselective heterogeneous catalytic systems. Computations provided reasonable explanations for the experimentally observed selectivities in many cases. Thus, it is worthwhile to use molecular modeling tools to support experimental studies and to even assess selectivities of catalytic systems not tested experimentally. As the theoretical methods, algorithms, and computers continue to develop, computational studies of asymmetric heterogeneous catalysis become more and more important. The challenges lie in the complexity of the catalytic systems. Molecular modeling of asymmetric heterogeneous catalysis will continue to be balancing between the accuracy of the computational methods and the amount of details that can be included in the model systems.

Appendix A

Abbreviations

AO	atomic orbital
BSSE	basis set superposition error
CBS	complete basis set
CC	coupled cluster
CCSD	CC with single and double excitations
CD	cinchonidine
CGF	contracted Gaussian function
CI	configuration interaction
CN	cinchonine
COMPASS	condensed-phase optimized molecular potentials for atomistic simulation studies
COSMO	conductor-like screening model
CP	counterpoise
CPU	central processing unit
de	diastereomeric excess
DFT	density functional theory
DHCD	10,11-dihydrocinchonidine
DZ	double-zeta
ee	enantiomeric excess
ECP	effective core potential
EL	ethyl lactate
EP	ethyl pyruvate
ESP	electrostatic potential
FF	force field
GGA	generalized gradient approximation
Gn	Gaussian-n
GTO	Gaussian-type orbital

HF	Hartree–Fock
HK	Hohenberg–Kohn
KPL	ketopantolactone
KS	Kohn–Sham
LCAO	linear combination of atomic orbitals
LDA	local density approximation
LSDA	local spin density approximation
M	molar (mol dm^{-3})
MARI	multipole-accelerated-resolution-of-identity
MBC	methylbenzoylcarbinol
MeOCD	*O*-methylcinchonidine
MeOCN	*O*-methylcinchonine
MM	molecular mechanics
MO	molecular orbital
MP	methyl pyruvate
MPn	Møller–Plesset perturbation theory of order n
MPPT	Møller–Plesset perturbation theory
NMR	nuclear magnetic resonance
PA	proton affinity
PAC	phenylacetylcarbinol
PCM	polarized continuum model
PDMSODHCD	*O*-(propyldimethylsilyl)-10,11-dihydrocinchonidine
PES	potential energy surface
PhOCD	*O*-phenylcinchonidine
PhOCN	*O*-phenylcinchonine
PPD	1-phenyl-1,2-propanedione
QC	quantum chemistry
QM	quantum mechanics
RI	resolution-of-identity
ROHF	restricted open-shell HF
SCF	self-consistent field
SCRF	self-consistent reaction-field
SD	Slater determinant
STO	Slater-type orbital
SV	split-valence
TBDMSOCD	*O*-(*tert*-butyldimethylsilyl)cinchonidine
TS	transition state
TZ	triple-zeta
UHF	unrestricted HF
WFT	wave function theory
ZPV	zero-point vibration

Appendix B

Chirality, catalysis, and molecular modeling

In this chapter, additional information on chirality, catalysis, and molecular modeling is given. The three concepts are clarified and some remarks on their discovery, development and significance today are made.

B.1 Chirality

B.1.1 Concept of chirality

An object that is non-superimposable on its mirror image is said to be chiral. In terms of symmetry, the object is chiral if it does not have any S_n symmetry element (i.e., an n-fold rotation–reflection axis) with any value of n.[281] Otherwise the object is achiral (i.e., non-chiral). For example, gloves and shoes are chiral but mittens and socks are often achiral. Chiral objects are not necessarily devoid of all symmetry elements (i.e., asymmetric) since they may possess one or more rotation axes.

Chirality is often due to the presence of a stereogenic/chirality center in a molecule. For example, a carbon atom bonded to four different substituents, a so-called "asymmetric" carbon atom, is such a center (see Figure 1.1). However, the presence of a stereogenic center is neither a necessary nor sufficient condition for chirality. For example, 1,3-dimethylallene has no stereogenic center but is, nevertheless, chiral. On the other hand, there are compounds that contain stereogenic atoms but are still achiral. They are called *meso* compounds.

The physical properties such as melting points, boiling points and densi-

ties of the enantiomers (i.e., a chiral molecule and its mirror image isomer[†]) are identical except that one enantiomer rotates the plane of plane-polarized light clockwise, whereas the other enantiomer rotates the plane the same amount but in counterclockwise direction. The two enantiomers of a racemate have identical chemistries with achiral molecules but interact differently with other chiral molecules. This phenomenon is referred to as chiral discrimination or chiral recognition. An analogy from everyday life is that our left and right hands fit differently into a left-hand glove. Instead, they would grip a water bottle (an achiral object) equally.

Enantiomers belong to a class of isomers called stereoisomers[‡]. Diastereomers are stereoisomers not related as mirror images. They are characterized by differences in physical properties and by some differences in chemical behavior towards achiral as well as chiral compounds.[4] Conformational isomers are stereoisomers which are generated through rotations about chemical bonds. They can be either enantiomeric or diastereomeric. A stable conformation corresponding to a potential energy minimum is called a conformer.

Chemical reactions by which unequal amounts of two product stereoisomers are formed are called stereoselective. An enantioselective reaction involves the preferential formation of one enantiomer from a prochiral molecule, whereas a diastereoselective reaction yields an excess amount of one diastereomer by the creation of a new stereogenic center in a chiral molecule.[21] In an enantioselective catalytic reaction, the asymmetry is induced by a chiral catalyst (or environment), whereas a diastereselective catalytic reaction does not require a chiral catalyst.

In connection with stereoselective reactions, the terms enantiodifferentiation and diastereodifferentiation or, collectively, stereodifferentiation are often used. In this thesis, stereodifferentiation means differentiation of stereoheterotopic faces of a molecule by a reagent/catalyst. For example, the ketone shown in Figure 1.5 has stereoheterotopic faces provided that $R_1 \neq R_2$: the approach of hydrogen from one or the other face of the C=O double bond affords a pair of stereoisomers. Depending on whether the stereoisomers are enantiomers or diastereomers, the faces are enantiotopic or diastereotopic, respectively.

B.1.2 Discovery of chirality

The realization that some chemical compounds are chiral emerged from the discovery of optical activity by the French physicist Jean Baptiste Biot in

[†] Isomer is one of several chemical compounds that have the same composition (molecular formula) but different structure. [‡] Stereoisomers have identical identity and connectivity of their atoms, but differ in the arrangement of their atoms in space.[4]

the early years of the 19th century.[282,283] Biot noticed that some substances such as quartz crystals and certain organic liquids rotated the plane of plane-polarized light. In 1848, the French chemist and microbiologist Louis Pasteur connected optical activity to the dissymmetry of individual molecules. This dissymmetry was christened chirality by Lord Kelvin in 1904. Pasteur observed that the sodium ammonium salt of optically inactive paratartaric acid crystallized in two distinguishable mirror-image forms. When dissolved in water, they rotated the plane of plane-polarized light equal amounts but in opposite directions. Pasteur inferred that paratartaric acid consisted of equal amounts of tartaric acid molecules that were mirror images of each other. An explanation for molecular chirality was not clear until the idea of four valences of carbon atom by Friedrich August Kekulé in 1858 and direction of these valences towards the corners of a tetrahedron in 1874, independently suggested by Jacobus Henricus van't Hoff and Joseph Achille Le Bel. In the 20th century, it became clear that molecules may be chiral even if they do not contain any asymmetric carbon atoms.

B.2 Catalysis

B.2.1 Concept of catalysis

Chemical catalysis is the acceleration of the rate of a chemical reaction by the presence of a substance, the catalyst, that is itself not consumed in the reaction. The catalyst affects only the reaction kinetics, not the overall reaction thermodynamics, that is, the extent of the reaction.

Why are catalysts then needed? The rate of a reaction could also be enhanced by simply raising the temperature. However, if the activation barrier of the reaction is very high, the temperature required to achieve a reasonable rate of product formation may be so high that it leads to various problems: (a) the walls of the reaction vessel could fail, (b) the reaction could be so fast that it would get out of control and lead to explosion, (c) the cost of the energy needed to increase the temperature sufficiently high would become prohibitive, (d) some reactants may decompose into useless products.

The catalyst works by providing an alternative pathway and free-energy landscape for the reaction. By interacting with the reactants—forming chemical bonds with them—the catalyst provides different transition states with lower activation barriers compared to those of an uncatalyzed reaction (Figure B.1). The amount of energy needed to carry out a chemical reaction is thus reduced. Catalysis also allows to control the product distibution of chemical reactions (i.e., selectivity) by increasing the formation rates of de-

sired products and reducing those of undesired ones. The main advantages of catalysis are thus that the desired products are made faster, using fewer resources, and generating less waste.[84]

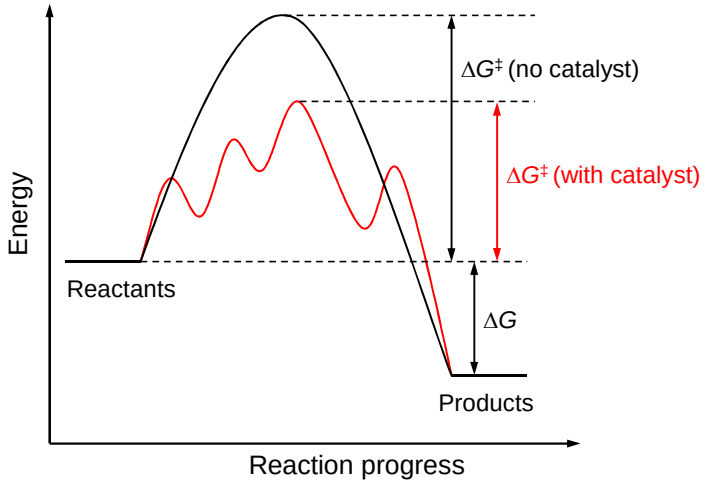

Figure B.1. Energy vs reaction coordinate for a catalyzed and non-catalyzed reaction.

There are many kinds of catalysts such as acids and bases, organometallic complexes, organic and inorganic polymers, supported metal particles, and enzymes.[84] Catalysis can be classified into three different categories: homogeneous catalysis, heterogeneous catalysis, and biocatalysis. In homogeneous catalysis the catalyst and the reactants are molecularly dispersed in the same phase, most commonly liquid. Heterogeneous catalysis covers all the cases where the catalyst and reactants are in different phases; usually the catalysts are solids and the reactants liquids or gases. In biocatalytic processes, isolated Nature's catalysts, enzymes, or whole microorganisms (e.g., bacteria) are utilized.

B.2.2 Discovery of catalysis

Catalytic processes have been important for mankind for thousands of years. For example, production of food and beverages such as cheese, wine, and beer have relied on the effects of microorganisms. However, catalysis as a scientific discipline started not before the first decades of the 19th century.[284] The starting point can be considered year 1814 when the Russian chemist Gottlieb Kirchhoff recognized that acids enable the hydrolysis of starch to a sugar

(glucose).[285] A few years later it was found that hydrogen can be oxidized by fine platinum powder even at room temperature. The first technological application of this discovery was a lighter invented by the German chemist Johann Döbereiner in 1823.[286] The terms catalysis and catalyst were coined by the Swedish chemist Jöns Jacob Berzelius in 1835.

At the end of the 19th century a rich chemical knowledge of catalysis existed. However, the field started to develop mainly in the 20th century due to the advances in chemical thermodynamics and kinetics made by Jacobus van't Hoff, Svante Arrhenius, and Friedrich Ostwald who were awarded the Nobel Price in 1901, 1903, and 1909, respectively.[285] Later, many such large-scale catalytic industrial processes were invented that are used even today to prepare bulk chemicals, for example, Haber–Bosch process for ammonia synthesis in 1909, Fischer–Tropsch process for synthesis of hydrocarbons in 1930, and Ziegler–Natta catalysis for polymers in 1953. Catalysis is still a strongly developing field as witnessed by the recent Nobel Prices, awarded to Y. Chauvin, R. H. Grubbs, and R. R. Schrock for the development of the metathesis method in organic synthesis in 2005 and to G. Ertl for his studies of chemical processes on solid surfaces in 2007.

B.2.3 Significance of catalysis

Chemical catalysis affects our lives in numerous ways. Enzymes make possible essentially all biochemical reactions which are necessary for living. Catalysts are used to produce foodstuffs, clothes, medicines, cosmetics, fuels, and other materials.[26,253] Catalysis-based chemical synthesis accounts for 60% of chemical products and 90% of current chemical processes.[287]

Today, mankind faces a variety of challenges in creating alternative fuels, reducing harmful by-products in manufacturing, cleaning up the environment and preventing future pollution, dealing with the causes of global warming, protecting people from toxic substances and infectious agents, and creating safe pharmaceuticals.[26] Catalysis offers a way to eliminate or at least substantially reduce pollution from chemical processes and vehicular emissions. Dealing with CO_2 emissions is a great challenge and requires new catalytic methods that can reduce CO_2. More active catalysts would lower dramatically the temperature and, consequently, the energy demands of inefficient chemical processes. For example, synthesis of ammonia, a major ingredient of dynamite and agricultural fertilizers, and petroleum reforming are huge energy consumers. 110 million tons of ammonia was produced in 2005, accounting for 1% of the global energy consumption.[84]

One of the major challenges facing mankind is the production of energy resources. Catalysis is likely to play an important role in it because, for

the present and foreseeable future, the major source of energy is found in chemical bonds.[26,288] Novel catalysts are needed for use in new conversion technologies such as fuel cells and devices for photolytic splitting of water to form hydrogen and oxygen. Chemical and biological catalysts that convert renewable bio-based feedstocks into fuels and chemicals are very attractive from the environmental standpoint.

All in all, catalysis-based technology will be of great significance in the future. Being able to understand and thereby control the relationship between catalyst structure and catalytic activity and selectivity is the grand challenge for catalysis science in the 21st century.[26] It requires a fundamental atomic-scale and nanoscale understanding of catalysis. Meeting the grand challenge will allow the design of new catalysts and catalytic processes that approach the ultimate goal of highly active, stable catalysts which provide near-100% selectivity to a desired product with minimal use of energy. Success in this endeavor will result in deeper insights in the catalysis and in the development of new technology that will benefit society in ways that today are almost unimaginable.[26]

B.3 Molecular modeling

B.3.1 Concept of molecular modeling

Computational science is a field that uses advanced computational capabilities to understand and solve complex problems and phenomena. Due to the revolution of information technology, computational science has emerged as a basic tool of scientific inquiry besides experiments and theory, and is becoming more and more important in all disciplines. Perhaps the most significant feature of computational science is that it enables such problems to be investigated that would otherwise be impractical or impossible to address, like forecasting the weather. In addition, computer simulations can yield considerable savings by replacing expensive and time-consuming experiments. Computational technologies have also developed into an important tool in almost all areas of chemistry and chemical industry and have many applications ranging from molecular modeling to the simulation and control of chemical processes.[289] For example, computational methods are used in drug design in the pharmaceutical industry and in modeling atmospheric chemistry, thus having an important role in the study of climate change.[289]

Molecular modeling deals with investigation of molecules and molecular systems by theoretical or computational techniques. It involves a mathematical description of the system which at the most basic molecular level means

solving the (non-relativistic) Schrödinger equation or the (relativistic) Dirac equation for electronic and/or nuclear motion, or Newton's equations for motion of atoms. As a correct description of a particular phenomenon through mathematical equations or algorithms may require millions or billions of calculations, most phenomena could not be studied without computers. Molecular modeling is thus often considered synonymous with computational chemistry. The increasing power of computers and better algorithms constantly extend the range of models and systems that can be studied.

Molecular modeling can give quantitative information about the physical and chemical phenomena of the system at different length and time scales. At the quantum/electronic scale, first-principles (ab initio) electronic structure calculations can provide, for example, ground state or excited state energies, molecular geometries, dipole moments, and spectroscopic data of chemical species. Chemical system of hundreds of atoms can be modeled at this scale. The results of quantum mechanical calculations can be used to provide a connection to more approximate atomic/molecular scale computations, which can handle systems up to millions of atoms, depending on the time scale. These computations are usually performed by molecular dynamics or Monte Carlo methods. Properties described at this scale range from structure and thermodynamic properties (pressures, phase equilibria, etc.) to sorption and transport properties (mass and heat transfer).

The results from the atomic scale calculations can in turn be applied to describe behavior at the mesoscale, that is, between atomic calculations and the continuum assumption of traditional materials engineering.[289] The mesoscale computations are intended to describe properties of systems that still reflect molecular composition of material but consist of too many, even billions or trillions of atoms to calculate atom by atom. These calculations usually cover time scales over 100 ns and length scales from 10 nm to 10 μm. The upper bound of the length scale is the one at which the material behaves as an effective continuous medium. No theory has been developed yet to fully describe the phenomena at the mesoscale, and current models extrapolate calculations from either the atomic or bulk scales and involve a lot of empiricism.[289] The breadth and power of molecular modeling applied to complex chemical systems has been illustrated, for example, in the publications of the third *JACS* Select issue.[290]

B.3.2 Development of molecular modeling

The theoretical groundwork of computational chemistry (molecular modeling) was laid down by the development of quantum mechanics in the 1920s. However, at that time the mathematical relations of quantum mechanics were

too complicated to be handled for such complex systems as molecules. One of the founders of quantum mechanics, Paul Dirac, expressed the problem in his famous remark in 1929:[291] "The fundamental laws necessary for the mathematical treatment of large parts of physics and the whole of chemistry are thus fully known, and the difficulty lies only in the fact that application of these laws leads to equations that are too complex to be solved." Modern computational chemistry has been considered to have started in the 1960s when computers came into use for solving these equations.[292] Since then computational methods and codes have developed enormously and the consequences have revolutionalized the whole of chemistry. This was recognized in 1998 by awarding the Nobel Prize to Walter Kohn and John A. Pople for their development of the density functional theory and computational methods in quantum chemistry, respectively.[293,294]

B.3.3 Molecular modeling of catalysis

One of the main goals in catalytic science is to be able to design rationally, rather than discover more or less randomly, new and improved catalytic systems (the catalyst and the catalytic process) with desired properties. Two grand challenges have been identified as integral in achieving this goal: (a) understanding mechanisms and dynamics of catalyzed transformations and (b) design and controlled synthesis of catalytic structures.[288] Multidisciplinary advances in chemistry, materials science, engineering, and physics are required to meet these challenges.

Detailed understanding of the mechanism and kinetics of the individual reaction steps comprising the catalytic cycle is the key to effectively design new catalysts and improve the existing ones. In this endeavor, theoretical and computational methods are crucial. It is extremely difficult to obtain all the necessary details of catalytic reactions from currently available experimental techniques, especially for transition state regions that are visited for extremely short times.[288] In addition, the experimental methods are almost exclusively based on techniques that provide an average value for a quantity over all catalytically active sites. Instead, molecular modeling can provide fundamental aspects (energetics, dynamics, etc.) of reactions at individual active sites. Whole reaction pathways from the reactants, through all transition states and intermediates, to products including the effects of reaction environment can be studied. Consequently, molecular modeling can help to understand the relationship between catalytic activity/selectivity and the local structure/composition of single sites.

Catalysis provides many challenges for molecular modeling. Many of the most important industrial catalysts are composed of nanoparticles dispersed

on a support material. The size and shape of the metal particles, defect sites (steps, kinks, etc.) on the metal surface, the support, pressure, and solvent may all influence surface coverage and composition as well as the structure and activity of chemical species considerably. Thus, the environmental factors play an important role in catalyst activity and selectivity and should be taken into consideration. In addition, the working catalyst is an intricate, dynamic entity that can change continuously. The success in modeling catalytic systems depends not only on the accuracy of the methods employed but also on the reality of the model studied.

The complete understanding of the electronic, molecular, and mesoscale phenomena of catalysis requires a multiscale approach that can simulate the myriads of atomic scale transformations occurring on the catalyst surface as a function of time, processing conditions as well as catalyst structure and composition. The multiscale approach would cover time scale ranging from 10^{-15} s for electronic transitions to even months or years for deactivation phenomena, and length scale from picometers to meters.[253] The current theoretical and computational methods are far from this scope and, therefore, new and improved simulation methods are needed.[26,288] At the electronic scale, for example, the goal is to develop a method that can provide accurate (within 5 kJ mol^{-1}) predictions of ground- and transition-state energies routinely for molecules and catalysts involving tens to hundreds of atoms.[288] With currently available density functionals, the computed adsorption and reaction energies are typically within 20–35 kJ mol^{-1} of the experimental results.[253] Methods used to simulate processes occurring at various length and time scales in heterogeneous catalysis have been reviewed in the literature.[215,253,295–303]

Accurate calculations (< 4.0 kJ mol^{-1} error in thermodynamics, $< 50\%$ error in reaction rates) have been estimated to require computing power of 250 teraflops[†] for heterogeneous catalysts in vacuum and 1000 teraflops for heterogeneous catalysts in the presence of gases and liquids.[26] This is quite far from what currently can be done routinely. Nevertheless, the computations have already enhanced the understanding of catalysis and are becoming reliable enough for the development of quantitative concepts that can be used to search for new processes and catalysts (see, e.g., ref 105). As computers, software, and algorithms continue to develop, the computational tools will become more and more important.

[†] According to the list of most powerful computers, the maximal LINPACK performance of the ten highest performance supercomputers in the world vary between 430 and 1760 teraflops.[304]

Appendix C

Details of computational methods

In this chapter, details of the computational methods applied in the thesis are given. First, some basic concepts in quantum mechanics and quantum chemistry are considered. After that, the theory behind various methods is presented. The methods based on quantum mechanics (QM) are discussed in Sections C.1–C.8 and the molecular mechanics (MM) methods in Section C.9. More information about the methods can be found in the literature.[183–185,238,305–313]

C.1 Foundations of quantum chemistry

C.1.1 Introduction

According to the present knowledge, there exist four fundamental interactions/forces in the universe: electromagnetic (incl. electrostatic), gravitational, strong interaction, and weak interaction.[308] Electromagnetism is the force that acts between electrically charged particles and is the only force that needs to be considered in the context of chemical phenomena—the other ones are much weaker or too short-ranged to have any effect.[308]

It is believed that the underlying physical laws necessary for the mathematical theory of a large part of physics and the whole of chemistry are completely known.[291] For example, the dynamics of the particles (nuclei and electrons) is governed by relativistic quantum mechanics and the interactions between particles by quantum electrodynamics. QM is today the most significant and the most successful theory that has been constructed to describe Nature. It is a general theory and is presumed to apply to everything, from subatomic particles to galaxies. The concept of quantum emerged from the problematics of black-body radiation in 1900. The foundations of QM

were established during the first half of the 20th century. Some fundamental aspects of the theory are still actively studied.

Quantum chemistry (QC) is a field that applies quantum mechanics to problems in chemistry. QM methods are used to calculate molecular properties (e.g., bond lengths and bond angles, dipole moments, barriers to internal rotation, relative stabilities of conformers) and thermodynamic properties (e.g., entropy, heat capacity), to analyze spectra (IR, NMR), to investigate the mechanism of chemical reactions, and to understand intermolecular interactions.

C.1.2 Basic theoretical concepts in quantum mechanics

QM is formulated in a well-defined mathematical language which, however, is much more abstract and less intuitive than that of classical mechanics. The whole of QM can be expressed in terms of a small set of postulates. When their consequences are developed, they embrace the behaviour of all known forms of matter, including the molecules, atoms, and electrons that are at the centre of QC.

In the traditional Hilbert space formalism of QM, each physical system $\mathcal{S}$ (e.g., a molecule) is associated with a complex, separable and often infinite-dimensional Hilbert space $\mathcal{H}$[†]. Each physical observable, dynamical variable $\mathbf{R}$ of the system $\mathcal{S}$ is represented by a self-adjoint operator R on $\mathcal{H}$. For example, the total energy E of the system is represented by the Hamiltonian operator H (see Section C.1.3). Further, each state of the system is represented by a state operator ρ which is nonnegative and of unit trace. When the system $\mathcal{S}$ is in the state represented by ρ, the average value of the observable $\mathbf{R}$ in a series of measurements is equal to the expectation value of the corresponding operator

$$\langle \mathbf{R} \rangle = \mathrm{Exp}(R, \rho) = \mathrm{tr}[\rho R] \tag{C.1.1}$$

where "tr" means "trace". If the state ρ is pure, that is, $\rho = |\Psi\rangle\langle\Psi|$, where the unit-normed vector $\Psi \in \mathcal{H}$ is called the state vector (also called state function or wave function especially in QC), then the average value of the observable $\mathbf{R}$ in the state is

$$\mathrm{Exp}(R, \rho) = \langle \Psi | R | \Psi \rangle \ . \tag{C.1.2}$$

If the operator R has a purely discrete spectrum it may be expressed in terms

[†] See, e.g., refs 305 and 306 for the definition of Hilbert space and other concepts in this section.

of its eigenvalues r_i and orthonormal eigenvectors $|r_{ij}\rangle$ as

$$R = \sum_{ij} r_i |r_{ij}\rangle\langle r_{ij}| \tag{C.1.3}$$

where i enumerates the eigenspaces and j enumerates the basis of every eigenspace. The eigenvalues r_i ($\in \mathbb{R}$) of the operator R are the possible measured values of $\mathbf{R}$ and their probabilities are

$$\text{Prob}(\mathbf{R} = r_i|\Psi) = \sum_j |\langle r_{ij}|\Psi\rangle|^2 \ . \tag{C.1.4}$$

Solving the eigenvalue equation

$$R|r_{ij}\rangle = r_i|r_{ij}\rangle \tag{C.1.5}$$

is one of the most important problems in QM and QC.

C.1.3 Schrödinger equation

In QC the goal is often to solve the non-relativistic, time-independent Schrödinger equation

$$H\Phi = E\,\Phi \tag{C.1.6}$$

where H is the Hamiltonian operator for the system, Φ is an eigenstate of the system and E is the total energy of that eigenstate. The most general form of the Hamiltonian H for a spinless particle is the sum of the kinetic and potential energy operators

$$H = \frac{(\mathbf{P} - \mathbf{A})^2}{2m} + W(\mathbf{Q}) \tag{C.1.7}$$

where $\mathbf{P}$, $\mathbf{Q}$, $\mathbf{A}(\mathbf{Q})$ and W($\mathbf{Q}$) are operators for the momentum, position, vector potential and scalar potential, respectively, and m is the mass of the particle. Despite its simple form, analytical solutions to the Schrödinger equation can be obtained only for relative simple systems such as harmonic oscillator and hydrogen atom. For most systems, one must resort to approximate solutions. All the quantum chemical methods presented in this chapter are used to find an approximate solution to the Schrödinger equation.

In coordinate representation of an abstract linear vector space $\mathcal{H}$, the state vector Φ is represented by a "wave" function of a continuous variable $\phi(\mathbf{x})$ and the actions of the position and momentum operators are

$$\mathbf{Q}\phi(\mathbf{x}) = \mathbf{x}\phi(\mathbf{x}) \tag{C.1.8}$$

and

$$\mathbf{P}\phi(\mathbf{x}) = -i\hbar\boldsymbol{\nabla}\phi(\mathbf{x}) \tag{C.1.9}$$

where $\boldsymbol{\nabla}$ is the del operator.

For a system of N particles, the state vector Φ is represented by a function of many variables, $\Phi(\mathbf{x}_1, \ldots, \mathbf{x}_N)$, and its interpretation is as a statistical state function in an abstract $3N$-dimensional configuration space, a function from which probability distributions for all observables may be calculated. In particular, $|\Phi(\mathbf{x}_1, \ldots, \mathbf{x}_N)|^2$ is the probability density in configuration space for particle 1 being at the position $\mathbf{x}_1$, particle 2 being at $\mathbf{x}_2$, etc. The Hamiltonian is the sum of the single particle kinetic and potential energies plus the interparticle interaction $V(\mathbf{x}_1, \ldots, \mathbf{x}_N)$. If there is no vector field (and, hence, no magnetic field), the Hamiltonian for N particles in the scalar potential $\sum_{n=1}^{N} W(\mathbf{x}_n)$ becomes

$$H = \left[\sum_{n=1}^{N} \frac{-\hbar^2}{2M_n} \nabla_n^2 + \sum_{n=1}^{N} W(\mathbf{x}_n) + V(\mathbf{x}_1, \ldots, \mathbf{x}_N) \right] . \tag{C.1.10}$$

Typical form of the Hamiltonian operator in QC takes into account five contributions to the total energy of the chemical system: the kinetic energies of the electrons and nuclei, the attraction of the electrons to the nuclei, and the interelectronic and internuclear repulsion. Other terms are required in the Hamiltonian in more complicated situations, for example in the presence of an external electric and/or magnetic field, in the event of significant spin–orbit coupling in heavy elements, etc. In atomic units (see Section C.1.4), the Hamiltonian for a system consisting of N electrons and M nuclei is

$$\begin{aligned} H = &- \sum_{i=1}^{N} \frac{1}{2} \nabla_i^2 - \sum_{A=1}^{M} \frac{1}{2M_A} \nabla_A^2 - \sum_{i=1}^{N} \sum_{A=1}^{M} \frac{Z_A}{r_{iA}} \\ &+ \sum_{i=1}^{N} \sum_{i>j}^{N} \frac{1}{r_{ij}} + \sum_{A=1}^{M} \sum_{A>B}^{M} \frac{Z_A Z_B}{R_{AB}} \end{aligned} \tag{C.1.11}$$

where i and j run over electrons, A and B run over nuclei, M_A is the ratio of the mass of nucleus A to the mass of an electron, Z_A is the atomic number of the nucleus A, ∇^2 is the Laplacian operator, and r_{pq} (as well as R_{pq}) is the distance between particles p and q.

C.1.4 Atomic units

The quantum chemical equations describing molecules and atoms can be rendered more clearly by working in atomic units (a.u.), where the charge of

the proton (e), the mass of the electron (m_e), $\hbar$ (Planck's constant h divided by 2π), and $4\pi\varepsilon_0$ (ε_0 is the permittivity of the vacuum) are all defined to have magnitude 1. For example, one atomic unit of length (bohr) equals ca. 5.2918×10^{-11} m, and one atomic unit of energy (hartree, E_h) equals ca. $4.3597 \times 10^{-18}\mathrm{J} \equiv 2625.5$ kJ mol^{-1}. Henceforth, all equations in this chapter will be expressed in a.u. unless otherwise stated.

C.1.5 Born–Oppenheimer approximation

Accurate wave functions for many-particle molecular systems are extremely difficult to express because of the correlated motion of particles. The Hamiltonian (C.1.11) contains pairwise attraction and repulsion terms, implying that no particle is moving independently of all of the others. The Born–Oppenheimer approximation is the first of several approximations used to simplify the solution of the Schrödinger equation.

As nuclei are much, typically thousands of times heavier than electrons, they move much more slowly. Because of this, the electrons can respond almost instantaneously to the displacement of the nuclei. Hence, to a good approximation, electronic motion can be decoupled from nuclear motion, that is, one can consider the electrons in a molecule moving in the field of fixed nuclear positions. As a result, the nuclear kinetic energy term is taken to be independent of the electrons, correlation in the attractive electron–nuclear potential energy term is eliminated, and the repulsive nuclear–nuclear potential energy term becomes a constant for a given geometry. The electronic Hamiltonian describing the motion of N electrons in the field of M point charges is

$$H_\mathrm{el} = -\sum_{i=1}^{N} \frac{1}{2}\nabla_i^2 - \sum_{i=1}^{N}\sum_{A=1}^{M} \frac{Z_A}{r_{iA}} + \sum_{i=1}^{N}\sum_{i>j}^{N} \frac{1}{r_{ij}} \,. \tag{C.1.12}$$

The solution to the Schrödinger equation involving the electronic Hamiltonian

$$H_\mathrm{el}\Phi_\mathrm{el} = E_\mathrm{el}\Phi_\mathrm{el} \tag{C.1.13}$$

is the electronic wave function $\Phi_\mathrm{el}(\{\mathbf{x}_i\};\{\mathbf{X}_A\})$ where the electronic coordinates $\{\mathbf{x}_i\}$ are independent variables but the nuclear coordinates $\{\mathbf{X}_A\}$ are only parameters. The total energy for fixed nuclei also includes the constant nuclear repulsion:

$$E_\mathrm{tot} = E_\mathrm{el} + \sum_{A=1}^{M}\sum_{A>B}^{M} \frac{Z_A Z_B}{R_{AB}} \,. \tag{C.1.14}$$

E_{tot} of Eq. (C.1.14) is usually called the total energy or the total electronic energy whereas E_{el} is the pure electronic energy. After the electronic problem of equations (C.1.12) to (C.1.14) has been solved, it is subsequently possible to solve the motion of the nuclei (describing the vibration, rotation, and translation) of a molecule. Henceforth, only the electronic problem and, thus, electronic Hamiltonians and wave functions will be considered and the subscript "el" will be dropped. Where it is convenient or necessary, a distinction between E_{el} and E_{tot} is made.

In general, the Born–Oppenheimer approximation is extremely mild one and is justified in most cases. With this approximation, one can for example construct a potential energy surface (PES[†]) for a molecule and identify the equilibrium geometry of the molecule with the lowest point on this surface.

C.1.6 Pauli principle

Electrons are particles having a spin of $\frac{1}{2}$. Spin is a natural consequence of the application of Einstein's theory of special relativity in the equations of QM as first shown by Dirac. The electron spin function is an eigenfunction of the operator S_z and has two eigenvalues, $m_s = \pm\hbar/2$, which correspond to the orthonormal spin eigenfunctions $\alpha(\omega)$ and $\beta(\omega)$ corresponding spin up, $\uparrow$, and spin down, $\downarrow$, respectively. The electron is described not only by its spatial coordinates $\mathbf{x}$ but also by its spin coordinate ω, which are denoted collectively by $\mathbf{q} = (\mathbf{x}, \omega)$. Particles with half-integral spin (i.e., fermions) require antisymmetric wave functions and, thus, a many-electron wave function must change sign whenever the coordinates $\mathbf{q}$ of any two electrons are interchanged

$$\Phi(\mathbf{q}_1, \ldots, \mathbf{q}_i, \ldots, \mathbf{q}_j, \ldots, \mathbf{q}_N) = -\Phi(\mathbf{q}_1, \ldots, \mathbf{q}_j, \ldots, \mathbf{q}_i, \ldots, \mathbf{q}_N) \; . \quad \text{(C.1.15)}$$

This requirement is sometimes called the antisymmetry principle. It is a general statement of the Pauli exclusion principle which states that no two electrons can occupy the same state, or equivalently, that all quantum numbers of two electrons cannot be equal.

The antisymmetry of the wave function can be achieved by building it from Slater determinants[‡] (SD). For the general case of N electrons and N spin orbitals, the Slater determinant is given as

[†] PES is the surface defined by E_{tot} over all possible nuclear coordinates. [‡] A single Slater determinant is the simplest antisymmetric wave function, which can be used to describe the ground state of a many-electron system.

$$\Phi_{\mathrm{SD}} = \frac{1}{\sqrt{N!}} \begin{vmatrix} \chi_1(1) & \chi_2(1) & \cdots & \chi_N(1) \\ \chi_1(2) & \chi_2(2) & \cdots & \chi_N(2) \\ \vdots & \vdots & & \vdots \\ \chi_1(N) & \chi_2(N) & \cdots & \chi_N(N) \end{vmatrix} \tag{C.1.16}$$

where the factor $(N!)^{-1/2}$ is a normalization factor. The columns in the SD are one-electron wave functions (spin orbitals) which are called molecular orbitals (MO) for molecules. Spin orbitals are a product of a spatial orbital and a spin function

$$\chi(\mathbf{q}) = \begin{cases} \phi(\mathbf{x})\alpha(\omega) \\ \quad \text{or} \\ \phi(\mathbf{x})\beta(\omega) \end{cases} . \tag{C.1.17}$$

In (C.1.16), the orbital χ_j occupied by electron i with coordinate $\mathbf{q}_i$ is denoted as $\chi_j(i)$. Therefore, the electron coordinates are along the rows in the SD.

C.1.7 Variational theorem

The Schrödinger equation cannot be solved exactly for atoms or molecules with a few exceptions. However, the so-called variational method can be used to systematically find the exact ground state of a system. This method is based on the variational theorem which states that if E_0 is the lowest eigenvalue of the Hamiltonian H (i.e., the exact ground state energy), then for any normalizable trial function Φ the inequality

$$E_0 \leq \frac{\langle \Phi | H | \Phi \rangle}{\langle \Phi | \Phi \rangle} \quad \left(= \frac{\int \Phi^* H \Phi \, d\tau}{\int \Phi^* \Phi \, d\tau} \right) \tag{C.1.18}$$

holds. In words, the energy computed from any approximate trial wave function is an upper bound to the the exact ground state energy. The equality holds only if the wave function is the exact function. The variational method, applied to define the ground state wave function and energy of a system, consists of choosing, for example, a trial function Φ that depends on one or more parameters. Those parameters are varied to obtain the lowest value of the expression on the right hand side of (C.1.18). Regardless of how the trial functions are constructed, the theorem guarantees that the quality of the guess will be determined by how low value is obtained.

In practice, it is impossible to go through all possible and acceptable N-electron wave functions when searching for the best approximation for the true wave function of the system under consideration. First, one has to make an assumption of the form of the wave function and then try to find such a wave function which is as close as possible to the true wave function.

C.2 Hartree–Fock method

In the Hartree–Fock (HF) approximation, the trial N-electron wave function is taken to consist of a single SD. The spin orbitals that give the 'best' wave function are found by minimizing the electronic energy of the wave function (corresponding to the Hamiltonian in Eq. (C.1.12)) subject to the orthonormalization constraint of the orbitals. This procedure gives the Hartree–Fock equations

$$f_i\chi_i = \varepsilon_i\chi_i \qquad i = 1, 2, \ldots, N \tag{C.2.1}$$

where ε_i is the energy of the spin orbital χ_i and

$$f_i = h_i + \sum_{j=1}^{N}(J_j - K_j) \tag{C.2.2}$$

is the Fock operator. It is an effective one-electron energy operator which describes the kinetic energy of an electron and its attraction to all the nuclei and repulsion to all the other electrons. The one-electron core-Hamiltonian, coulomb, and exchange operators in (C.2.2) are defined by

$$h_1\,\chi_i(1) = \left[-\frac{1}{2}\nabla_1^2 - \sum_{A=1}^{M}\frac{Z_A}{r_{1A}}\right]\chi_i(1) \tag{C.2.3}$$

$$J_j\,\chi_i(1) = \int |\chi_j(2)|^2 \frac{1}{r_{12}}\chi_i(1)\,d\mathbf{q}_2 \tag{C.2.4}$$

$$K_j\,\chi_i(1) = \int \chi_j^*(2)\chi_i(2)\frac{1}{r_{12}}\chi_j(1)\,d\mathbf{q}_2\ . \tag{C.2.5}$$

The HF equations form a set of pseudo-eigenvalue equations, as the Fock operator depends on all the occupied spin orbitals (via J_j and K_j) and, thus, the solutions of (C.2.1). Therefore, iterative methods must be imployed for determining the orbitals. The technique is called the self-consistent field (SCF) method.

The HF equations can be solved numerically only for small highly symmetric systems like atoms. Essentially all calculations use a basis set expansion to express the unknown spatial parts of the spin orbitals in terms of known functions. Any type of basis functions may in principle be used: exponential, Gaussian, polynomial, plane wave etc. The chosen basis functions should have a behaviour which agrees with the physics of the problem. At the same time, all the required integrals should be easy to calculate. The basis sets are discussed further in Section C.3.

If a set of K basis functions $\{\eta_\nu(\mathbf{x})|\nu = 1, 2, \ldots, K\}$, located on the nuclei, is chosen, each MO ϕ_i can be expanded as a linear combination of the basis functions

$$\phi_i = \sum_{\nu=1}^{K} c_{\nu i}\eta_\nu \qquad i = 1, 2, \ldots, K \ . \tag{C.2.6}$$

Conventionally, these basis functions are called atomic orbitals (AOs) and the procedure is called linear combination of atomic orbitals (LCAO). To exactly represent the MOs $\{\phi_i\}$, a complete set (i.e., an infinite number) of basis functions η_ν would be required. In that limit called the HF limit, the results are identical to those obtained by the numerical HF method. However, if K is large enough and the functions η_ν well chosen, one can present the MOs with negligible error.

By using the LCAO procedure, the problem of calculating the HF spin orbitals from (C.2.1) reduces to the problem of calculating the set of expansion coefficients $c_{\nu i}$ from the Roothaan equations† which can be expressed as a single matrix equation

$$\mathbf{FC} = \mathbf{SC}\boldsymbol{\varepsilon} \ . \tag{C.2.7}$$

In (C.2.7), $\mathbf{C}$ is a $K \times K$ matrix of the expansion coefficients $c_{\nu i}$ and $\boldsymbol{\varepsilon}$ is a diagonal matrix of the orbital energies ε_i. The overlap matrix $\mathbf{S}$ has the elements

$$S_{\mu\nu} = \int \eta_\mu^*(1)\eta_\nu(1)\, d\mathbf{x}_1 \tag{C.2.8}$$

and the Fock matrix $\mathbf{F}$ has the elements

$$F_{\mu\nu} = H_{\mu\nu}^{\text{core}} + \sum_{\lambda,\sigma=1}^{K} D_{\lambda\sigma}\Big[(\mu\nu|\sigma\lambda) - \frac{1}{2}(\mu\lambda|\sigma\nu)\Big] \tag{C.2.9}$$

where

$$H_{\mu\nu}^{\text{core}} = \int \eta_\mu^*(1)h_1\eta_\nu(1)d\mathbf{x}_1 \tag{C.2.10}$$

are the one-electron elements of the core-Hamiltonian matrix $\mathbf{H}^{\text{core}}$,

$$D_{\lambda\sigma} = 2\sum_{j=1}^{N/2} c_{\lambda j}c_{\sigma j}^* \tag{C.2.11}$$

are the density matrix elements, which are interpreted as the total electron density in the overlap region of η_λ and η_σ, and

$$(\mu\nu|\sigma\lambda) = \iint \eta_\mu^*(1)\eta_\nu(1)\frac{1}{r_{12}}\eta_\sigma^*(2)\eta_\lambda(2)d\mathbf{x}_1 d\mathbf{x}_2 \tag{C.2.12}$$

† The Roothaan equations apply to a restricted closed shell system, see page 94. For unrestricted systems, analogous Pople–Nesbet equations are used.

are two-electron integrals. $\mathbf{H}^{\text{core}}$ needs to be evaluated only once as it remains unchanged during the iterative calculation. However, the density matrix needs to be re-evaluated at each iteration. At convergence, the energy of the system

$$E_0^{\text{HF}} = \frac{1}{2}\sum_{\mu\nu} D_{\mu\nu}(H_{\mu\nu}^{\text{core}} + F_{\mu\nu}) \tag{C.2.13}$$

is at a minimum, and the potential/field generated by the SCF electron density is identical to that produced by solving for the electron distribution (to within a certain threshold).

Solving the Roothaan equations produces a total of K spatial MOs, of which $N/2$ are occupied and $K - N/2$ are unoccupied (virtual). For K basis functions, the number of one-electron and two-electron integrals to evaluate is of the order of K^2 and K^4, respectively. Even small basis sets for moderately-sized molecules can rapidly approach millions of two-electron integrals. Their efficient evaluation and manipulation is the major difficulty in an HF–SCF calculation.

The main chemical limitation of the HF theory is the one-electron nature of the Fock operator. All electron correlation except exchange is ignored; each electron sees all the other electrons as an average distribution. Higher-level methods attempt to remedy this neglect in various ways shown in the next sections.

Restricted and unrestricted HF

The vast majority of all 'normal' compounds, such as water, methane and most other ground state species in organic or inorganic chemistry, have even number of electrons which are all paired to give a singlet type of wave function (a closed shell system). In such instances the restriction that each spatial orbital should have two electrons, one with α and one with β spin, is normally made. Such wave functions are called restricted Hartree–Fock (RHF) wave functions. The RHF picture is inadequate in open-shell situations where the system contains an odd number of electrons (e.g., methyl radical) or the system has an even number of electrons but not all electrons occupy the spatial orbitals pairwise (e.g., the triplet ground state of methylene CH_2). There are two possibilities to treat such systems within the HF approximation. In the restricted open-shell Hartree–Fock (ROHF) method, the electrons that are paired with each other are forced to occupy the same spatial orbital. In the unrestricted Hartree–Fock (UHF) formalism, each spin orbital is allowed to have its own spatial part and orbital energy. The energy of a UHF wave function is always lower than or equal to a corresponding R(O)HF type wave

function. For singlet states near the equilibrium geometry, it is usually not possible to lower the energy of the system by allowing the α and β MOs to be different.

C.3 Basis sets

The basis functions used to represent spin orbitals should be of a proper functional form and the number of them should be small enough to minimize the computational effort for the evaluation of the two-electron integrals, for example, in the HF method. At the same time, the error due to the incompleteness of the basis should be small.

Slater-type orbitals (STOs) are attractive basis functions primarily because they closely resemble the atomic orbitals of the hydrogen atom. However, the four-index integrals (C.2.12) can only be solved numerically which is more difficult than analytical solution. This fact severely limits the utility of STOs in molecular systems of any significant size. In the Gaussian-type orbitals (GTOs) the radial decay of the STOs is changed from e^{-r} to e^{-r^2} which allows the analytical solution of the general four-index integral. In order to combine the best feature of GTOs (computational efficiency) with that of STOs (proper radial shape), several GTOs are often combined linearly together to form contracted Gaussian functions (CGFs).

The simplest type of basis set is a minimal basis set in which one basis function or CGF is used to represent each of the atomic orbitals. Such is, for example, the STO-3G basis set (Slater-Type Orbital approximated by 3 Gaussians). Accurate calculations need more extensive basis sets. A significant improvement is achieved by adopting a double-zeta (DZ) or triple-zeta (TZ) basis set, in which each basis function in the minimal basis set is replaced by two or three basis functions, respectively.

A split-valence (SV) basis set is a compromise between the inadequacy of a minimal basis set and the computational demands of DZ and TZ basis sets. Each valence shell atomic orbital is represented by two basis functions while each inner-shell atomic orbital is represented by a single basis function. Typical examples are 3-21G and 6-31G Gaussian basis sets developed by Pople and co-workers. In most applications such basis sets are augmented by polarization functions which are functions of higher angular momentum than those occupied in an atom, for example, p-functions for hydrogen and d-functions for the first-row elements. Polarization functions ensure that the orbitals can distort from their original atomic symmetry and better adapt to the molecular environment. The 6-31G(d,p) set by Pople et al. and the SVP (split-valence polarization) set by Schäfer, Horn, and Ahlrichs are typical

examples of these kinds of basis sets. Polarized DZ and SV basis sets are the mainstay of routine quantum chemical applications since they usually offer a balanced compromise between accuracy and efficiency. The basis sets can be further improved by increasing the number of functions in the various categories. Diffuse functions can also be added so that the basis set have the flexibility necessary to allow a weakly bound electron to localize far from the remaining density in certain systems.

Basis set superposition error

An important consequence of the use of a finite basis set is the so-called basis set superposition error (BSSE). This error may arise, for example, when dealing with a complex of two weakly bound molecular species. The interaction energy in such a case is calculated by substracting the energies of the isolated species from the energy of the complex (assuming a size-extensive method[†]) using the same basis set. In the complex, the basis functions from one molecule can help compensate for the basis set incompleteness on the other molecule, and vice versa. The complex will, therefore, be artificially lowered in energy, and the strength of the intermolecular interaction is overestimated. In the limit of a complete basis set, BSSE is zero.

An approximate way of correcting BSSE is the counterpoise (CP) correction.[314] In this method, the BSSE is estimated as the difference between monomer energies with the regular basis and the energies calculated with the full set of basis functions for the whole complex

$$E_{\mathrm{BSSE}}^{\mathrm{CP}} = E^{a\cup b}(\mathrm{A}) - E^{a}(\mathrm{A}) + E^{a\cup b}(\mathrm{B}) - E^{b}(\mathrm{B})\ . \qquad \text{(C.3.1)}$$

The energies in (C.3.1) are calculated using the geometries of the species A and B in the complex AB. The superscripts a and b denote the basis functions associated with A and B, respectively. The borrowing of basis is only partly a mathematical artifact and, thus, CP correction always overestimates the BSSE.[238]

Pseudopotentials

For systems involving elements from the third row or higher in the periodic table of elements there is a large number of core electrons which in general are unimportant in a chemical sense. However, a large number of basis functions should be used to represent the corresponding orbitals since otherwise the valence orbitals will not be properly described. In addition, the relativistic

[†] For the definition of size-extensivity and size-consistency, see Section C.4.1

effects of the core electrons are important in very heavy elements. These problems may be solved by introducing a pseudopotential (also called effective core potential, ECP). It replaces the strong Coulomb potential of the nucleus and the effects of the tightly bound core electrons by an effective ionic potential acting on the valence electrons. In other words, the core electrons are modeled by a suitable function, and only the valence electrons are treated explicitly. The use of ECP basis sets for heavy elements improves computational efficiency by reducing the scale of the electronic structure problem. In addition, part of the relativistic effects, especially the scalar effects may be taken care of without having to perform the full relativistic calculation.

C.4 Post-Hartree–Fock methods

The Hartree–Fock theory provides an inadequate treatment of the correlation between the motions of the electrons. In a sufficiently large basis, the HF wave function is able to account for $\sim 99\%$ of the total energy of the system, but the remaining $\sim 1\%$ is often very important for describing chemical phenomena. The difference in energy between the HF and the lowest possible energy in a given basis set is called the electron correlation energy. A large variety of computational techniques has been devised to deal with the electron correlation problem in the context of traditional wave function based ab initio quantum chemistry. Some of the most popular ones, that have also been applied in this work, are introduced here.

C.4.1 Configuration interaction methods

Let us assume that the molecule of interest has an even number of electrons and is adequately represented, to a first approximation, by a closed shell restricted HF determinant, Φ_{HF}. The exact ground state or excited state wave function Φ_{exact} can be expressed as a linear combination of all possible N-electron Slater determinants arising from a complete set of spin orbitals

$$\begin{aligned}\Phi_{\mathrm{exact}} &= C_0\Phi_{\mathrm{HF}} + \sum_{i}^{\mathrm{occ.}}\sum_{r}^{\mathrm{virt.}} C_i^r\Phi_i^r + \sum_{i<j}^{\mathrm{occ.}}\sum_{r<s}^{\mathrm{virt.}} C_{ij}^{rs}\Phi_{ij}^{rs} + \sum_{i<j<k}^{\mathrm{occ.}}\sum_{r<s<t}^{\mathrm{virt.}} C_{ijk}^{rst}\Phi_{ijk}^{rst} + \cdots \\ &= \sum_{J=0}^{L} C_J\Phi_J \ . \end{aligned} \tag{C.4.1}$$

The symbols C in (C.4.1) are the expansion coefficients, Φ_i^r (Φ_S) are the singly excited determinants which differ from the 'reference' wave function

Φ_{HF} in having an occupied spin orbital χ_i replaced by a virtual (unoccupied) one χ_r, Φ_{ij}^{rs} (Φ_D) are the doubly excited determinants, etc. Eq. (C.4.1) includes up to and even the N-tuply excited determinants.

An ab initio method in which the wavefunction is expressed in the form of (C.4.1) is called configuration interaction (CI). As the total number of different Slater determinants that can be constructed in (C.4.1) gets extremely large even for small molecules and basis sets, the expansion must almost always be truncated to some finite value of L. The expansion coefficients are determined variationally, and the MOs used for building the excited determinants are taken from a HF calculation and held fixed. Limitation of the list of determinants to Φ_{HF} and those that are singly and doubly excited with respect to Φ_{HF} is denoted CISD. In the large basis set limit the CISD method scales as K^6 where K is the number of basis functions. Inclusion of also the triply excited determinants yields the CISDT method, which scales as K^8. The only CI method which is generally applicable for a large variety of systems is CISD. For medium sized molecules and basis sets, it typically recovers 80–90% of the available electron correlation energy.

One serious deficiency with truncated CI methods such as CISD is the lack of size-consistency. A method is size-consistent if the energy of a system AB comprised of subsystems A and B infinitely far apart is equal to the sum of the energies of A and B computed separately using the same method. Full CI is size-consistent and size-extensive. The energy calculated with a size-extensive method scales correctly (i.e., as the exact energy does) with the number of particles in the system. A size-extensive method allows straightforward comparisons between calculations involving variable numbers of electrons, for example ionization processes. RHF, UHF, coupled cluster methods (see below), and Møller–Plesset perturbation theory (see below) are size-extensive. Instead, RHF is not necessarily size-consistent.

C.4.2 Coupled cluster methods

CI methods provide a systematic approach for going beyond the HF level. They are variational providing upper bounds to the exact energy. Coupled cluster (CC) methods are size-consistent but not variational. It is thus possible that the energy of the system is calculated to be lower than the exact energy. However, this is rarely a problem because the interest is often not in absolute energies but in relative energies (energy differences).

The CC theory introduces the cluster operator T, which relates the exact electronic wave function Φ_{exact} to the HF wavefunction Φ_{HF} through

$$\Phi_{\mathrm{exact}} = e^T \Phi_{\mathrm{HF}} \tag{C.4.2}$$

where

$$e^T = 1 + T + \frac{1}{2!}T^2 + \frac{1}{3!}T^3 + \ldots = \sum_{k=0}^{\infty} \frac{1}{k!}T^k \ . \tag{C.4.3}$$

T is defined as

$$T = T_1 + T_2 + T_3 + \ldots + T_N \tag{C.4.4}$$

where N is the total number of electrons and the various T_i operators generate all possible determinants having i excitations from the reference wave function. For example,

$$\begin{aligned} T_1\Phi_{\mathrm{HF}} &= \sum_{i}^{\text{occ.}} \sum_{r}^{\text{virt.}} t_i^r \Phi_i^r \\ T_2\Phi_{\mathrm{HF}} &= \sum_{i<j}^{\text{occ.}} \sum_{r<s}^{\text{virt.}} t_{ij}^{rs} \Phi_{ij}^{rs} \end{aligned} \tag{C.4.5}$$

and likewise for T_3 to T_N. The t_i^r are called single-excitation amplitudes, t_{ij}^{rs} double-excitation amplitudes, and so on. The excitation amplitudes are determined by solving the coupled cluster equations that are derived by substituting $e^T\Phi_{\mathrm{HF}}$ into the electronic Schrödinger equation.

To apply the CC theory, two approximations are made. First, one uses a finite basis set to express the spin orbitals in the HF wave function. Second, the operator T is approximated by including only some of the operators $T_1, T_2, \ldots, T_N$. The most important contribution to T is made by T_2. Inclusion of T_2 only gives an approximate CC approach called the coupled cluster doubles (CCD) method. The cost of including single excitations T_1 in addition to doubles is worth the increase of accuracy; this is the CCSD model. CCSD scales as K^6 in the limit of a large basis set. Inclusion of connected triples excitations T_3 defines CCSDT, but it is computationally very costly, scaling as K^8. The effects of the connected triples can be estimated using perturbation theory. The most commonly used approach is in the CCSD(T) method. A method that is closely related to the CC theory is quadratic configuration interaction including singles and doubles (QCISD). It was originally developed by Pople et al.[315] as a way to correct for size-consistency errors in CISD. The QCISD(T) method includes the same perturbative correction for contribution from triples as the CCSD(T) method.

C.4.3 Møller–Plesset perturbation theory

Møller–Plesset perturbation theory (MPPT) provides an alternative systematic approach to finding the correlation energy. The calculations are size-consistent but not variational.

In the general case of the perturbation theory, an operator R is expressed as a combination of an operator $R^{(0)}$ for which the eigenfunctions can be found and a perturbing operator $R^{(1)}$

$$R = R^{(0)} + \lambda R^{(1)} \ . \tag{C.4.6}$$

λ varies from 0 to 1 determining the strength of the perturbation, that is, λ maps $R^{(0)}$ into R. In MPPT of a many-body system, the zero-order Hamiltonian $H^{(0)}$ is the sum of the one-electron Fock operators defined in (C.2.2)

$$H^{(0)} = \sum_{i=1}^{N} f_i \ . \tag{C.4.7}$$

The perturbation $H^{(1)}$ is thus

$$H^{(1)} = H - \sum_{i=1}^{N} f_i \tag{C.4.8}$$

where H is the electronic Hamiltonian (C.1.12). The HF determinant is the zero-order wave function and the zero-order energy $E^{(0)}$ is the sum of all orbital energies of the occupied spin orbitals. The first-order energy is exactly the HF energy, E_{HF}. The first correction to E_{HF} is given by the second-order MPPT (MP2) as

$$E^{(2)} = \sum_{i<j}^{\text{occ.}} \sum_{r<s}^{\text{virt.}} \frac{|\langle ij|rs\rangle - \langle ij|sr\rangle|^2}{\varepsilon_i + \varepsilon_j - \varepsilon_r - \varepsilon_s} \tag{C.4.9}$$

where the notation

$$\langle ij|rs\rangle = \iint \chi_i^*(1)\chi_j^*(2)\frac{1}{r_{12}}\chi_r(1)\chi_s(2)d\mathbf{q}_1 d\mathbf{q}_2 \tag{C.4.10}$$

has been used.

MP2 scales roughly as K^5 and typically accounts for ∼80–90% of the correlation energy. It is the most economical method for including electron correlation of the ab initio wave function based methods. It is possible to extend MPPT to include higher-order energy corrections, and the procedures are then denoted MP3, MP4, etc. At the MP4 level, integrals involving triply and quadruply excited determinants appear. The computational cost of MP4 involving contribution from singles to quadruples (i.e., MP4(SDTQ)) scales as K^7 and is still a computationally feasible model for many molecular systems, requiring a time similar to CISD. The full fourth order energy typically accounts for ∼95–98% of the correlation energy.

C.5 Density functional theory

The electron correlation treatments described in Section C.4 are all based on approximating the many-electron wave function Φ. Historically, this approach has been the subject of most research effort in the electronic structure theory community. However, an alternative approach that has been widely used for over 40 years by physicists working on the electronic structure of solids, surfaces, etc., has also become popular in QC over the past 20 years. This is the density functional theory (DFT). DFT is an (in principle) exact electronic structure theory and, as its name implies, is based on the electron density distribution $n(\mathbf{x})$. While the N-electron wave function $\Phi(\mathbf{x}_1, \ldots, \mathbf{x}_N)$ is a function of $3N$ variables, $n(\mathbf{x})$ is a function of only three variables. Thus, DFT has the potential to notably simplify electronic structure calculations.

In 1964, Hohenberg and Kohn[316] proved two theorems on which all modern DFTs rest. According to the first Hohenberg–Kohn (HK) theorem, the ground state density $n_0(\mathbf{x})$ of a system uniquely (to within a constant) determines the external potential $v(\mathbf{x})$ and, thus, the full Hamiltonian H and all properties determined by it. The second HK theorem states that of all v-representable densities[†] only the true ground state density $n_0(\mathbf{x})$ corresponds to the minimum energy of the system, that is,

$$E_{v(\mathbf{x})}[n(\mathbf{x})] \geq E_{v(\mathbf{x})}[n_0(\mathbf{x})] \equiv E_0 \tag{C.5.1}$$

where E_0 is the ground state energy. The theorem is analogous to the variational theorem for wave functions (C.1.18). The major problem in the second HK theorem is that many "reasonable" densities have been shown to be non-v-representable.[317,318] The serious difficulty associated with the v-representability of trial densities was eliminated by Levy in his constrained-search formulation of the ground state energy minimization procedure.[317,318] In it, the minimization is carried out over all N-representable densities. This is easier than (C.5.1) because virtually all practical DFT applications are in one way or the other related to wave function techniques where all densities trivially satisfy the N-representability condition.

C.5.1 Kohn–Sham method

The first attempts to use the electron density rather than the wave function for obtaining information about atomic and molecular systems date back

[†] A density is v-representable if it is associated with the antisymmetric ground state wave function of a Hamiltonian H with some external potential $v(\mathbf{x})$ (not necessarily a Coulomb potential). A density is N-representable if it can be obtained from some antisymmetric wave function.

to the work of Thomas and Fermi in 1927. In Thomas–Fermi and related models, the functional $F[n(\mathbf{x})]$ delivering the sum of kinetic and interaction energies of the system is approximated by an explicit functional of $n(\mathbf{x})$. These approaches are simple but due to the crude level of approximation involved (especially in the way the kinetic energy is determined), they lead to a great loss in accuracy.

In 1965, Kohn and Sham[191] suggested an indirect but more accurate way to approach the unknown functional $F[n(\mathbf{x})]$. Considering a system of N nonrelativistic, interacting electrons in a nonmagnetic state, the functional delivering the energy of the system can be written as

$$E[n(\mathbf{x})] = \sum_{i=1}^{N} \int \chi_i^*(\mathbf{x}) \Big(-\frac{1}{2}\nabla^2 \Big) \chi_i(\mathbf{x}) d\mathbf{x} + \frac{1}{2} \iint \frac{n(\mathbf{x}) n(\mathbf{x}')}{|\mathbf{x} - \mathbf{x}'|} \, d\mathbf{x} \, d\mathbf{x}' + E_{\mathrm{xc}}[n(\mathbf{x})] + \int v(\mathbf{x}) n(\mathbf{x}) d\mathbf{x} \tag{C.5.2}$$

where

$$n(\mathbf{x}) = \sum_{i=1}^{N} |\chi_i(\mathbf{x})|^2 \ . \tag{C.5.3}$$

The sum of the first three terms in (C.5.2) represents the functional $F[n(\mathbf{x})]$, whereas the fourth term is the energy due to the external potential $v(\mathbf{x})$. The first term in (C.5.2) is the true kinetic energy of the ground state of noninteracting electrons with density $n(\mathbf{x})$ (i.e., a single Slater determinant) and the second term is the classical expression for the interaction energy. The third term $E_{\mathrm{xc}}[n(\mathbf{x})]$ is the so-called exchange-correlation energy defined by (C.5.2). It contains the difference between the kinetic energies of the interacting and noninteracting systems and the nonclassical part of the interelectronic interaction term $\sum_{i=1}^{N} \sum_{j<i}^{N} |\mathbf{x}_i - \mathbf{x}_j|^{-1}$.

Minimization of (C.5.2) subject to the orthonormalization constraint of the orbitals leads to a set of equations, the so-called Kohn–Sham (KS) equations

$$\Big[-\frac{1}{2}\nabla^2 + v(\mathbf{x}) + \int \frac{n(\mathbf{x}')}{|\mathbf{x} - \mathbf{x}'|} d\mathbf{x}' + v_{\mathrm{xc}}(\mathbf{x}) \Big] \chi_i = \varepsilon_i \chi_i \tag{C.5.4}$$

with the exchange-correlation potential

$$v_{\mathrm{xc}}(\mathbf{x}) = \frac{\delta E_{\mathrm{xc}}[n(\mathbf{x})]}{\delta n(\mathbf{x})} \ . \tag{C.5.5}$$

The eigenfunctions and eigenvalues, χ_i and ε_i, of the KS equations have no strict physical significance with the exception of the connection (C.5.3)

between χ_i and the true physical density, and the fact that the highest eigenvalue ε_N is the negative of the exact, many-body ionization potential. However, all χ_i and ε_i are of great semiquantitative value, much like HF energies and wavefunctions, and often more so, because they also reflect correlation effects and are consistent with the exact physical density, $n(\mathbf{x})$.[319]

Analogous to the HF equations, the KS equations (C.5.4) must be solved self-consistently. Numerical procedures can be applied only for small systems. The KS orbitals are expanded using basis sets essentially in all calculations. Inserting the basis set expansion in (C.5.4) leads to a matrix equation

$$\mathbf{h_{KS}C} = \mathbf{SC}\boldsymbol{\varepsilon} \tag{C.5.6}$$

where $\mathbf{h_{KS}}$ is analogous to the Fock matrix in the HF method. The one-electron and Coulomb parts of $\mathbf{h_{KS}}$ are identical to the corresponding Fock matrix elements. The exchange-correlation parts

$$\int \eta_\mu(\mathbf{x}) v_{\mathrm{xc}} \eta_\nu(\mathbf{x}) d\mathbf{x} \tag{C.5.7}$$

cannot be evaluated analytically since even the most simple approximations of v_{xc} are fairly sophisticated mathematical constructs. Instead, the integrals (C.5.7) have to be generated by numerical integration techniques based on a grid. The selection of the grid depends on the desired numerical accuracy in the final results. For typical applications 1000–10000 integration grid points are used for each atom. The grid plays the same role for E_{xc} as the basis set for the other terms.

RI-J and MARI-J approximations

Due to the four-center two-electron Coulomb integrals the KS method scales as K^4 where K is the number of basis functions. However, it is possible to reduce this scaling to K^2K' by approximating the two-electron integrals with three-center expansions. This is done by fitting the electron density $n(\mathbf{x})$ to a linear combination of atom-centered auxiliary basis functions $\{\omega_\kappa(\mathbf{x}) | \kappa = 1, 2, \ldots, K'\}$

$$n(\mathbf{x}) \approx \tilde{n}(\mathbf{x}) = \sum_{\kappa=1}^{K'} c_\kappa \omega_\kappa(\mathbf{x}) \tag{C.5.8}$$

and using the fitted density in evaluating the $J_{\mu\nu}$ integrals

$$J_{\mu\nu} = \iint \eta_\mu(\mathbf{x}) \eta_\nu(\mathbf{x}) \frac{n(\mathbf{x}')}{|\mathbf{x} - \mathbf{x}'|} \, d\mathbf{x} \, d\mathbf{x}' \tag{C.5.9}$$

$$\approx \sum_{\kappa=1}^{K'} c_\kappa \iint \eta_\mu(\mathbf{x})\eta_\nu(\mathbf{x}) \frac{\omega_\kappa(\mathbf{x}')}{|\mathbf{x}-\mathbf{x}'|}\, d\mathbf{x}\, d\mathbf{x}' \ . \qquad \text{(C.5.10)}$$

The coefficients c_κ are determined, for example, by minimizing the Coulomb self-repulsion of the residual density

$$\iint \frac{\big[n(\mathbf{x})-\tilde{n}(\mathbf{x})\big]\big[n(\mathbf{x}')-\tilde{n}(\mathbf{x}')\big]}{|\mathbf{x}-\mathbf{x}'|}\, d\mathbf{x}\, d\mathbf{x}' \ . \qquad \text{(C.5.11)}$$

This procedure is called the resolution of identity for J (RI-J) as its derivation utilizes a mathematical trick called the 'resolution of the identity'. The functions in the auxiliary basis set are of the same type as the functions used in the LCAO expansion but the number of them must be 2–3 times larger than in the LCAO basis set in order to get results of reasonable accuracy (e.g., energies within 10^{-4} a.u. per atom[202]). The RI approximation can also be used in conjunction with HF and MP2 methods. It reduces the CPU time required by a DFT calculation by a factor of ∼10 and in conjunction with HF and MP2 by a factor of ∼5–30 depending on the basis set used. The efficiency and accuracy of the approximation are nearly independent of molecule's geometry, electronic structure, composition, and size.

The multipole accelerated resolution of identity for J (MARI-J) method saves CPU time further by partitioning the Coulomb interactions in the near- and far-fields.[205] The calculation of the far-field part is performed by application of the multipole expansion and the near-field part is evaluated employing the RI-J approximation. MARI-J reduces calculation times significantly—it offers up to 6.5-fold CPU time savings compared to full RI-J calculations and shows scalings as favorable as $K^{1.5}$.

C.5.2 Exchange-correlation functionals

To put DFT to practical tool, good approximations for the exchange-correlation functional E_{xc} are needed. Two different philosophies for developing new functionals exist: nonempirical and semiempirical. The nonempirical functionals are constructed from first principles and subject to known exact constraints whereas the semiempirical functionals include one or more parameters fitted to a set of experimental data.

The functionals can be assigned to various rungs of "Jacob's Ladder" stretching from the Hartree world up to the heaven of chemical accuracy.[320,321] There are five rungs corresponding to increasingly complex ingredients in the functionals. The local density approximation (LDA)—and its extension to

systems with unpaired spins, the local spin density approximation (LSDA)—constitutes the lowest rung using only density as its ingredient as

$$E_{\mathrm{xc}}^{\mathrm{LDA}}[n(\mathbf{x})] \equiv \int \varepsilon_{\mathrm{xc}}[n(\mathbf{x})]\, n(\mathbf{x})\, d\mathbf{x} \tag{C.5.12}$$

where $\varepsilon_{\mathrm{xc}}[n(\mathbf{x})]$ is the exchange-correlation energy per particle of a uniform interacting electron gas of density $n(\mathbf{x})$. The second rung of Jacob's Ladder is the generalized gradient approximation (GGA) where the density functional depends on density and its gradient

$$E_{\mathrm{xc}}^{\mathrm{GGA}} = \int f[n(\mathbf{x}), |\nabla n(\mathbf{x})|]\, d\mathbf{x} \tag{C.5.13}$$

in order to account for the non-homogeneity of the true electron density. The third rung is the meta-GGA which adds the further ingredients $\nabla^2 n(\mathbf{x})$ and kinetic energy density or at least either of them. The fourth rung is the hyper-GGA which also employs the exact exchange energy density, a fully nonlocal functional of the occupied KS orbitals. Two kinds of functionals belong to the fourth rung of Jacob's Ladder: hybrid GGA, which is a combination of GGA with HF exchange, and hybrid meta-GGA, which is a combination of meta-GGA with HF exchange.[322] Both of these types of functionals are semiempirical and have been very successful for chemistry as exemplified by B3LYP, currently maybe the most popular functional in chemistry.[193–196] The fifth rung consists of functionals that combine exact exchange with exact partial correlation, making use not only of the occupied KS orbitals but also of the unoccupied ones.[320]

Most of the calculations on heterogeneous catalytic systems today use DFT methods. They allow a first-principles-based treatment (including electron correlation) of complex metal and metal oxide systems at significantly reduced CPU cost compared to, for example, the CC methods. DFT is often stated to be inappropriate for weak interactions due to dispersion (van der Waals type interactions) but today there are approaches to improving DFT for these interactions.[322] The bond lengths and angles predicted by DFT calculations are typically accurate to within 5 pm and 1–2°, whereas overall adsorption and reaction energies are typically within 20–35 kJ mol^{-1} of experimental data.[253]

C.6 Thermochemistry

Information about the energetic properties of molecules is at the heart of every quantum chemical investigation. Energy calculation and geometry optimization of a molecule yield a quantum mechanical estimate of the total

electronic energy E_{tot} [see Eq. (C.1.14)]. This energy, however, does not include any contribution from the motion of the nuclei. Even at 0 K the nuclei of a molecule vibrate about their equilibrium positions. This motion contributes to the total molecular energy[†] with a term called zero-point vibrational energy (E_{ZPV}). It is important to compute E_{ZPV} if accurate quantum mechanical estimates of, for instance, relative stabilities of two isomers are desired. In addition, the thermal corrections to the energy need to be calculated in order to get thermodynamic quantities such as internal energy, enthalpy, and entropy of a chemical system at some finite temperature. For example, the experimentally measured reaction energies are always in the form of some thermodynamic quantity, typically enthalpy or free energy, and can be compared correctly to computational results only if theoretically determined single-molecule energies are converted to thermodynamic variables of ensembles of molecules. Calculation of the thermodynamic quantities requires knowing the molecular vibrational frequencies. In addition, theoretical vibrational frequencies help in analyzing experimental infrared (IR) spectra.

C.6.1 Vibrational frequencies and zero-point energy

In the lowest approximation the molecular vibrations may be described as those of a harmonic oscillator. This results from first approximating the total electronic potential energy $V(\mathbf{x})$ where the nuclei move by a second-order Taylor expansion around the stationary geometry $\mathbf{x}_0$ as a function of the nuclear coordinates

$$V(\mathbf{x}) \simeq V(\mathbf{x}_0) + (\mathbf{x}-\mathbf{x}_0)^{\mathrm{T}}\left(\frac{dV}{d\mathbf{x}}\right) + \frac{1}{2}(\mathbf{x}-\mathbf{x}_0)^{\mathrm{T}}\left(\frac{d^2V}{d\mathbf{x}^2}\right)(\mathbf{x}-\mathbf{x}_0) \quad \text{(C.6.1)}$$

The derivates in (C.6.1) are evaluated at $\mathbf{x} = \mathbf{x}_0$ and T means "transpose". The energy for the expansion point, $V(\mathbf{x}_0)$, may be taken as zero, and the first derivative is zero since $\mathbf{x}_0$ is a stationary point. Consequently, (C.6.1) becomes

$$V(\Delta\mathbf{x}) = \frac{1}{2}\Delta\mathbf{x}^{\mathrm{T}}\,\mathbf{k}\,\Delta\mathbf{x}\ . \quad \text{(C.6.2)}$$

$\mathbf{k}$ is a $3N \times 3N$ matrix called the force constant matrix or Hessian matrix (N is the number of atoms in the molecule) and its elements are the second derivatives of the electronic potential energy with respect to the coordinates of the nuclei at the equilibrium geometry

$$k_{ij} = \left(\frac{\partial^2 V}{\partial x_i \partial x_j}\right)_{\mathbf{x}=\mathbf{x}_0}\ . \quad \text{(C.6.3)}$$

[†] The total molecular energy is approximately the sum of translational, rotational, vibrational, and electronic energies.

The nuclear Schrödinger equation for an N-atom system is then

$$\left[-\sum_{i=1}^{3N} \frac{1}{2m_i} \frac{\partial^2}{\partial x_i^2} + \frac{1}{2} \Delta \mathbf{x}^{\mathrm{T}} \mathbf{k} \Delta \mathbf{x} \right] \Xi(\mathbf{x}) = E\, \Xi(\mathbf{x}) \tag{C.6.4}$$

where m_i refers to the atomic mass. By a transformation into a unique set of mass-dependent spatial coordinates $\mathbf{q}$, so-called vibrational normal coordinates, the $3N$-dimensional Schrödinger equation (C.6.4) can be separated into $3N$ one-dimensional Schrödinger equations, which are in the form of a standard harmonic oscillator of unit mass and force constant λ_i

$$\left[-\frac{1}{2} \frac{\partial^2}{\partial q_i^2} + \frac{1}{2} \lambda_i q_i^2 \right] \Xi(q_i) = E_i\, \Xi(q_i) \qquad i = 1, 2, \ldots, 3N\ . \tag{C.6.5}$$

Each component q_i corresponds to a molecular vibration or a "normal mode" for the system and is associated with a set of harmonic oscillator wave functions $\Xi(q_i)$ and energy eigenvalues

$$E_{i,n_i} = \left(n_i + \frac{1}{2} \right) h\nu_i \qquad n_i = 0, 1, 2, \ldots \tag{C.6.6}$$

where n_i is the vibrational quantum number and $\nu_i = \sqrt{\lambda_i}/2\pi$ is the vibrational frequency for the ith normal mode. Six/five of the frequencies ν_i of a non-linear/linear molecule should be zero or very close to it corresponding to the translational and rotational modes. The remaining $3N-6$ / $3N-5$ frequencies are the molecular harmonic vibrational frequencies. The zero-point vibrational energy of a non-linear molecule in the harmonic approximation is

$$E_{\mathrm{ZPV}} = \sum_{i}^{3N-6} \frac{1}{2} h\nu_i\ . \tag{C.6.7}$$

Frequency calculations are diagnostic as to the nature of stationary points on the potential energy surface. If the stationary point is a local or global minimum on the PES, all normal mode force constants λ_i are positive. If the stationary point is not a minimum but a saddle-point, one or more λ_i are negative, thus leading to imaginary frequencies. A transition state (TS) structure is associated with one and only one imaginary frequency and the corresponding eigenvector (reaction coordinate) leads downhill from the TS towards an energy minimum (e.g., reactant or product).

The differences between the harmonic oscillator approximation and the true system are intrinsic to the truncation of the Taylor expansion and will remain even for an exact level of electronic structure theory. The true potential energy of, for example, a bond stretch curve is lower than that predicted

by the parabolic potential of the harmonic approximation. The calculated harmonic frequency will thus be higher than the true frequency. The vibrational frequencies calculated at the HF level are systematically too high by about 10% due to overestimation of bonding in the HF theory. Therefore, they are often scaled by a factor of ca. 0.89–0.91 to partly compensate these systematic errors. Inclusion of electron correlation normally decreases the vibrational frequencies. For example, MP2 shows significant improvement over HF—the anharmonicity can be approximately accounted for by scaling the MP2 harmonic frequencies by ca. 0.94–0.97. CCSD(T) and some of the hybrid density functionals in DFT, such as B3LYP and B3PW91, are even more accurate with scaling factors of ca. 0.95–0.99. The value of the scaling factor depends also on the basis set in addition to the level of electronic structure theory.

C.6.2 Thermal corrections to energy

Dealing with collections of molecules in order to calculate macroscopic, measurable properties of matter requires the use of statistical mechanics. As thermodynamic properties can often be calculated with about the same accuracy with which they can be measured, computations are often an attractive alternative to experiments.

The fundamental function in statistical mechanics is the partition function Z that encodes the statistical properties of a system in thermodynamic equilibrium. Z is a function of temperature and other parameters, such as the volume V enclosing a gas. Most of the thermodynamic functions of the system (e.g., internal energy, free energy, entropy, and pressure) can be expressed in terms of the partition function or its derivatives. There are actually several different types of partition functions, each corresponding to a different type of statistical ensemble. The canonical partition function applies to a canonical ensemble, a collection of systems which have the same temperature, volume, and number of particles, and which are allowed to exchange energy (as heat) with the environment. The canonical partition function for a single particle is

$$z = \sum_{i}^{\text{all states}} e^{-\varepsilon_i / k_\mathrm{B} T} \tag{C.6.8}$$

where ε_i is the energy of the state i and k_B is Boltzmann constant. Increasing the temperature T means increasing population of the upper energy levels which, for one, is reflected in the increasing value for z. For a system of N identical indistinguishable particles (e.g., gas particles), the partition

function is

$$Z = \frac{z^N}{N!} \ . \tag{C.6.9}$$

In order to calculate z, all possible quantum states are needed. Because the energy of a molecule can be approximated as a sum of terms involving translational, rotational, vibrational, and electronical states

$$\varepsilon = \varepsilon_{\text{trans}} + \varepsilon_{\text{rot}} + \varepsilon_{\text{vib}} + \varepsilon_{\text{elec}} \ , \tag{C.6.10}$$

the partition function can be written as a product of various terms as

$$z = z_{\text{trans}} z_{\text{rot}} z_{\text{vib}} z_{\text{elec}} \ . \tag{C.6.11}$$

Therefore, partition function for each contribution can be assessed individually. As calculating the thermodynamic functions such as enthalpy and entropy involves taking the logarithm of z (Z)

$$\begin{aligned} H &= k_{\text{B}} T^2 \left(\frac{\partial \ln Z}{\partial T} \right)_{V,N} + k_{\text{B}} T V \left(\frac{\partial \ln Z}{\partial V} \right)_{T,N} \\ S &= k_{\text{B}} T \left(\frac{\partial \ln Z}{\partial T} \right)_{V,N} + k_{\text{B}} T \ln Z \ , \end{aligned} \tag{C.6.12}$$

the values of these functions consist of sums of values for individual terms

$$\begin{aligned} H &= H_{\text{trans}} + H_{\text{rot}} + H_{\text{vib}} + H_{\text{elec}} \\ S &= S_{\text{trans}} + S_{\text{rot}} + S_{\text{vib}} + S_{\text{elec}} \ . \end{aligned} \tag{C.6.13}$$

For one mole of non-linear, non-interacting ideal gas particles, the enthalpy terms are (R is the gas constant)

$$\begin{aligned} H_{\text{trans}} &= \frac{5}{2} RT \\ H_{\text{rot}} &= \frac{3}{2} RT \\ H_{\text{vib}} &= \frac{Rh}{k_{\text{B}}} \sum_{i=1}^{3N-6} \nu_i \left(\frac{1}{2} + \frac{1}{e^{h\nu_i / k_{\text{B}} T} - 1} \right) \\ H_{\text{elec}} &= 0 \ . \end{aligned} \tag{C.6.14}$$

In (C.6.14), it is assumed that the first and higher electronically excited states are entirely inaccessible. The expression for H_{vib} is valid within the harmonic oscillator approximation and is comprised of two parts: the first part consists of the zero-point energies and the second part, that depends on temperature, is a contribution from molecules which are not in the vibrational ground state. Thus, the total enthalpy at temperature T is a sum of total electronic energies defined in (C.1.14) and the terms in (C.6.14).

C.7 Compound methods

A desirable goal in thermochemistry is to compute a thermodynamic energy such as enthalpy of formation or proton affinity with "chemical accuracy", which generally means an accuracy of ± 1 kcal mol^{-1} as compared to experimental data. In principle this accuracy can be achieved by high-level methods such as CCSD(T) and QCISD(T) with large basis sets but these calculations are computationally too expensive to be practical except for very small molecules. To allow accurate calculations on molecules containing several nonhydrogen atoms, various compound methods have been developed.[323] These methods consist of a number of predefined component calculations whose results are combined together with empirical corrections in a specified matter. Two such families of methods, namely the Gaussian-n (Gn) methods[324] and the Complete Basis Set (CBS) methods[325] were applied in this thesis and are reviewed here. The main difference between them is the way they try to extrapolate the correlation energy.

C.7.1 Gaussian-n methods

In the G1, G2, and G3 methods[326–329] as well as their variants,[200,201,330–332] the "complete correlation, complete basis set" total energy limit of molecular species is approached by using relative small basis sets, additivity approximations, and empirical corrections. Let us consider the G3 method[329] as an example. In it, the total energy is effectively calculated at the QCISD(T,full)/-G3large level but in much less CPU time than required by such a calculation. Above, G3large is an improved version of the 6-311+G(3df,2p) basis set and the symbol 'full' means that the calculation includes all electrons instead of the valence electrons in the treatment of electron correlation[†].

In the G3 method, an initial equilibrium geometry of a species is obtained at the HF/6-31G(d) level. This geometry is used to calculate harmonic frequencies which are scaled by a factor of 0.8929 and used to evaluate the zero-point energy and, when desired, thermal effects. The final equilibrium geometry used in various subsequent high-level single-point energy calculations is optimized at the MP2(full)/6-31G(d) level. The total energy at 0 K (the G3 energy) is calculated as

$$\begin{aligned} E^0_{\mathrm{G3}} = {} & E_{\mathrm{MP4/d}} + E_{\mathrm{plus}} + E_{\mathrm{2df,p}} + E_{\mathrm{QCI}} \\ & + E_{\mathrm{G3large}} + E_{\mathrm{SO}} + E_{\mathrm{HLC}} + E_{\mathrm{ZPV}} \ . \end{aligned} \tag{C.7.1a}$$

[†] Often only the valence electrons are included in the computational treatment of electron correlation. This is called the frozen core approximation. It saves CPU time and is often a reasonable approximation because much of the chemistry that one is interested in is localized around the valence band.

Here $E_{\mathrm{MP4/d}} = E\big[\mathrm{MP4/6\text{-}31G(d)}\big]$ is a so-called base energy which is modified by a series of corrections from additional calculations: a correction for diffuse functions

$$E_{\mathrm{plus}} = E\big[\mathrm{MP4/6\text{-}31{+}G(d)}\big] - E\big[\mathrm{MP4/6\text{-}31G(d)}\big] \,, \tag{C.7.1b}$$

a correction for higher polarization functions

$$E_{\mathrm{2df,p}} = E\big[\mathrm{MP4/6\text{-}31G(2df,p)}\big] - E\big[\mathrm{MP4/6\text{-}31G(d)}\big] \,, \tag{C.7.1c}$$

a correction for correlation effects beyond fourth-order perturbation theory

$$E_{\mathrm{QCI}} = E\big[\mathrm{QCISD(T)/6\text{-}31G(d)}\big] - E\big[\mathrm{MP4/6\text{-}31G(d)}\big] \,, \tag{C.7.1d}$$

a correction for larger basis set effects and for the non-additivity

$$\begin{aligned} E_{\mathrm{G3large}} = {} & E\big[\mathrm{MP2(full)/G3large}\big] - E\big[\mathrm{MP2/6\text{-}31G(2df,p)}\big] \\ & - E\big[\mathrm{MP2/6\text{-}31{+}G(d)}\big] + E\big[\mathrm{MP2/6\text{-}31G(d)}\big] \,. \end{aligned} \tag{C.7.1e}$$

E_{SO} is the spin-orbit correction term taken from experiments or accurate theoretical calculations, whereas E_{HLC} is a term for "higher level correction" to take into account remaining (basis set) deficiencies in the energy calculations

$$E_{\mathrm{HLC}} = -An_\beta - B(n_\alpha - n_\beta) \,. \tag{C.7.1f}$$

In (C.7.1f), n_α and n_β are the number of α and β valence electrons, respectively. The A and B values are chosen to give the smallest average absolute deviation from experiment for the G2/97 test set.[333,334] For molecules, $A = 6.386$ mE_{h} and $B = 2.977$ mE_{h} in the G3 theory.

The MP4 calculations are the most time-consuming steps in the G2 and G3 methods and limit their applicability to rather small molecules. The G2(MP2) and G3(MP2) methods[200,330] are modifications of G2 and G3; they replace MP4 calculations with MP2 calculations thereby allowing somewhat larger molecules to be treated. The G3//B3LYP and G3(MP2)//B3LYP methods[201] are variations of the G3 and G3(MP2) methods. In them, the geometries and zero-point energies are obtained at the B3LYP/6-31G(d) level. Table C.1 shows performance of various Gn methods in the G2/97 test set.[201,330] For comparison, the mean absolute deviation at the B3LYP/6-311+G(3df,2p)//B3LYP/6-31G(d) level of theory† using a scale factor of 0.96

† The notation *level2/basis2//level1/basis1* indicates that the energy is calculated at the *level2/basis2* level of theory using the geometry optimized at the *level1/basis1* level of theory. High-level calculations are often carried out using geometries optimized at a lower level since geometries are usually much less sensitive to the theoretical level than relative energies.

for zero-point energies is 5.5 kJ mol^{-1} for the 8 proton affinities and 13.8 kJ mol^{-1} for all 299 energies in the G2/97 test set.[201]

Table C.1. Comparison of mean absolute deviation (kJ mol^{-1}) from 299 experimental values for enthalpies of formation, ionization potentials, electron affinities, and proton affinities in the G2/97 test set.[201,330]

Type	G2	G2(MP2)	G3	G3(MP2)	G3(MP2)//B3LYP
Proton affinities[a]	4.5	3.2	5.6	4.3	3.7
All	6.2	7.9	4.2	5.4	5.2

[a] The G2/97 test set contains the proton affinities of H_2, NH_3, H_2O, C_2H_2, SiH_4, PH_3, H_2S, and HCl.

C.7.2 Complete basis set methods

Whereas the G*n* methods assume basis set additivity and add an empirical correction to recover some of the remaining correlation energy, the CBS methods try to explicitly extrapolate the value of correlation energy to the complete basis set limit.[199,335–338] The main part of the correlation energy is due to electron pairs (i.e., those described by double excited configurations) and is reasonably well described at the MP2 level (p. 165 in ref 308). The MP2 energy at the limit of complete basis set is estimated by employing the asymptotic convergence of pair natural orbital expansions. Empirical corrections are also involved due to remaining correlation effects.

The CBS-4M model chemistry[199] employes the very fast UHF/3-21G(d) method for geometry optimization and zero-point energies. This makes studies of large and flexible molecules practical.[337] However, the UHF/3-21(d) geometries are sometimes inaccurate, which in many cases leads to large errors in the final results. Further, CBS-4M uses a large basis set SCF calculation as a base energy and an MP2 calculation with complete basis set extrapolation to correct the energy through second order. An MP4(SDQ)/6-31G calculation is used to approximate higher order contributions. The model includes some additional empirical corrections, too. The mean absolute deviation of the CBS-4M method is 7.3 kJ mol^{-1} for the eight proton affinities and 13.6 kJ mol^{-1} for all energies in the G2/97 test set.[199]

C.8 Continuum solvation models

All computational methods presented so far have considered isolated, non-interacting molecular species. In fact, molecules in the gas phase at low to moderate pressures may be treated as such species. This facilitates theoretical treatment substantially. However, most chemical processes occur in solution. The solvent can have a major effect on molecular properties and reactions (equilibrium and rates). Especially, the relative populations of different conformations of a molecule in solution may vary substantially from those in the gas phase.

Methods for evaluating the effect of a solvent may broadly be divided into explicit and implicit ones. Explicit models include individual solvent molecules whereas implicit models ignore the molecular structure of the solvent. The solvent is rather represented as a structureless homogeneous medium. The explicit models are clearly more physically realistic but due to the huge number (hundreds or thousands) of solvent molecules needed to describe solvation properly, these models are usually impractical to be treated with quantum mechanics within the confines of present computational resources. The implicit solvation models, also called continuum solvation models, are more practical and may be accurate enough if the role of the solvent is merely to act as a continuous medium bathing the solute. The second advantage of continuum solvation models is that they provide a very accurate way to treat the strong, long-range electrostatic forces that dominate many solvation phenomena. A considerable variety of continuum solvation models has been proposed.

The most important fundamental quantity describing the interaction of a solute with a surrounding solvent is the standard Gibbs free energy of solvation $\Delta G^{\ominus}_{\mathrm{solv}}$. It is the free energy change to transfer a molecule from vacuum to solvent at some standard state conditions and can be considered to have three main components (although they are not separate thermodynamic observables):

$$\Delta G^{\ominus}_{\mathrm{solv}} = \Delta G^{\ominus}_{\mathrm{cav}} + \Delta G^{\ominus}_{\mathrm{vdW}} + \Delta G^{\ominus}_{\mathrm{elec}} \ . \tag{C.8.1}$$

The first term on the right-hand side of (C.8.1), $\Delta G^{\ominus}_{\mathrm{cav}}$, is the cavitation energy. It is the free energy cost associated with the work to form cavities in the solvent that are occupied by the solute molecules. The van der Waals contribution $\Delta G^{\ominus}_{\mathrm{vdW}}$ results from favorable dispersion interactions $\Delta G^{\ominus}_{\mathrm{dis}}$ between the solute and solvent and a repulsion contribution $\Delta G^{\ominus}_{\mathrm{rep}}$. The cavitation and van der Waals energies are often combined and usually assumed to be proportional to the surface area of the cavity. They can be parameterized by fitting to experimental solvation energies.

$\Delta G^{\ominus}_{\text{elect}}$ in (C.8.1) accounts for electrostatic interactions between the charge distribution of the solute and the dielectric medium (solvent) characterized by its dielectric constant ε. This contribution is always non-positive and particularly important for polar and charged solutes. The electrical moments of the solute induce polarization in the surrounding medium, which in turn generates an electric field (also called the 'reaction field') at the solute molecule. Thus, a term describing the interaction between the solute and the reaction field should be included in the solute Hamiltonian as

$$H = H^{(0)} + \frac{1}{2} V_{\text{RF}}(\Psi) \tag{C.8.2}$$

where $H^{(0)}$ is the Hamiltonian for an isolated molecule and $V_{\text{RF}}(\Psi)$ is the potential energy operator associated with the reaction field[†]. As V_{RF} depends on the wave function Ψ, the corresponding Schrödinger equation is nonlinear. Iterative solutions are referred to as self-consistent reaction-field (SCRF) calculations. Many SCRF models exist. They differ in how the size and shape of the cavity that contains the solute is chosen and how V_{RF} is calculated.

In the COSMO formalism[219] (COSMO stands for 'conductor-like screening model'), calculation of $\Delta G^{\ominus}_{\text{elect}}$ starts by forming a molecular shaped cavity within the dielectric continuum. The charge distribution of the solute polarizes the dielectric medium whose response is described by the generation of screening charges on the cavity surface. Due to the non-analytical nature of the cavity shapes, it is necessary to find the solute–solvent interaction potential energy term (V_{RF}) numerically. In these respects COSMO resembles the famous polarized continuum model (PCM).[339,340] However, in the COSMO formalism the screening charges are initially calculated using the condition that the surrounding medium is conducting having an infinite dielectric constant. The charges are finally scaled by a factor of $(\varepsilon-1)/(\varepsilon+0.5)$ to recover the effects of the finite dielectric constant ε of the medium. Such a procedure simplifies the electrostatics calculations considerably and makes COSMO computationally fast. Accounting for nonelectrostatic effects with the original COSMO formulation tends to be ad hoc, but a novel statistical scheme, called COSMO for real solvents (COSMO-RS), has been proposed to compute the full solvation free energy for neutral solutes.[341,342]

In addition to the three components of $\Delta G^{\ominus}_{\text{solv}}$ presented in (C.8.1), there may be explicit terms for other contributions. For example, terms for specific structural interactions between the solute and solvent molecules such as hydrogen bonding $\Delta G^{\ominus}_{\text{hb}}$ can be included. Changes in molecular mo-

[†] The factor of 1/2 in (C.8.2) derives from assuming a linear response of the surrounding medium to the solute's charge distribution. Half of the induced favorable solute–solvent interaction is canceled by the cost of polarizing the solvent.

tions on going from the gas to the solution phase also contribute by a term $\Delta G^{\ominus}_{\mathrm{mm}} = -RT \ln(z_{\mathrm{A(sln)}}/z_{\mathrm{A(g)}})$, where $z_{\mathrm{A(sln)}}$ and $z_{\mathrm{A(g)}}$ are the molecular partition functions of solute A in the solution and in the gas phase, respectively, at the temperature T and the standard state concentration 1 M both in the gas phase and in solution. If a vibrational frequency calculation is done in both phases, one can calculate $\Delta G^{\ominus}_{\mathrm{mm}}$, but most commonly it is omitted assuming that its contribution is negligible.

To find the theoretical value for the equilibrium constant for a reaction (or conformational equilibrium) in solution at the desired temperature, one starts by calculating the gas-phase $\Delta G^{\ominus}_{\mathrm{(gas)}}$ for the process. Then one calculates the $\Delta G^{\ominus}_{\mathrm{solv}}$ for each reactant and product (or conformers) and combines these values with $\Delta G^{\ominus}_{\mathrm{(gas)}}$ to find $\Delta G^{\ominus}_{\mathrm{(sol)}}$ for the process in solution. The molecular geometries should be reoptimized in the presence of the reaction field, but this step is sometimes omitted because changes in geometry when going from the gas phase to the solution phase are usually small. For isomerizations and conformational changes, it is usually a good approximation to assume that the species have nearly the same cavitation and van der Waals contributions. Consequently, these contributions will essentially cancel and need not be calculated.

C.9 Molecular mechanics methods

Classically a molecule can be thought as being a set of balls connected by springs. The balls represent the atoms of various masses and the springs the various forces acting between the atoms. This model is the basis of the MM methods, also called force field (FF) methods. The MM methods neglect the electrons as individual particles and the quantum aspects of the nuclear motion. Instead, the energy of a molecule is expressed as a sum of terms which desribe the energy needed to distort the molecule in a specific fashion

$$E_{\mathrm{MM}} = E_{\mathrm{str}} + E_{\mathrm{bend}} + E_{\mathrm{tors}} + E_{\mathrm{el}} + E_{\mathrm{vdw}} + E_{\mathrm{cross}} \ . \qquad \text{(C.9.1)}$$

E_{str} is the energy function for stretching a bond between two atoms, E_{bend} represents the energy required for bending a bond angle, and E_{tors} is the torsional energy for rotation around a bond. E_{el} and E_{vdw} represent the electrostatic and van der Waals energies. E_{cross} covers coupling between the other terms, but usually only between the first three terms. For example, in water molecule the lowest energy O−H bond distance depends on the bond angle, and this effect cannot be taken into account without including a term that depends on both bond length and angle. Cross terms are part of all FFs designed to achieve a high accuracy.

Each potential energy term in (C.9.1) is a parametric function of nuclear coordinates and a specified set of these functions comprises a force field. The FF parameters are determined by data from experiments or ab initio electronic structure calculations. The simplest possible energy function for stretching a bond between atom types A and B[†] around a "natural" bond length b_0 (a parameter) is that of a harmonic oscillator

$$E_{\mathrm{str}}^{\mathrm{AB}} = k_2(b - b_0)^2 \tag{C.9.2}$$

where k_2 is the "force constant" (a parameter) for the A−B bond. Eq. (C.9.2) is sufficient for most equilibrium geometries but if more accurate results are desired, the functional form has to be improved, for example, by including higher-order (cubic, quartic, etc.) terms

$$E_{\mathrm{str}}^{\mathrm{AB}} = k_2(b - b_0)^2 + k_3(b - b_0)^3 + k_4(b - b_0)^4 + \ldots \tag{C.9.3}$$

General expressions for other energy terms can be found, for example, in refs 238 and 308.

The MM calculations in this thesis were performed using the COMPASS (Condensed-phase Optimized Molecular Potentials for Atomistic Simulation Studies) force field.[212] The functional form of COMPASS is

$$\begin{aligned}
E_{\mathrm{MM}} = & \sum_{b} \left[k_2(b - b_0)^2 + k_3(b - b_0)^3 + k_4(b - b_0)^4\right] \\
& + \sum_{\theta} \left[k_2(\theta - \theta_0)^2 + k_3(\theta - \theta_0)^3 + k_4(\theta - \theta_0)^4\right] \\
& + \sum_{\phi} \left[k_1(1 - \cos\phi) + k_2(1 - \cos 2\phi) + k_3(1 - \cos 3\phi)\right] \\
& + \sum_{\chi} k_2\chi^2 + \sum_{b,b'} k(b - b_0)(b' - b'_0) + \sum_{b,\theta} k(b - b_0)(\theta - \theta_0) \\
& + \sum_{b,\phi} (b - b_0)\left[k_1\cos\phi + k_2\cos 2\phi + k_3\cos 3\phi\right] \\
& + \sum_{\theta,\phi} (\theta - \theta_0)\left[k_1\cos\phi + k_2\cos 2\phi + k_3\cos 3\phi\right] \\
& + \sum_{\theta,\theta'} k(\theta - \theta_0)(\theta' - \theta'_0) + \sum_{\theta,\theta',\phi} k(\theta - \theta_0)(\theta' - \theta'_0)\cos\phi \\
& + \sum_{i,j} \frac{q_i q_j}{r_{ij}} + \sum_{i,j} \epsilon_{ij}\left[2\left(\frac{r_{ij}^0}{r_{ij}}\right)^9 - 3\left(\frac{r_{ij}^0}{r_{ij}}\right)^6\right]
\end{aligned} \tag{C.9.4}$$

[†] The atom type depends on the atomic number and the type of chemical bonding it is involved in.

where the valence terms represent internal coordinates of bond (b), angle (θ), torsion angle (ϕ), and out-of-plane angle (χ) and the cross-coupling terms include combinations of two or three internal coordinates. The nonbond interactions include a coulombic function for an electrostatic interaction and a Lennard-Jones 9-6 function for the van der Waals interaction.[212] The COMPASS force field is parameterized to predict both intramolecular properties for isolated molecules and intermolecular properties for molecules in condensed phases. The parameterization is based on a combined ab initio and empirical procedure. The root mean square deviation of calculated structural parameters (bond lengths and angles), vibrational frequencies, and conformational energies from experimental values in a set of 178 common organic molecules are approximately 1%, 41 cm^{-1}, and 1.6 kJ mol^{-1}, respectively.[212]

FF methods have difficulties in describing the electrostatic interaction properly. At the lowest approximation, this interaction may be modeled by assigning point charges to each atom center or bond dipole moments to each bond. The atomic charges may be treated as fitting parameters. More commonly their values are based on fitting to the electrostatic potential calculated by electronic structure methods; these charges are called electrostatic potential (ESP) charges. In the MM calculations for this thesis, the atomic charges of the molecules were determined by the charge equilibration (QEq) method[213] as implemented in the Forcite molecular mechanics module in Materials Studio (Accelrys Software Inc.). The QEq approach uses only experimental atomic ionization potentials, electron affinities and atomic radii to predict the atomic charges, and leads to charge distributions in excellent agreement with those obtained from ESPs of accurate ab initio calculations.[213]

When studying time-independent phenomena, FF calculations are used to predict minimum energy geometries, relative stabilities, and barriers for interconversion of different conformations. The numerical value of the FF energy by itself has no meaning. It can be regarded as the steric or excess energy relative to a hypothetical molecule with non-interacting fragments. Instead, relative energies of different conformations of the same molecule can be calculated directly by comparing the E_{MM} values.

The main advantage of the FF methods with respect to electronic structure methods is that the calculations are several orders of magnitude faster. Therefore, large systems containing thousands or even millions of atoms can be treated. In addition, the non-bonded, especially van der Waals interactions which are very difficult to calculate reliably by electronic structure methods, can be modeled properly by the FFs. A downside of the FF methods is that they are traditionally inherently unable to describe the details of chemical reactions with bond breaking/formation and rehybridization of atoms

which require modeling the rearrangement of electrons. An exception is the ReaxFF force field[343] which allows for continuous bond breaking/formation. As the FF parameters are often optimized to predict properties for certain classes of molecules, unusual molecules may be poorly represented. It is not possible to assess the quality of the results without comparison with calculated results on similar types of molecules for which experimental data exists.

There exist many different FFs today. Three main aspects in which they differ are the functional form of each energy term, the number of cross terms included, and the type of information used for fitting the parameters. In one class are the generic FFs that in the extreme case can in principle cover molecules composed of elements from the whole periodic table. Such an FF is, for example, the Universal Force Field (UFF).[344] Because of the generality of the parameterization and simple functional forms, these FFs normally yield reasonable predictions of molecular structure only. Another class includes FFs that are designed primarily to treat large biomolecules with a better accuracy. The functional forms are kept as simple as possible and no cross terms are included. AMBER[345] and CHARMM[346] are examples of such force fields. The third class of FFs strives to accurately reproduce a number of molecular properties such as structures, conformational energies, vibrational frequencies, and heats of formation of small to medium size molecules. Achieving this goal requires complicated functional forms and cross terms. Force fields such as MM2,[347] MM3,[348–350] CFF93,[351] and MMFF[352] belong to this class.

References and notes

(1) Barron, L. D. *Space Sci. Rev.* **2008**, *135*, 187–201.

(2) Cohen, J. *Science* **1995**, *267*, 1265–1266.

(3) Avalos, M.; Babiano, R.; Cintas, P.; Jiménez, J. L.; Palacios, J. C. *Tetrahedron: Asymmetry* **2000**, *11*, 2845–2874.

(4) IUPAC Compendium of Chemical Terminology – the Gold Book. `http://goldbook.iupac.org` (accessed Jun 2010).

(5) The figure is taken from Wikimedia Commons. `http://commons.wikimedia.org/wiki/File:Chirality_with_hands.jpg` (accessed Jun 2010).

(6) Zhang, J.; Chen, S.; Zingiryan, A.; Bu, X. *J. Am. Chem. Soc.* **2008**, *130*, 17246–17247.

(7) Yuasa, S. *J. Biol. Phys.* **1994**, *20*, 229–233.

(8) Quack, M. *Angew. Chem. Int. Ed.* **2002**, *41*, 4618–4630.

(9) Tsogoeva, S. B.; Wei, S.; Freund, M.; Mauksch, M. *Angew. Chem. Int. Ed.* **2009**, *48*, 590–594.

(10) The figures are taken from Wikimedia Commons. `http://en.wikipedia.org/wiki/File:Myoglobin.png` and `http://commons.wikimedia.org/wiki/File:DNA_double_helix_vertikal.PNG` (accessed Jun 2010).

(11) Cahn, R. S.; Ingold, C.; Prelog, V. *Angew. Chem. Int. Ed. Eng.* **1966**, *5*, 385–415.

(12) Prelog, V.; Helmchen, G. *Angew. Chem. Int. Ed. Eng.* **1982**, *21*, 567–583.

(13) Brenna, E.; Fuganti, C.; Serra, S. *Tetrahedron: Asymmetry* **2003**, *14*, 1–42.

(14) Bentley, R. *Chem. Rev.* **2006**, *106*, 4099–4112.

(15) Thayer, A. M. *Chem. Eng. News* **2007**, *85*, 11–19.

(16) Suh, I.-H.; Park, K. H.; Jensen, W. P.; Lewis, D. E. *J. Chem. Educ.* **1997**, *74*, 800–805.

(17) Rouhi, A. M. *Chem. Eng. News* **2004**, *82*, 47–62.

(18) Stinson, S. C. *Chem. Eng. News* **2000**, *78*, 55–78.

(19) Stinson, S. C. *Chem. Eng. News* **2001**, *79*, 45–57.
(20) Rouhi, A. M. *Chem. Eng. News* **2004**, *81*, 45–55.
(21) Sheldon, R. A. *Chirotechnology: industrial synthesis of optically active compounds*; Marcel Dekker: New York, 1993.
(22) Blaser, H.-U. *Chem. Rev.* **1992**, *92*, 935–952.
(23) Jacoby, M. *Chem. Eng. News* **2004**, *82*, 37–41.
(24) Thayer, A. *Chem. Eng. News* **2005**, *83*, 40–48.
(25) Thayer, A. M. *Chem. Eng. News* **2006**, *84*, 15–25.
(26) Opportunities for Catalysis in the 21st Century: A Report from the Basic Energy Sciences Advisory Committee, 2002. `http://www.sc.doe.gov/bes/reports/files/OC_rpt.pdf` (accessed Jun 2010).
(27) Schoemaker, H. E.; Mink, D.; Wubbolts, M. G. *Science* **2003**, *299*, 1694–1697.
(28) Leresche, J. E.; Meyer, H.-P. *Org. Process Res. Dev.* **2006**, *10*, 572–580.
(29) Trost, B. M. *Proc. Nat. Acad. Sci. U.S.A.* **2004**, *101*, 5348–5355.
(30) Yoon, T. P.; Jacobsen, E. N. *Science* **2003**, *299*, 1691–1693.
(31) Knowles, W. S. *Angew. Chem. Int. Ed.* **2002**, *41*, 1998–2007.
(32) Noyori, R. *Angew. Chem. Int. Ed.* **2002**, *41*, 2008–2022.
(33) Sharpless, K. B. *Angew. Chem. Int. Ed.* **2002**, *41*, 2024–2032.
(34) Murzin, D. Y.; Mäki-Arvela, P.; Toukoniitty, E.; Salmi, T. *Catal. Rev.* **2005**, *47*, 175–256.
(35) Blaser, H.-U. *Chem. Commun.* **2003**, 293–296.
(36) McMorn, P.; Hutchings, G. J. *Chem. Soc. Rev.* **2004**, *33*, 108–122.
(37) Heitbaum, M.; Glorius, F.; Escher, I. *Angew. Chem. Int. Ed.* **2006**, *45*, 4732–4762.
(38) Trindade, A. F.; Gois, P. M. P.; Afonso, C. A. M. *Chem. Rev.* **2009**, *109*, 418–514.
(39) Davis, M. E.; Katz, A.; Ahmad, W. R. *Chem. Mater.* **1996**, *8*, 1820–1839.
(40) Davis, M. E. *Top. Catal.* **2003**, *25*, 3–7.
(41) Corma, A. *Catal. Rev.* **2004**, *46*, 369–417.
(42) Klabunovskii, E.; Smith, G. V.; Zsigmond, Á. *Heterogeneous Enantioselective Hydrogenation: Theory and Practice*; Catalysis by Metal Complexes; Springer: Dordrecht, 2006.
(43) Hazen, R. M.; Sholl, D. S. *Nat. Mater.* **2003**, *2*, 367–374.
(44) Hazzazi, O. A.; Attard, G. A.; Wells, P. B. *J. Mol. Catal. A: Chem.* **2004**, *216*, 247–255.
(45) Horvath, J. D.; Baker, L.; Gellman, A. J. *J. Phys. Chem. C* **2008**, *112*, 7637–7643.
(46) Lorenzo, M. O.; Baddeley, C. J.; Muryn, C.; Raval, R. *Nature* **2000**, *404*,

376–379.

(47) Barlow, S. M.; Raval, R. *Surf. Sci. Rep.* **2003**, *50*, 201–341.

(48) Baiker, A. *Catal. Today* **2005**, *100*, 159–170.

(49) Studer, M.; Blaser, H.-U.; Exner, C. *Adv. Synth. Catal.* **2003**, *345*, 45–65.

(50) Blaser, H.-U.; Studer, M. *Acc. Chem. Res.* **2007**, *40*, 1348–1356.

(51) Mallat, T.; Orglmeister, E.; Baiker, A. *Chem. Rev.* **2007**, *107*, 4863–4890.

(52) Baiker, A. *J. Mol. Catal. A: Chem.* **1997**, *115*, 473–493.

(53) Baiker, A. *J. Mol. Catal. A: Chem.* **2000**, *163*, 205–220.

(54) Blaser, H.-U.; Jalett, H.-P.; Müller, M.; Studer, M. *Catal. Today* **1997**, *37*, 441–463.

(55) Wells, P. B.; Wilkinson, A. G. *Top. Catal.* **1998**, *5*, 39–50.

(56) Baiker, A. *J. Mol. Catal. A: Chem.* **2000**, *163*, 205–220.

(57) von Arx, M.; Mallat, T.; Baiker, A. *Top. Catal.* **2002**, *19*, 75–87.

(58) Bürgi, T.; Baiker, A. *Acc. Chem. Res.* **2004**, *37*, 909–917.

(59) Orito, Y.; Imai, S.; Niwa, S.; Nguyen, G. H. *J. Synth. Org. Chem. Jpn.* **1979**, *37*, 173–174.

(60) Orito, Y.; Imai, S.; Niwa, S. *J. Chem. Soc. Jpn.* **1979**, 1118–1120.

(61) Hess, R.; Mallat, T.; Baiker, A. *J. Catal.* **2003**, *218*, 453–456.

(62) von Arx, M.; Mallat, T.; Baiker, A. *Tetrahedron: Asymmetry* **2001**, *12*, 3089–3094.

(63) Varga, T.; Felföldi, K.; Forgó, P.; Bartók, M. *J. Mol. Catal. A: Chem.* **2004**, *216*, 181–187.

(64) Li, X.; Dummer, N.; Jenkins, R.; Wells, R. P. K.; Wells, P. B.; Willock, D. J.; Taylor, S. H.; Johnston, P.; Hutchings, G. J. *Catal. Lett.* **2004**, *96*, 147–151.

(65) Zuo, X.; Liu, H.; Guo, D.; Yang, X. *Tetrahedron* **1999**, *55*, 7787–7804.

(66) Schürch, M.; Schwalm, O.; Mallat, T.; Weber, J.; Baiker, A. *J. Catal.* **1997**, *169*, 275–286.

(67) Sutyinszki, M.; Szöri, K.; Felföldi, K.; Bartók, M. *Catal. Commun.* **2002**, *3*, 125–127.

(68) Toukoniitty, E.; Mäki-Arvela, P.; Kumar, N.; Salmi, T.; Murzin, D. Y. *Catal. Lett.* **2004**, *95*, 179–183.

(69) Balázsik, K.; Bucsi, I.; Cserényi, S.; Szöllősi, G.; Bartók, M. *J. Mol. Catal. A: Chem.* **2008**, *280*, 87–95.

(70) Blaser, H. U.; Jalett, H. P.; Lottenbach, W.; Studer, M. *J. Am. Chem. Soc.* **2000**, *122*, 12675–12682.

(71) Diezi, S.; Mallat, T.; Szabo, A.; Baiker, A. *J. Catal.* **2004**, *228*, 162–173.

(72) Exner, C.; Pfaltz, A.; Studer, M.; Blaser, H.-U. *Adv. Synth. Catal.* **2003**, *345*, 1253–1260.

(73) Hess, R.; Vargas, A.; Mallat, T.; Bürgi, T.; Baiker, A. *J. Catal.* **2004**, *222*,

117–128.

(74) Busygin, I.; Wärnå, J.; Toukoniitty, E.; Murzin, D. Y.; Leino, R. *J. Catal.* **2008**, *254*, 339–348.

(75) Toukoniitty, E.; Busygin, I.; Leino, R.; Murzin, D. Y. *J. Catal.* **2004**, *227*, 210–216.

(76) Busygin, I.; Toukoniitty, E.; Leino, R.; Murzin, D. Y. *J. Mol. Catal. A: Chem.* **2005**, *236*, 227–238.

(77) Sonderegger, O. J.; Ho, G. M.-W.; Bürgi, T.; Baiker, A. *J. Mol. Catal. A: Chem.* **2005**, *229*, 19–24.

(78) Blaser, H.-U.; Jalett, H.-P.; Garland, M.; Studer, M.; Thies, H.; Wirth-Tijani, A. *J. Catal.* **1998**, *173*, 282–294.

(79) Toukoniitty, E.; Ševčíková, B.; Mäki-Arvela, P.; Wärnå, J.; Salmi, T.; Murzin, D. Y. *J. Catal.* **2003**, *213*, 7–16.

(80) Künzle, N.; Hess, R.; Mallat, T.; Baiker, A. *J. Catal.* **1999**, *186*, 239–241.

(81) Blaser, H. U.; Garland, M.; Jallet, H. P. *J. Catal.* **1993**, *144*, 569–578.

(82) LeBlond, C.; Wang, J.; Liu, J.; Andrews, A. T.; Sun, Y.-K. *J. Am. Chem. Soc.* **1999**, *121*, 4920–4921.

(83) Jenkins, D. J.; Alabdulrahman, A. M. S.; Attard, G. A.; Griffin, K. G.; Johnston, P.; Wells, P. B. *J. Catal.* **2005**, *234*, 230–239.

(84) Rothenberg, G. *Catalysis: Concepts and Green Applications*; Wiley-VCH: Weinheim, 2008.

(85) Wehrli, J. T.; Baiker, A.; Monti, D. M.; Blaser, H. U. *J. Mol. Catal.* **1989**, *49*, 195–203.

(86) Wehrli, J. T.; Baiker, A.; Monti, D. M.; Blaser, H. U. *J. Mol. Catal.* **1990**, *61*, 207–226.

(87) Webb, G.; Wells, P. B. *Catal. Today* **1992**, *12*, 319–337.

(88) Toukoniitty, E.; Mäki-Arvela, P.; Kalantar Neyestanaki, A.; Salmi, T.; Villela, A.; Leino, R.; Sjöholm, R.; Laine, E.; Väyrynen, J.; Ollonqvist, T. *Stud. Surf. Sci. Catal.* **2000**, *130*, 3363–3368.

(89) Toukoniitty, E.; Mäki-Arvela, P.; Kalantar Neyestanaki, A.; Salmi, T.; Sjöholm, R.; Leino, R.; Laine, E.; Kooyman, P. J.; Ollonqvist, T.; Väyrynen, J. *Appl. Catal., A* **2001**, *216*, 73–83.

(90) Zuo, X.; Liu, H.; Liu, M. *Tetrahedron Lett.* **1998**, *39*, 1941–1944.

(91) Meheux, P. A.; Ibbotson, A.; Wells, P. B. *J. Catal.* **1991**, *128*, 387–396.

(92) Augustine, R. L.; Tanielyan, S. K. *J. Mol. Catal. A: Chem.* **1997**, *118*, 79–87.

(93) Griffiths, S. P.; Johnston, P.; Wells, P. B. *Appl. Catal., A* **2000**, *191*, 193–204.

(94) Toukoniitty, E.; Mäki-Arvela, P.; Villela, A. N.; Kalantar Neyestanaki, A.; Salmi, T.; Leino, R.; Sjöholm, R.; Laine, E.; Väyrynen, J.; Ollonqvist, T.; Kooyman, P. J. *Catal. Today* **2000**, *60*, 175–184.

(95) Mallat, T.; Bodnar, Z.; Minder, B.; Borszeky, K.; Baiker, A. *J. Catal.* **1997**, *168*, 183–193.

(96) Blaser, H. U.; Jalett, H. P.; Wiehl, J. *J. Mol. Catal.* **1991**, *68*, 215–222.

(97) Wehrli, J. T.; Baiker, A.; Monti, D. M.; Blaser, H. U.; Jalett, H. P. *J. Mol. Catal.* **1989**, *57*, 245–257.

(98) Toukoniitty, E.; Mäki-Arvela, P.; Kuusisto, J.; Nieminen, V.; Päivärinta, J.; Hotokka, M.; Salmi, T.; Murzin, D. Y. *J. Mol. Catal. A: Chem.* **2003**, *192*, 135–151.

(99) Bürgi, T.; Baiker, A. *J. Am. Chem. Soc.* **1998**, *120*, 12920–12926.

(100) Wang, J.; Sun, Y.; LeBlond, C.; Landau, R. N.; Blackmond, D. G. *J. Catal.* **1996**, *161*, 752–758.

(101) Wandeler, R.; Künzle, N.; Schneider, M. S.; Mallat, T.; Baiker, A. *J. Catal.* **2001**, *200*, 377–388.

(102) Toukoniitty, E.; Mäki-Arvela, P.; Kalantar Neyestanaki, A.; Salmi, T.; Murzin, D. Y. *Appl. Catal., A* **2002**, *235*, 125–138.

(103) Garland, M.; Blaser, H.-U. *J. Am. Chem. Soc.* **1990**, *112*, 7048–7050.

(104) Avery, K. A.; Mann, R.; Norton, M.; Willock, D. J. *Top. Catal.* **2003**, *25*, 89–102.

(105) Honkala, K.; Hellman, A.; Remediakis, I. N.; Logadottir, A.; Carlsson, A.; Dahl, S.; Christensen, C. H.; Nørskov, J. K. *Science* **2005**, *307*, 555–558.

(106) Neurock, M.; van Santen, R. A. *J. Phys. Chem. B* **2000**, *104*, 11127–11145.

(107) Vargas, A.; Bürgi, T.; Baiker, A. *New J. Chem.* **2002**, *26*, 807–810.

(108) Vargas, A.; Bürgi, T.; von Arx, M.; Hess, R.; Baiker, A. *J. Catal.* **2002**, *209*, 489–500.

(109) Sutherland, I. M.; Ibbotson, A.; Moyes, R. B.; Wells, P. B. *J. Catal.* **1990**, *125*, 77–88.

(110) Simons, K. E.; Meheux, P. A.; Griffiths, S. P.; Sutherland, I. M.; Johnston, P.; Wells, P. B.; Carley, A. F.; Rajumon, M. K.; Roberts, M. W.; Ibbotson, A. *Recl. Trav. Chim. Pays-Bas* **1994**, *113*, 465–474.

(111) Schwalm, O.; Weber, J.; Margitfalvi, J.; Baiker, A. *J. Mol. Struct.* **1993**, *297*, 285–293.

(112) Schwalm, O.; Minder, B.; Weber, J.; Baiker, A. *Catal. Lett.* **1994**, *23*, 271–279.

(113) Vargas, A.; Ferri, D.; Baiker, A. *J. Catal.* **2005**, *236*, 1–8.

(114) Lee, I. C.; Masel, R. I. *J. Phys. Chem. B* **2002**, *106*, 368–373.

(115) Diezi, S.; Reimann, S.; Bonalumi, N.; Mallat, T.; Baiker, A. *J. Catal.* **2006**, *239*, 255–262.

(116) Vargas, A.; Hoxha, F.; Bonalumi, N.; Mallat, T.; Baiker, A. *J. Catal.* **2006**, *240*, 203–212.

(117) Lavoie, S.; Laliberté, M.-A.; Temprano, I.; McBreen, P. H. *J. Am. Chem.*

Soc. **2006**, *128*, 7588–7593.

(118) Lavoie, S.; Mahieu, G.; McBreen, P. H. *Angew. Chem. Int. Ed.* **2006**, *45*, 7404–7407.

(119) Lavoie, S.; McBreen, P. H. *J. Phys. Chem. B* **2005**, *109*, 11986–11990.

(120) Lavoie, S.; Laliberté, M.-A.; McBreen, P. H. *Catal. Lett.* **2004**, *97*, 111–114.

(121) Lavoie, S.; Laliberté, M.-A.; McBreen, P. H. *J. Am. Chem. Soc.* **2003**, *125*, 15756–15757.

(122) Augustine, R. L.; Taneilyan, S. K.; Doyle, L. K. *Tetrahedron: Asymmetry* **1993**, *4*, 1803–1827.

(123) Augustine, R. L.; Taneilyan, S. K. *J. Mol. Catal. A: Chem.* **1996**, *112*, 93–104.

(124) Saus, A.; Zimmermann, K.; Gürtler, O. *Chem.-Ztg.* **1991**, *115*, 252–253.

(125) Blaser, H. U.; Jalett, H. P.; Monti, D. M.; Baiker, A.; Wehrli, J. T. *Stud. Surf. Sci. Catal.* **1991**, *67*, 147–155.

(126) Szőri, K.; Balázsik, K.; Felföldi, K.; Bartók, M. *J. Catal.* **2006**, *241*, 149–154.

(127) Bartók, M.; Sutyinszki, M.; Bucsi, I.; Felföldi, K.; Szöllősi, G.; Bartha, F.; Bartók, T. *J. Catal.* **2005**, *231*, 33–40.

(128) Balázsik, K.; Bartók, M. *J. Catal.* **2004**, *224*, 463–472.

(129) Bartók, M.; Sutyinszki, M.; Felföldi, K.; Szöllősi, G. *Chem. Commun.* **2002**, 1130–1131.

(130) Bartók, M.; Balázsik, K.; Notheisz, F. *React. Kinet. Catal. Lett.* **2002**, *77*, 363–370.

(131) Bartók, M.; Balázsik, K.; Kele, Z. *Catal. Lett.* **2003**, *87*, 235–240.

(132) Vayner, G.; Houk, K. N.; Sun, Y.-K. *J. Am. Chem. Soc.* **2004**, *126*, 199–203.

(133) Felföldi, K.; Varga, T.; Forgó, P.; Bartók, M. *Catal. Lett.* **2004**, *97*, 65–70.

(134) Orglmeister, E.; Mallat, T.; Baiker, A. *J. Catal.* **2005**, *234*, 242–246.

(135) Margitfalvi, J. L.; Hegedüs, M. *J. Catal.* **2002**, *156*, 175–179.

(136) Margitfalvi, J. L.; Hegedüs, M.; Tfirst, E. *Stud. Surf. Sci. Catal.* **1996**, *101*, 241–250.

(137) Margitfalvi, J. L.; Hegedüs, M.; Tfirst, E. *Tetrahedron: Asymmetry* **1996**, *7*, 571–580.

(138) Margitfalvi, J. L.; Hegedüs, M. *J. Mol. Catal. A: Chem.* **1996**, *107*, 281–289.

(139) Margitfalvi, J. L.; Tfirst, E. *J. Mol. Catal. A: Chem.* **1999**, *139*, 81–95.

(140) Toukoniitty, E. Ph.D. thesis, Åbo Akademi University: Turku, 2002.

(141) Busygin, I. Ph.D. thesis, Åbo Akademi University: Turku, 2007.

(142) Toukoniitty, E.; Mäki-Arvela, P.; Kuzma, M.; Villela, A.; Kalantar Neyestanaki, A.; Salmi, T.; Sjöholm, R.; Leino, R.; Laine, E.; Murzin, D. Y. *J. Catal.* **2001**, *204*, 281–291.

(143) Lindholm, A.; Mäki-Arvela, P.; Toukoniitty, E.; Pakkanen, T. A.;

Hirvi, J. T.; Salmi, T.; Murzin, D. Y.; Sjöholm, R.; Leino, R. *J. Chem. Soc., Perkin Trans. 1* **2002**, 2605–2612.

(144) Toukoniitty, B.; Toukoniitty, E.; Mäki-Arvela, P.; Mikkola, J.-P.; Salmi, T.; Murzin, D. Y.; Kooyman, P. J. *Ultrason. Sonochem.* **2006**, *13*, 68–75.

(145) Toukoniitty, B.; Toukoniitty, E.; Kuusisto, J.; Mikkola, J.-P.; Salmi, T.; Murzin, D. Y. *Chem. Eng. J.* **2006**, *120*, 91–98.

(146) Vargas, A.; Bürgi, T.; Baiker, A. *J. Catal.* **2004**, *222*, 439–449.

(147) Bonello, J. M.; Lambert, R. M.; Künzle, N.; Baiker, A. *J. Am. Chem. Soc.* **2000**, *122*, 9864–9865.

(148) Bürgi, T.; Atamny, F.; Knop-Gericke, A.; Hävecker, M.; Schedel-Niedrig, T.; Schlögl, R.; Baiker, A. *Catal. Lett.* **2000**, *66*, 109–112.

(149) Castonguay, M.; Roy, J.-R.; Rochefort, A.; McBreen, P. H. *J. Am. Chem. Soc.* **2000**, *122*, 518–524.

(150) Bonello, J. M.; Williams, F. J.; Santra, A. K.; Lambert, R. M. *J. Phys. Chem. B* **2000**, *104*, 9696–9703.

(151) Bonello, J. M.; Sykes, E. C. H.; Lindsay, R.; Williams, F. J.; Santra, A. K.; Lambert, R. M. *Surf. Sci.* **2001**, *482–485*, 207–214.

(152) Ferri, D.; Bürgi, T.; Baiker, A. *Chem. Commun.* **2001**, 1172–1173.

(153) Kubota, J.; Zaera, F. *J. Am. Chem. Soc.* **2001**, *123*, 11115–11116.

(154) Ferri, D.; Bürgi, T. *J. Am. Chem. Soc.* **2001**, *123*, 12074–12084.

(155) Bakos, I.; Szabó, S.; Bartók, M.; Kálmán, E. *J. Electroanal. Chem.* **2002**, *532*, 113–119.

(156) Chu, W.; LeBlanc, R. J.; Williams, C. T. *Catal. Commun.* **2002**, *3*, 547–552.

(157) LeBlanc, R. J.; Chu, W.; Williams, C. T. *J. Mol. Catal. A: Chem.* **2004**, *212*, 277–289.

(158) Vargas, A.; Bürgi, T.; Baiker, A. *J. Catal.* **2004**, *226*, 69–82.

(159) Calvo, S. R.; LeBlanc, R. J.; Williams, C. T.; Balbuena, P. B. *Surf. Sci.* **2004**, *563*, 57–73.

(160) Bonalumi, N.; Vargas, A.; Ferri, D.; Bürgi, T.; Mallat, T.; Baiker, A. *J. Am. Chem. Soc.* **2005**, *127*, 8467–8477.

(161) von Arx, M.; Wahl, M.; Jung, T. A.; Baiker, A. *Phys. Chem. Chem. Phys.* **2005**, *7*, 273–277.

(162) Vargas, A.; Baiker, A. *J. Catal.* **2006**, *239*, 220–226.

(163) Vargas, A.; Baiker, A. *J. Catal.* **2007**, *247*, 387.

(164) Bonello, J. M.; Williams, F. J.; Lambert, R. M. *J. Am. Chem. Soc.* **2003**, *125*, 2723–2729.

(165) Schneider, M. S.; Urakawa, A.; Grunwaldt, J.-D.; Bürgi, T.; Baiker, A. *Chem. Commun.* **2004**, 744–745.

(166) Bonalumi, N.; Bürgi, T.; Baiker, A. *J. Am. Chem. Soc.* **2003**, *125*, 13342–13343.

(167) de M. Carneiro, J. W.; da S. B. de Oliveira, C.; Passos, F. B.; Aranda, D. A. G.; de Souza, P. R. N.; Antunes, O. A. C. *Catal. Today* **2005**, *107–108*, 31–39.

(168) Bürgi, T.; Baiker, A. *J. Catal.* **2000**, *194*, 445–451.

(169) Vargas, A.; Bürgi, T.; Baiker, A. *J. Catal.* **2001**, *197*, 378–384.

(170) Schwalm, O.; Weber, J.; Minder, B.; Baiker, A. *J. Mol. Struct. THEOCHEM* **1995**, *330*, 353–357.

(171) Rauls, E.; Hammer, B. *Catal. Lett.* **2006**, *106*, 111–114.

(172) Diezi, S.; Ferri, D.; Vargas, A.; Mallat, T.; Baiker, A. *J. Am. Chem. Soc.* **2006**, *128*, 4048–4057.

(173) Vargas, A.; Santarossa, G.; Iannuzzi, M.; Baiker, A. *J. Phys. Chem. C* **2008**, *112*, 10200–10208.

(174) Frisch, M. J. et al. *Gaussian 98, Revision A.3*, Gaussian, Inc., Pittsburgh, PA, 1998.

(175) Frisch, M. J. et al. *Gaussian 98, Revision A.11.3*, Gaussian, Inc., Pittsburgh, PA, 2002.

(176) Frisch, M. J. et al. *Gaussian 03, Revision C.02*, Gaussian, Inc., Wallingford, CT, 2004.

(177) Ahlrichs, R.; Bär, M.; Häser, M.; Horn, H.; Kölmel, C. *Chem. Phys. Lett.* **1989**, *162*, 165–169.

(178) Häser, M.; Ahlrichs, R. *J. Comput. Chem.* **1989**, *10*, 104–111.

(179) Treutler, O.; Ahlrichs, R. *J. Chem. Phys.* **1995**, *102*, 346–354.

(180) von Arnim, M.; Ahlrichs, R. *J. Comput. Chem.* **1998**, *19*, 1746–1757.

(181) Bahn, S. R.; Jacobsen, K. W. *Comput. Sci. Eng.* **2002**, *4*, 56–66.

(182) Dacapo program. `https://wiki.fysik.dtu.dk/dacapo` (accessed Jun 2010).

(183) Szabo, A.; Ostlund, N. S. *Modern Quantum Chemistry: Introduction to Advanced Electronic Structure Theory*; Dover: Mineola, NY, 1996.

(184) Parr, R. G.; Yang, W. *Density-Functional Theory of Atoms and Molecules*; Oxford University Press: New York, 1989.

(185) Koch, W.; Holthausen, M. C. *A Chemist's Guide to Density Functional Theory*; Wiley-VCH: Weinheim, 2000.

(186) Møller, C.; Plesset, M. S. *Phys. Rev.* **1934**, *46*, 618–622.

(187) Frisch, M. J.; Head-Gordon, M.; Pople, J. A. *Chem. Phys. Lett.* **1990**, *166*, 281–289.

(188) Krishnan, R.; Pople, J. A. *Int. J. Quant. Chem.* **1978**, *14*, 91–100.

(189) Purvis, G. D., III; Bartlett, R. J. *J. Chem. Phys.* **1982**, *76*, 1910–1918.

(190) Scuseria, G. E.; Janssen, C. L.; Schaefer, H. F., III *J. Chem. Phys.* **1988**, *89*, 7382–7387.

(191) Kohn, W.; Sham, L. J. *Phys. Rev.* **1965**, *140*, A1133–A1138.

(192) Rajagopal, A. K.; Callaway, J. *Phys. Rev. B* **1973**, *7*, 1912–1919.
(193) Lee, C.; Yang, W.; Parr, R. G. *Phys. Rev. B* **1988**, *37*, 785–789.
(194) Becke, A. D. *Phys. Rev. A* **1988**, *38*, 3098–3100.
(195) Becke, A. D. *J. Chem. Phys.* **1993**, *98*, 5648–5652.
(196) Stevens, P. J.; Devlin, F. J.; Chabalowski, C. F.; Frisch, M. J. *J. Phys. Chem.* **1994**, *98*, 11623–11627.
(197) Perdew, J. P. *Phys. Rev. B* **1986**, *33*, 8822–8824.
(198) Perdew, J. P. *Phys. Rev. B* **1986**, *34*, 7406.
(199) Montgomery, J. A., Jr.; Frisch, M. J.; Ochterski, J. W.; Petersson, G. A. *J. Chem. Phys.* **2000**, *112*, 6532–6542.
(200) Curtiss, L. A.; Raghavachari, K.; Pople, J. A. *J. Chem. Phys.* **1993**, *98*, 1293–1298.
(201) Baboul, A. G.; Curtiss, L. A.; Redfern, P. C.; Raghavachari, K. J. *J. Chem. Phys.* **1999**, *110*, 7650–7657.
(202) Eichkorn, K.; Treutler, O.; Öhm, H.; Häser, M.; Ahlrichs, R. *Chem. Phys. Lett.* **1995**, *240*, 283–290.
(203) Eichkorn, K.; Treutler, O.; Öhm, H.; Häser, M.; Ahlrichs, R. *Chem. Phys. Lett.* **1995**, *242*, 652–660.
(204) Eichkorn, K.; Weigend, F.; Treutler, O.; Ahlrichs, R. *Theor. Chem. Acc.* **1997**, *97*, 119–124.
(205) Sierka, M.; Hogekamp, A.; Ahlrichs, R. *J. Chem. Phys.* **2003**, *118*, 9136–9148.
(206) Andrae, D.; Häußermann, U.; Dolg, M.; Stoll, H.; Preuß, H. *Theor. Chim. Acta* **1990**, *77*, 123–141.
(207) Schäfer, A.; Horn, H.; Ahlrichs, R. *J. Chem. Phys.* **1992**, *97*, 2571–2577.
(208) Perdew, J. P.; Chevary, J. A.; Vosko, S. H.; Jackson, K. A.; Pederson, M. R.; Singh, D. J.; Fiolhais, C. *Phys. Rev. B* **1992**, *46*, 6671–6687.
(209) Perdew, J. P.; Burke, K.; Ernzerhof, M. *Phys. Rev. Lett.* **1996**, *77*, 3865–3868.
(210) Hammer, B.; Hansen, L. B.; Nørskov, J. K. *Phys. Rev. B* **1999**, *59*, 7413–7421.
(211) Vanderbilt, D. *Phys. Rev. B* **1990**, *41*, 7892–7895.
(212) Sun, H. *J. Phys. Chem. B* **1998**, *102*, 7338–7364.
(213) Rappé, A. K.; Goddard, W. A., III *J. Phys. Chem.* **1991**, *95*, 3358–3363.
(214) Hammer, B.; Nørskov, J. K. In *Advances in Catalysis*; Gates, B. C., Knözinger, H., Eds.; Academic Press: San Diego, CA, 2000; Vol. 45, pp 71–129.
(215) Broadbelt, L. J.; Snurr, R. Q. *Appl. Catal., A* **2000**, *200*, 23–46.
(216) Watwe, R. M.; Cortright, R. D.; Nørskov, J. K.; Dumesic, J. A. *J. Phys. Chem. B* **2000**, *104*, 2299–2310.

(217) Saeys, M.; Reyniers, M.-F.; Marin, G. B.; Neurock, M. *J. Phys. Chem. B* **2002**, *106*, 7489–7498.

(218) Valcárcel, A.; Ricart, J. M.; Clotet, A.; Markovits, A.; Minot, C.; Illas, F. *Surf. Sci.* **2002**, *519*, 250–258.

(219) Klamt, A.; Schüürmann, G. *J. Chem. Soc., Perkin Trans. 2* **1993**, 799–805.

(220) Dijkstra, G. D. H.; Kellogg, R. M.; Wynberg, H. *J. Org. Chem.* **1990**, *55*, 6121–6131.

(221) Taskinen, A. Åbo Akademi University, Turku, Finland. Unpublished work, 2006.

(222) Nieminen, V.; Taskinen, A. Åbo Akademi University, Turku, Finland. Unpublished work, 2007.

(223) Bonalumi, N.; Vargas, A.; Ferri, D.; Baiker, A. *Chem. Eur. J.* **2007**, *13*, 9236–9244.

(224) Ma, Z.; Lee, I.; Zaera, F. *J. Am. Chem. Soc.* **2007**, *129*, 16083–16090.

(225) Busygin, I.; Tkachenko, O. P.; Nieminen, V.; Borovkov, V. Y.; Sillanpää, R.; Toukoniitty, E.; Kustov, L. M.; Murzin, D. Y.; Leino, R. *J. Phys. Chem. C* **2007**, *111*, 9374–9383.

(226) Ferri, D.; Bürgi, T.; Baiker, A. *J. Chem. Soc., Perkin Trans. 2* **1999**, 1305–1311.

(227) Bürgi, T.; Vargas, A.; Baiker, A. *J. Chem. Soc., Perkin Trans. 2* **2002**, 1596–1601.

(228) Taskinen, A. Åbo Akademi University, Turku, Finland. Unpublished work, 2007–2009.

(229) Nieminen, V.; Taskinen, A.; Sinkkonen, J.; Toukoniitty, E.; Murzin, D. Y. The role of modifier structure and conformation in heterogeneous enantioselective hydrogenation. Presented at the Europacat VIII conference, Turku, Finland, August 2007.

(230) Ma, Z.; Lee, I.; Kubota, J.; Zaera, F. *J. Mol. Catal. A: Chem.* **2004**, *216*, 199–207.

(231) Mink, L.; Ma, Z.; Olsen, R. A.; James, J. N.; Sholl, D. S.; Mueller, L. J.; Zaera, F. *Top. Catal.* **2008**, *48*, 120–127.

(232) Collier, P. J.; Hall, T. J.; Iggo, J. A.; Johnston, P.; Slipszenko, J. A.; Wells, P. B.; Whyman, R. *Chem. Commun.* **1998**, 1451–1452.

(233) Zaera, F. *J. Phys. Chem. C* **2008**, *112*, 16196–16203.

(234) Olsen, R. A.; Borchardt, D.; Mink, L.; Agarwal, A.; Mueller, L. J.; Zaera, F. *J. Am. Chem. Soc.* **2006**, *128*, 15594–15595.

(235) Minder, B.; Mallat, T.; Skrabal, P.; Baiker, A. *Catal. Lett.* **1994**, *29*, 115–124.

(236) Reichardt, C. *Solvents and Solvent Effects in Organic Chemistry*; Wiley-VCH: Weinheim, 1990.

(237) NIST Chemistry WebBook. `http://webbook.nist.gov` (accessed Jun 2010).

(238) Cramer, C. J. *Essentials of Computational Chemistry: Theories and Models*; Wiley: Chichester, 2002.

(239) Török, B.; Balázsik, K.; Felföldi, K.; Bartók, M. *Stud. Surf. Sci. Catal.* **2000**, *130*, 3381–3386.

(240) Vargas, A.; Bonalumi, N.; Ferri, D.; Baiker, A. *J. Phys. Chem. A* **2006**, *110*, 1118–1127.

(241) Trost, B. M. *Science* **1983**, *219*, 245–250.

(242) Sautet, P. *Top. Catal.* **2000**, *13*, 213–219.

(243) Toukoniitty, E.; Mäki-Arvela, P.; Nieminen, V.; Hotokka, M.; Päivärinta, J.; Salmi, T.; Murzin, D. Y. In *Catalysis of Organic Reactions*; Morrell, D. G., Ed.; Marcel Dekker: New York, 2003; Chapter 25, pp 341–348.

(244) Slipszenko, J. A.; Griffiths, S. P.; Johnston, P.; Simons, K. E.; Vermeer, W. A. H.; Wells, P. B. *J. Catal.* **1998**, *179*, 267–276.

(245) Shukla, V.; Kulkarni, P. *World J. Microbiol. Biotechnol.* **2000**, *16*, 499–506.

(246) Vargas, A.; Reimann, S.; Diezi, S.; Mallat, T.; Baiker, A. *J. Mol. Catal. A: Chem.* **2008**, *282*, 1–8.

(247) Jeffery, E. L.; Mann, R. K.; Hutchings, G. J.; Taylor, S. H.; Willock, D. J. *Catal. Today* **2005**, *105*, 85–92.

(248) Hall, T. J.; Johnston, P.; Vermeer, W. A. H.; Watson, S. R.; Wells, P. B. *Stud. Surf. Sci. Catal.* **1996**, *101*, 221–230.

(249) Toukoniitty, E.; Franceschini, S.; Vaccari, A.; Murzin, D. Y. *Appl. Catal., A* **2006**, *300*, 147–154.

(250) Boudart, M. *J. Mol. Catal.* **1985**, *30*, 27–38.

(251) Bond, G. C. *Surf. Sci.* **1985**, *156*, 966–981.

(252) Gates, B. C. *Chem. Rev.* **1995**, *95*, 511–522.

(253) van Santen, R. A.; Neurock, M. *Molecular Heterogeneous Catalysis*; Wiley-VCH: Weinheim, 2006.

(254) Haruta, M. *Catal. Today* **1997**, *36*, 153–166.

(255) Hutchings, G. J. *Catal. Today* **2005**, *100*, 55–61.

(256) Che, M.; Bennett, C. O. In *Advances in Catalysis*; Eley, D. D., Pines, H., Weisz, P. B., Eds.; Academic Press: San Diego, CA, 1989; Vol. 36, pp 55–172.

(257) Masson, A.; Bellamy, B.; Hadj Romdhane, Y.; Che, M.; Roulet, H.; Dufour, G. *Surf. Sci.* **1986**, *173*, 479–497.

(258) Lin, X.; Ramer, N. J.; Rappe, A. M.; Hass, K. C.; Schneider, W. F.; Trout, B. L. *J. Phys. Chem. B* **2001**, *105*, 7739–7747.

(259) Jacob, T.; Muller, R. P.; Goddard, W. A., III *J. Phys. Chem. B* **2003**, *107*, 9465–9476.

(260) Murzin, D. Y.; Toukoniitty, E. *React. Kinet. Catal. Lett.* **2007**, *90*, 19–25.

(261) Zhdanov, V. P.; Kasemo, B. In *Catalysis and Electrocatalysis at Nanoparticle Surfaces*; Wieckowski, A., Savinova, E. R., Vayenas, C. G., Eds.; Marcel Dekker: New York, 2003; pp 35–64.

(262) Hammer, B.; Nielsen, O. H.; Nørskov, J. K. *Catal. Lett.* **1997**, *46*, 31–35.

(263) Nilsson, A.; Pettersson, L. G. M.; Hammer, B.; Bligaard, T.; Christensen, C. H.; Nørskov, J. K. *Catal. Lett.* **2005**, *100*, 111–114.

(264) Pallassana, V.; Neurock, M. *J. Catal.* **2000**, *191*, 301–317.

(265) Evans, M. G.; Polanyi, M. *Trans. Faraday Soc.* **1936**, *32*, 1333–1360.

(266) Sen, B.; Vannice, M. A. *J. Catal.* **1988**, *113*, 52–71.

(267) Besson, M.; Pinel, C. *Top. Catal* **1998**, *5*, 25–38.

(268) Kukula, P.; Prins, R. *Top. Catal.* **2003**, *25*, 29–42.

(269) Besson, M.; Pinel, C. *Top. Catal.* **2003**, *25*, 43–61.

(270) Hoveyda, A. H.; Evans, D. A.; Fu, G. C. *Chem. Rev.* **1993**, *93*, 1307–1370.

(271) Studer, M.; Okafor, V.; Blaser, H.-U. *Chem. Commun.* **1998**, 1053–1054.

(272) Sonderegger, O. J.; Bürgi, T.; Baiker, A. *J. Catal.* **2003**, *215*, 116–121.

(273) Horiuti, J.; Polanyi, M. *Trans. Faraday Soc.* **1934**, *30*, 1164–1172.

(274) van Druten, G. M. R.; Ponec, V. *Appl. Catal., A* **2000**, *191*, 163–176.

(275) Lemcoff, N. O. *J. Catal.* **1977**, *46*, 356–364.

(276) Chang, N.-S.; Aldrett, S.; Holtzapple, M. T.; Davison, R. R. *Chem. Eng. Sci* **2000**, *55*, 5721–5732.

(277) Gao, F.; Allian, A. D.; Zhang, H.; Cheng, S.; Garland, M. *J. Catal.* **2006**, *241*, 189–199.

(278) Temkin, M. I.; Murzin, D. Y.; Kul'kova, N. V. *Kinet. Katal.* **1989**, *30*, 637.

(279) Smeds, S.; Murzin, D.; Salmi, T. *Appl. Catal., A* **1995**, *125*, 271–291.

(280) Kovtunov, K. V.; Beck, I. E.; Bukhtiyarov, V. I.; Koptyug, I. V. *Angew. Chem., Int. Ed.* **2008**, *47*, 1492–1495.

(281) Hollas, J. M. *Symmetry in Molecules*; Chapman & Hall: London, 1972; p 101.

(282) Hudson, J. *Suurin tiede: Kemian historia*; Art House: Jyväskylä, 1995; from the original book *The History of Chemistry*, © John Hudson (Chapman & Hall, 1992) translated in Finnish by Kimmo Pietiläinen.

(283) Brock, W. H. *The Fontana History of Chemistry*; Fontana Press: London, 1992.

(284) Roberts, M. W. *Catal. Lett.* **2000**, *67*, 1–4.

(285) van Santen, R. A.; Niemantsverdriet, H. *Chemical Kinetics and Catalysis*; Fundamental and Applied Catalysis; Plenum Press: New York, 1995.

(286) Hoffmann, R. *Am. Sci.* **1998**, *86*, 326.

(287) New Chemical Science and Engineering Technology: Vision 2020 Catalysis Report, 1998. `http://www.ccrhq.org/vision/index/roadmaps/catrep.`

html.

(288) Basic Research Needs: Catalysis for Energy – A Report from the U.S. Department of Energy, 2007. http://www.sc.doe.gov/bes/reports/files/CAT_rpt.pdf (accessed Jun 2010).

(289) Chemical Industry of the Future: Technology Roadmap for Computational Chemistry, 1999. http://www.chemicalvision2020.org/pdfs/compchem.pdf (accessed Jun 2010).

(290) Truhlar, D. G. *J. Am. Chem. Soc.* **2008**, *130*, 16824–16827.

(291) Dirac, P. A. M. *Proc. R. Soc. Lond. A* **1929**, *123*, 714–733.

(292) *Theory and Applications of Computational Chemistry: The First Forty Years*; Dykstra, C. E., Frenking, G., Kim, K. S., Scuseria, G. E., Eds.; Elsevier: Amsterdam, 2005.

(293) Kohn, W. *Rev. Mod. Phys.* **1999**, *71*, 1253–1266.

(294) Pople, J. A. *Rev. Mod. Phys.* **1999**, *71*, 1267–1274.

(295) Greeley, J.; Nørskov, J. K.; Mavrikakis, M. *Ann. Rev. Phys. Chem.* **2002**, *53*, 319–348.

(296) Andzelm, J. W.; Alvarado-Swaisgood, A. E.; Axe, F. U.; Doyle, M. W.; Fitzgerald, G.; Freeman, C. M.; Gorman, A. M.; Hill, J.-R.; Kölmel, C. M.; Levine, S. M.; Saxe, P. W.; Stark, K.; Subramanian, L.; van Daelen, M. A.; Wimmer, E.; Newsam, J. M. *Catal. Today* **1999**, *50*, 451–477.

(297) Neyman, K. M.; Illas, F. *Catal. Today* **2005**, *105*, 2–16.

(298) Bromley, S. T.; Catlow, C. R. A.; Maschmeyer, T. *CATTECH* **2003**, *7*, 164–175.

(299) Neurock, M. *J. Catal.* **2003**, *216*, 73–88.

(300) Ruette, F.; Sánchez, M.; Sierraalta, A.; Mendoza, C.; Añez, R.; Rodríguez, L.; Lisboa, O.; Daza, J.; Manrique, P.; Perdomo, Z.; Rosa-Brussin, M. *J. Mol. Catal. A: Chem.* **2005**, *228*, 211–225.

(301) Nørskov, J. K.; Scheffler, M.; Toulhoat, H. *MRS Bull.* **2006**, *31*, 669–674.

(302) Liu, Z.-P. *Pure Appl. Chem.* **2004**, *76*, 2069–2083.

(303) Groß, A. *Surf. Sci.* **2002**, *500*, 347–367.

(304) TOP500 Supercomputer Sites: TOP500 List – June 2010. http://www.top500.org/list/2010/06/100 (accessed Jun 2010).

(305) Thirring, W. *Quantum Mathematical Physics*, 2nd ed.; Springer-Verlag: New York, 2002; translated by E. M. Harrell.

(306) Ballentine, L. E. *Quantum Mechanics: A Modern Development*; World Scientific: Singapore, 1998.

(307) Atkins, P.; Friedman, R. *Molecular Quantum Mechanics*, 4th ed.; Oxford University Press: New York, 2005.

(308) Jensen, F. *Introduction to Computational Chemistry*; Wiley: Chichester, 1999.

(309) Levine, I. N. *Quantum Chemistry*, 5th ed.; Prentice-Hall: New Jersey, 2000.

(310) Leach, A. R. *Molecular Modelling: Principles and Applications*, 2nd ed.; Prentice Hall: Harlow, England, 2001.

(311) Noggle, J. H. *Physical Chemistry*, 3rd ed.; HarperCollins: New York, 1996.

(312) Foresman, J. B.; Frisch, Æ. *Exploring Chemistry with Electronic Structure Methods*, 2nd ed.; Gaussian, Inc.: Pittsburgh, PA, 1996.

(313) Martin, R. M. *Electronic Structure: Basic Theory and Practical Methods*; Cambridge University Press: Cambridge, UK, 2004.

(314) van Duijneveldt, F. B.; van Duijneveldt-van de Rijdt, J. G. C. M.; Lenthe, J. H. *Chem. Rev.* **1994**, *94*, 1873–1885.

(315) Pople, J. A.; Head-Gordon, M.; Raghavachari, K. *J. Chem. Phys.* **1987**, *87*, 5968–5975.

(316) Hohenberg, P.; Kohn, W. *Phys. Rev.* **1964**, *136*, B864–B871.

(317) Levy, M. *Proc. Nat. Acad. Sci. U.S.A.* **1979**, *76*, 6062–6065.

(318) Levy, M. *Phys. Rev. A* **1982**, *26*, 1200–1208.

(319) Kohn, W.; Becke, A. D.; Parr, R. G. *J. Phys. Chem.* **1996**, *100*, 12974–12980.

(320) Perdew, J. P.; Kurth, S. In *A Primer in Density Functional Theory*; Fiolhais, C., Noqueira, F., Marques, M., Eds.; Lecture Notes in Physics; Springer-Verlag: New York, 2003; Chapter 1, p 51.

(321) Perdew, J. P.; Ruzsinszky, A.; Constantin, L. A.; Sun, J.; Csonka, G. I. *J. Chem. Theory Comput.* **2009**, *5*, 902–908.

(322) Zhao, Y.; Truhlar, D. G. *J. Phys. Chem. A* **2005**, *109*, 5656–5667.

(323) *Quantum-Mechanical Prediction of Thermochemical Data*; Cioslowski, J., Ed.; Kluwer Academic: Dordrecht, 2001; Vol. 22.

(324) Raghavachari, K.; Curtiss, L. A. in ref 323.

(325) Petersson, G. A. in ref 323.

(326) Pople, J. A.; Head-Gordon, M.; Fox, D. J. *J. Chem. Phys.* **1989**, *90*, 5622–5629.

(327) Curtiss, L. A.; Jones, C.; Trucks, G. W.; Raghavachari, K.; Pople, J. A. *J. Chem. Phys.* **1990**, *93*, 2537–2545.

(328) Curtiss, L. A.; Raghavachari, K.; Trucks, G. W.; Pople, J. A. *J. Chem. Phys.* **1991**, *94*, 7221–7230.

(329) Curtiss, L. A.; Raghavachari, K.; Redfern, P. C.; Rassolov, V.; Pople, J. A. *J. Chem. Phys.* **1998**, *109*, 7764–7776.

(330) Curtiss, L. A.; Redfern, P. C.; Raghavachari, K. J.; Rassolov, V.; Pople, J. A. *J. Chem. Phys.* **1999**, *110*, 4703–4709.

(331) Curtiss, L. A.; Raghavachari, K.; Redfern, P. C.; Pople, J. A. *J. Chem. Phys.* **2000**, *112*, 1125–1132.

(332) Curtiss, L. A.; Redfern, P. C.; Raghavachari, K.; Pople, J. A. *J. Chem. Phys.* **2001**, *114*, 108–117.

(333) Curtiss, L. A.; Raghavachari, K.; Redfern, P. C.; Pople, J. A. *J. Chem. Phys.* **1997**, *106*, 1063–1079.

(334) Curtiss, L. A.; Redfern, P. C.; Raghavachari, K.; Pople, J. A. *J. Chem. Phys.* **1998**, *109*, 42–55.

(335) Petersson, G. A.; Braunstein, M. *J. Chem. Phys.* **1985**, *83*, 5129–5134.

(336) Montgomery, J. A., Jr.; Ochterski, J. W.; Petersson, G. A. *J. Chem. Phys.* **1994**, *101*, 5900–5909.

(337) Ochterski, J. W.; Petersson, G. A.; Montgomery, J. A., Jr. *J. Chem. Phys.* **1996**, *104*, 2598–2619.

(338) Montgomery, J. A., Jr.; Frisch, M. J.; Ochterski, J. W.; Petersson, G. A. *J. Chem. Phys.* **1999**, *110*, 2822–2827.

(339) Miertuš, S.; Scrocco, E.; Tomasi, J. *Chem. Phys.* **1981**, *55*, 117–129.

(340) Cammi, R.; Tomasi, J. *J. Comput. Chem.* **1995**, *16*, 1449–1458.

(341) Klamt, A. *J. Phys. Chem.* **1995**, *99*, 2224–2235.

(342) Cramer, C. J.; Truhlar, D. G. *Chem. Rev.* **1999**, *99*, 2161–2200.

(343) van Duin, A. C. T.; Dasgupta, S.; Lorant, F.; Goddard, W. A., III *J. Phys. Chem. A* **2001**, *105*, 9396–9409.

(344) Rappé, A. K.; Casewit, C. J.; Colwell, K. S.; Goddard, W. A., III; Skiff, W. M. *J. Am. Chem. Soc.* **1992**, *114*, 10024–10035.

(345) Cornell, W. D.; Cieplak, P.; Bayly, C. I.; Gould, I. R.; Merz, K. M., Jr.; Ferguson, D. M.; Spellmeyer, D. C.; Fox, T.; Caldwell, J. W.; Kollman, P. A. *J. Am. Chem. Soc.* **1995**, *117*, 5179–5197.

(346) MacKerell, A. D., Jr.; Wiórkiewicz-Kuczera, J.; Karplus, M. *J. Am. Chem. Soc.* **1995**, *117*, 11946–11975.

(347) Allinger, N. L. *J. Am. Chem. Soc.* **1977**, *99*, 8127–8134.

(348) Allinger, N. L.; Yuh, Y. H.; Lii, J.-H. *J. Am. Chem. Soc.* **1989**, *111*, 8551–8566.

(349) Lii, J.-H.; Allinger, N. L. *J. Am. Chem. Soc.* **1989**, *111*, 8566–8575.

(350) Lii, J.-H.; Allinger, N. L. *J. Am. Chem. Soc.* **1989**, *111*, 8576–8582.

(351) Hwang, M. J.; Stockfisch, T. P.; Hagler, A. T. *J. Am. Chem. Soc.* **1994**, *116*, 2515–2525.

(352) Halgren, T. A. *J. Comput. Chem.* **1996**, *17*, 490–519.

ISBN 978-952-12-2480-5
ISBN 978-952-12-2481-2 (digital)
Uniprint – Turku, Finland 2010